SIMULATION OF A MACHINE TOOL HYDRAULIC COPYING SYSTEM UNDER DYNAMIC LOADING

Laurent G. Tremblay

A DISSERTATION

in the

Faculty of Engineering

Presented in partial fulfillment of the requirements for
the Degree of Master of Engineering at
Sir George Williams University
Montreal, Canada

September, 1973

ABSTRACT

The mathematical modeling and computer simulation of a four-way spool valve controlled symmetrical linear actuator subjected to the cutting force fluctuations developed for a single cutting edge tool are presented.

The forcing function is developed by using a dynamic variation to the metal cutting relationships derived by Merchant for oblique cutting using a thin-shear-plane model. The effects on system performance of the stationary, deterministic cutting process and the sensitivity of the system to changes in fluid supply pressure, bulk modulus, actuator mass, leakage, spool valve area gradient, overlap, and mechanical servo linkage are examined.

Roughing and finishing operations in which the tracer template consists of straight line elements are simulated.

It is shown that the load applied to a single stage servo system is an important design consideration since the performance depends to a large extent on the load dynamics.

ACKNOWLEDGEMENTS

The author wishes to express his gratitude to his supervisor, Dr. M.O.M. Osman for initiating the project and for his suggestions and guidance during the investigation.

The author is also indebted to the analog computing facilities at Sir George Williams University and to its staff.

TABLE OF CONTENTS

	Page
ABSTRACT	i
ACKNOWLEDGEMENTS	ii
TABLE OF CONTENTS	iii
LIST OF TABLES	v
LIST OF FIGURES	vi
NOMENCLATURE	ix
CHAPTER 1: INTRODUCTION	1
1.1 Literature Survey	1
1.2 System Description	3
1.3 System Operation	7
1.4 Cutting Operations and Limitations	9
1.5 System Analysis	12
CHAPTER 2: OBLIQUE CUTTING AND THE COPYING SYSTEM	14
2.1 Geometry of Oblique Cutting	14
2.2 Force and Stress Relationships	16
CHAPTER 3: MATHEMATICAL MODEL OF THE SYSTEM	21
3.1 Spool Flow Equation	21
3.2 Actuator Flow Equation	23

Page

3.3 Mechanical Feedback Equation 24

3.4 Equilibrium Equation 25

3.5 Cutting Force Equation 25

3.6 Linear Analysis Transfer Function 26

CHAPTER 4: SYSTEM SIMULATION 29

4.1 Introduction 29

4.2 Results 33

CHAPTER 5: DISCUSSION AND CONCLUSIONS 55

REFERENCES 61

APPENDIX A: Actuator Flow Equations 64

Spool Valve Pressure-Flow Characteristics 68

APPENDIX B: Graphical Presentation of the Force Component and Force Constant 70

APPENDIX C: Analog Simulation of the Mathematical Model 75

LIST OF TABLES

		Page
4-1	Cutting conditions for simulated template profiles	32

LIST OF FIGURES

		Page
1-1	Spool-sleeve configuration	4
1-2	Positive spool displacement flow	5
1-3	Copying system with direct feedback	8
1-4	Sectional diagram of the copying system	10
1-5	Template slope - carriage velocity with parameter $\dot{X}_c$	11
2-1	Oblique cutting	14
2-2	Chip formation in oblique cutting	15
2-3	Cylinder effective feed rate	18
3-1	Mechanical feedback linkage	25
4-1	Simulated template profiles	30
4-2	Effect of increasing frequence of the force variation on the spool displacement and criterion; actuator extension under load condition B	34
4-3	Effect of increasing frequency of the force variation on the spool displacement and criterion; actuator extension under load condition B with fluctuating force magnitude ratio of .10	35
4-4	Effect of increasing frequency of the force variation on the spool displacement and criterion; actuator retraction under load condition B	36
4-5	Effect of spool valve overlap on the spool displacement and criterion; actuator retraction vs. extension under load condition B	37
4-6	Effect of spool valve overlap on the spool displacement and criterion; actuator retraction under load condition B	38
4-7	Effect of increasing frequency of the force variation on the spool displacement and criterion; actuator extension with spool valve overlap under load condition B	39
4-8	Effect of increasing spool valve area gradient on the spool displacement and criterion; actuator extension under load condition B	40
4-9	Effect of increasing frequency of the force variation on the spool displacement and criterion; actuator retraction under load condition C	41

		Page
4-10	Effect of increasing frequency of the force variation on the spool displacement and criterion; actuator extension with spool valve overlap under load condition C with fluctuating force magnitude ratio of .05	42
4-11	Effect of decreasing supply pressure on the spool displacement, criterion, and actuator displacement; actuator extension under load condition A	43
4-12	Effect of leakage, supply pressure, and axial piston hole dia. on the actuator displacement; .03 step input under cutting force component and force constant of load condition A	44
4-13	Effect of decreasing actuator leakage and axial piston hole dia. on the spool displacement and criterion; actuator extension under no external load condition	45
4-14	Effect of increasing actuator mass on the spool displacement, criterion, and actuator displacement; actuator extension under load condition A	46
4-15	Effect of increasing effective bulk modulus on the workpiece radial error and the load pressure; actuator extension under load condition A	47
4-16	Load pressure response to sawtooth input under load condition D	48
4-17	Load pressure response to sawtooth input under load condition D; actuator total leakage coefficient one half of normal value	49
4-18	Load pressure response to sawtooth input under load condition D; actuator total leakage coefficient one half of normal value, spool valve area gradient increased	50
4-19	Effect of increasing the fluctuating force magnitude ratio on the spool displacement and criterion; actuator extension with spool valve overlap under load condition E	51
4-20	Effect of increasing the spool valve area gradient on the actuator output displacement and velocity response to a .06 step input under no load	52

		Page
4-21	Effects of increasing the actuator mass on the actuator output displacement and velocity response to a .06 step input under no load	53
4-22	Effect of increasing actuator leakage, axial piston hole dia. and spool valve area gradient on the spool displacement response to a .06 step input under no load	54
A1-1	Actuator leakage flow	66
A1-2	Spool valve pressure-flow characteristics	69
A2-1 to A2-4	Force component and force constant	71, 72, 73, 74
A3-1	Scaled analog diagram	80

NOMENCLATURE

A	effective piston area of linear actuator, in^2.
A_h	area of sharp edged hole in piston, , in^2.
B	viscous damping coefficient, lb-sec/in.
B_s	time scale factor, dimensionless.
b	width of machine cut, in.
CTN	performance criterion: the time integral of the absolute value of the workpiece radial error, in.-sec.
C_d	turbulent orifice discharge coefficient, dimensionless.
C_s	tool side cutting edge angle, deg.
E	workpiece radial error, $= (X_c - Y_c) \sin \delta$, in.
e	spool valve error, or spool displacement from neutral, in.
e_o	spool valve overlap, in.
F_1	cutting force component, lb/rev.
F_2	cutting force constant associated with the cylinder feed rate in the direction of F_Q, lb-sec/in.-rev.
F_{dyn}	dynamic cutting force
F_P, F_Q, F_R	steady state cutting force components; parallel to the velocity approach vector, perpendicular to the finished work surface, and perpendicular to the first two respectively.
f	carriage feed rate, in./rev. of workpiece.
f_q	feed rate in the direction of force F_Q, in./rev.
G_a	spool valve area gradient, $in.^2$/in. of spool displacement.
G_m	mechanical linkage gain, dimensionless.
i	angle of inclination, or obliquity, deg.
K	material constant, dimensionless.
K_q	spool valve flow gain, $in.^3$/sec/in. of spool displacement.
L_e, L_i	actuator external, or internal laminar leakage coefficient, $in.^3$/sec/psi.
$L_t = L_i + \frac{L_e}{2}$	actuator total leakage coefficient, $in.^3$/sec/psi.
ℓ_1, ℓ_2	spool valve input linkage lengths, in.
m	mass of hydraulic cylinder, lb-$sec.^2$/in.

n	workpiece rotational speed, rev./sec.
P_1, P_2	pressure in cylinder forward and return chamber, psi.
$P_L = P_1 - P_2$	load pressure difference across ram, psi.
P_r	return, or exhaust pressure, psi.
P_s	supply pressure, psi.
Q_1, Q_2	volume flow rate into cylinder forward chamber, out of cylinder return chamber, $in.^3/sec.$
Q_L	load flow, = average of flows in the two actuator lines, $in.^3/sec.$
Q_{Le}, Q_{Li}	leakage flow rate at ends of piston rod, and across piston, $in.^3/sec.$
Q_h	flow rate through hole in piston, $in.^3/sec.$
r_t	t_1/t_2 = chip ratio, dimensionless, (value less than unity).
S	Laplace operator, $= d/dt$, sec^{-1}.
T	computer time, sec.
t	system time, sec.
t_1, t_2	uncut, and final chip thickness, in.
V_1, V_2	volume of forward and return chamber, $in.^3$
V_δ	one half the total trapped oil volume, $in.^3$
V_c, V_s, V_w	chip velocity component in the plane of the tool face, shear velocity component in the shear plane, and approach velocity component respectively, for the thin-shear-plane model.
V_{cq}	component of cylinder velocity in the direction of force component F_Q, in/sec.
X_c	cylinder linkage command input, parallel to the cylinder axis, in.
Y_c	cylinder output displacement, along cylinder axis, in.
α_n	normal rake angle, deg.
β	fluid bulk modulus of elasticity, psi.
β_e	effective bulk modulus, psi
β_n	normal friction angle in oblique cutting, deg.
γ	angle between cylinder and workpiece axis, deg.
δ_h	hydraulic damping ratio, dimensionless.

ϵ	magnitude ratio of fluctuating force.
η_c, η_s	chip, and shear flow angle, deg.
Θ	template profile slope(s), deg.
μ	fluid absolute viscosity, lb-sec/in.^{2}
ρ	fluid mass density, lb-sec^2/in.^{4}
τ_o	shear strength with zero normal stress, psi.
τ_s	shear strength on shear plane, psi.
Φ_n	normal shear angle, deg.
ω	frequency of force variation, rad/sec.
ω_h	hydraulic natural frequency, rad/sec.

Superscript $\cdot$ denotes differentiation with respect to time

CHAPTER 1

INTRODUCTION

1.1 Literature Survey

Hydraulic servomechanisms have a natural application in power systems due to their high power capacity, power to inertia ratio and power to weight ratio. They are widely applied - References [1] [2] [3], in designs of aircraft control surface systems, missile attitude control systems, rocket throttling controls, gimballed antennas, and numerous other fields. Machine tool control systems are a natural application since it is not uncommon that the loading of the member whose position is controlled is principally inertia.

Early development of hydraulic control was primarily on a trail and error procedure combined with experience from previous applications and experimental testing. Attempts at evolving design procedures by a purely analytical approach were hampered by the serious nonlinearities inherent in the differential and algebraic equations which described the system components. The most significant nonlinearity in the valve controlled system is the relationship between flow rate and pressure drop across the servovalve. By linearizing the valve flow equations, such dynamic characteristics as stability, transient and frequency response is obtained by deriving the incremental transfer function for the valve actuator and load combination, and applying automatic control system analysis such as described by D'Azzo and Houpis [5], Kuo [6] and others.

Analytical techniques now exist, such as described by Morse [10], Merritt [11], by which a preliminary dynamic analysis can be obtained of hydraulic control systems, particularly those using a flow control valve in the forward loop. The basic configuration of a hydraulic cylinder controlled by a four-way spool valve is the type of servo controlled positioning system discussed in an early paper by Harpur [12], in which a solution was given of the nonlinear equation of an error-actuated system using the classical method of small

perturbations. Shearer's [13] linear analysis of a balanced linear actuator connected to a mass plus friction load controlled by an open centre fourway spool valve included actuator laminar leakage and oil compressibility. Reeves [14] derived the linear equivalent of the valve flow by computing the fundamental component of the flow rate when spool displacement and output pressure are assumed to be sinusoidal.

The mathematical treatment of a mechanically actuated closed center spool valve, balanced linear actuator system under simple loading, excluding leakage and compressibility, but including the valve flow nonlinearity was further extended by Royle [19], Turnbull [20], and Butler [21].

If several system parameters are permitted to vary the manipulation of Nyquist criteria, Bode diagrams, Nichol's chart, root-locus plots and other graphical techniques become rather cumbersome [4]. With the introduction of nonlinearities such as backlash, pressure and flow saturation, stiction, coulomb friction, deadband, the analytical version of the problem becomes extremely time consuming. In studies of these systems, the analog computer offers a far greater flexibility than the graphical methods, makes possible a more accurate determination of frequency and transient response for large amplitudes where linearization techniques do not apply, and thus offers an excellent opportunity to study the effect of different parameters. Rererences [7] [8] [9] give a detailed account of simulation techniques. Reethoff [15] demonstrated the power of combined analog simulation and limited testing of a hydromechanical position servomechanism with an unbalanced linear actuator connected to a mass plus spring load. Rausch [16] compared solutions of the nonlinear equations obtained by analog simulation with solutions of the incremental linear transfer function for an inertially loaded hydromechanical servomechanism, consisting of an open center valve and balanced actuator. Davies and Lambert [17], and Glaze [18] simulated a hydromechanical servomechanism flexibility connected to an inertial load.

The literature survey revealed that an external axial load is often omitted in publications, although Khaimovitch [34] included a constant load in his analysis of a machine tool hydraulic control system. This dissertation, therefore, extends the analysis by including the influence of a dynamic loading, [35] [36], which is a function of the output signal of the servomotor.

1.2 System Description

The valve controlled hydraulic system for the position control under investigation consists of three main elements; a variable delivery pump, a mechanically operated sliding type servovalve, and a linear actuator. The sliding valve is of spool type construction, having three lands operating within a fixed sleeve which contains the matching sets of sharp edged rectangular ports symmetrically placed along its periphery, as shown in Fig. 1-1. By using rectangular ports a linear area gradient is obtained and sufficient inner circumferential sleeve bearing surface remains to eliminate the need for additional centering lands. The valve area gradient, which is the rate of change of orifice area with spool stroke, is the principal parameter in establishing the flow gain of the valve and hence has a direct influence on the stability of the system. Establishing the flow gain is especially important in hydromechanical servos since it is often the only method of gain control in the control loop.

The width of each land is made equal to, or greater than, that of the matching port. With such a closed center configuration there is zero flow through the spool when it is at its neutral or null position; assuming zero leaking at the spool. The equal land port condition is a zero lapped valve often termed critical closed center. As seen from Fig. 1-2, positive displacement of the spool results in flow through the set of orifices 1 and 4. In European terminology, the valve would be described as having two control edges, meaning that two land edges are in the flow path. For matched orifices, an equal flow area would be exposed through orifices 1 and 4; or 2 and 3 for an opposite spool displacement. For symmetrical orifices, the area exposed through orifice 1 is equal to that exposed through orifice 2 for an equal but opposite spool displacement; similarly

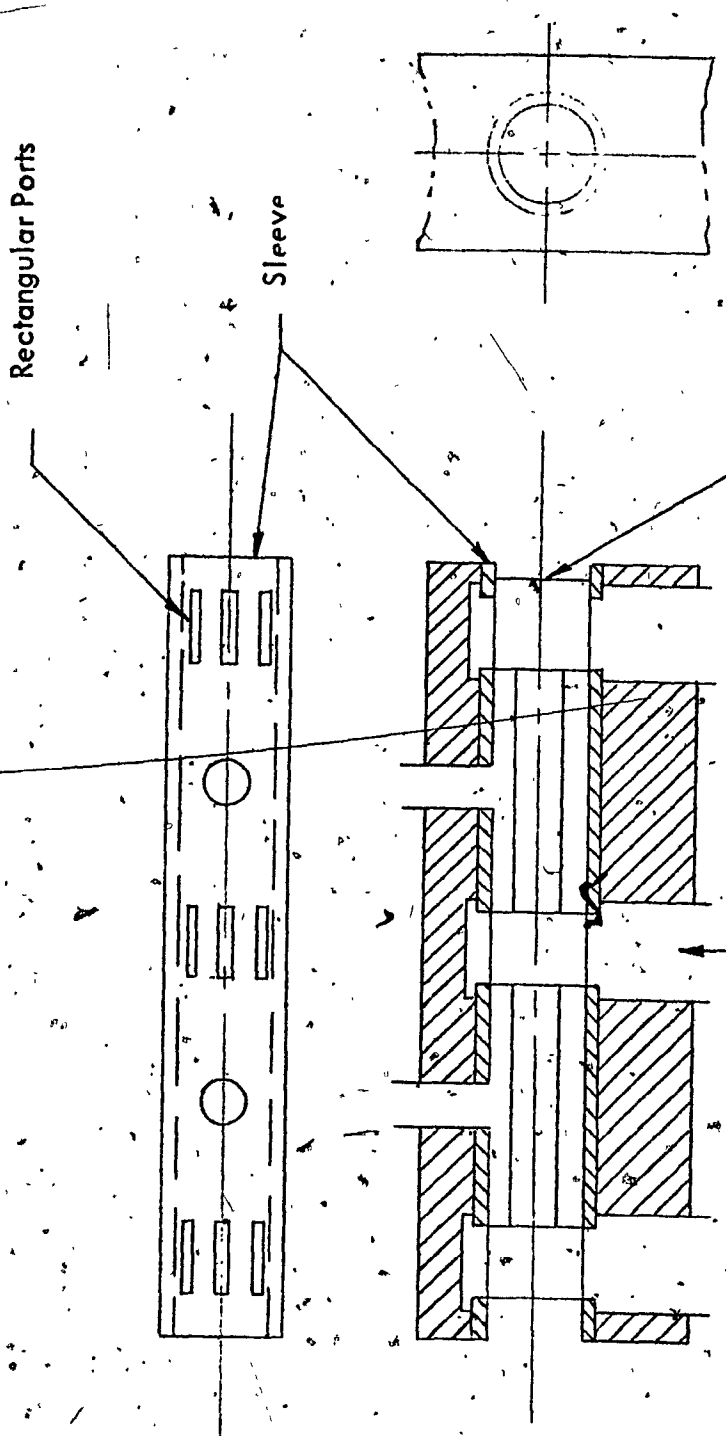

FIGURE 1-1 Spool-Sleeve Configuration

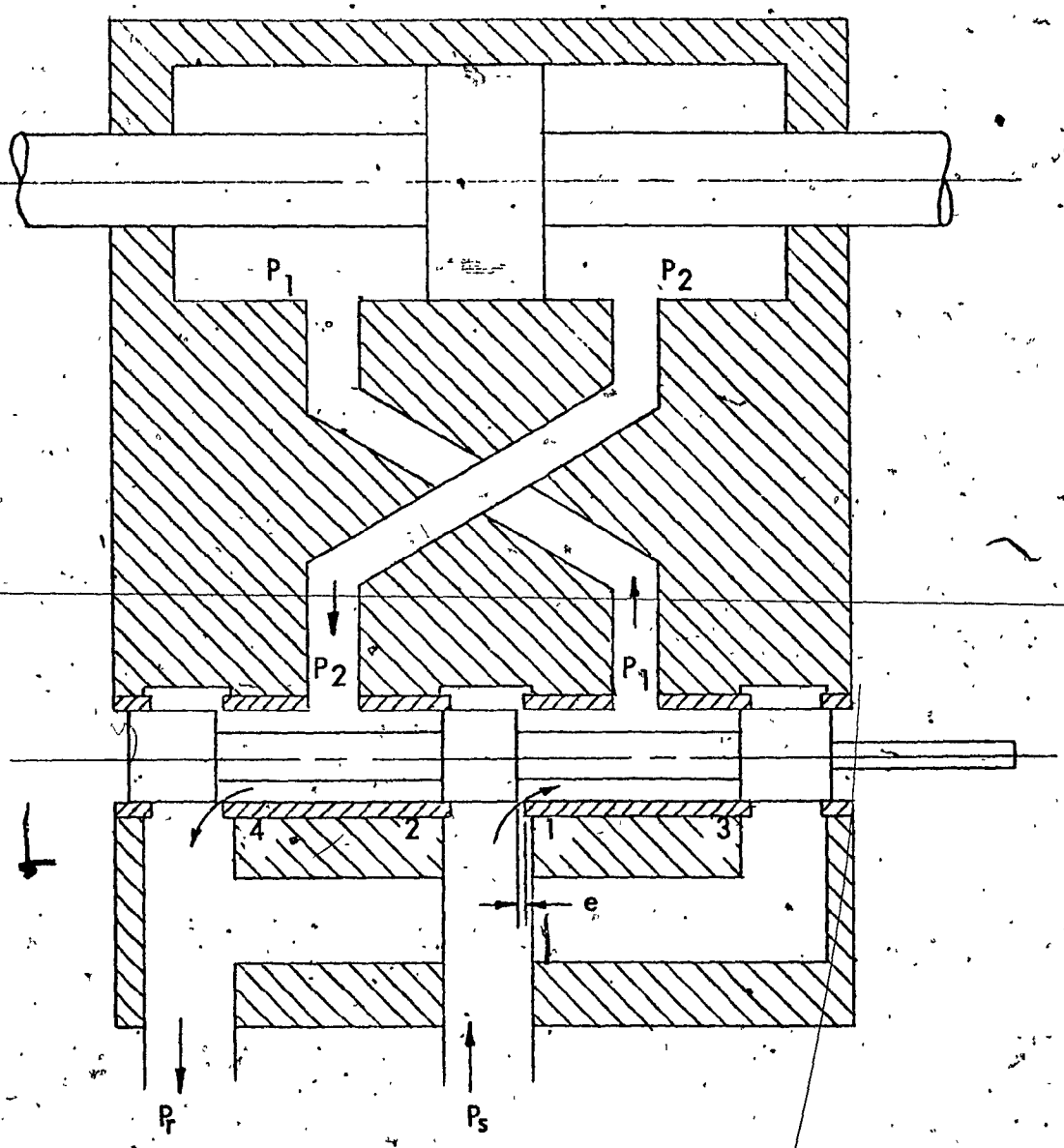

FIGURE 1-2 Positive Spool Displacement Flow

for orifices 3 and 4. In the overlapped case, the amount of overlap refers to the difference in length between the edge of the port and that of the land, when the land is centrally located along the port. Flow through either set of orifices will, therefore, not occur until the spool is displaced an amount greater than the overlap. The effect of this deadband on system accuracy is included in the study. In practice, manufacturing a critical center valve demands stringent machining tolerances, and a slight overlap is often desired to offset the leakage effect of radial clearances.

An open center spool configuration, in which the port width exceeds that of the matching land, could also be used, although it was not included in this investigation. The spool is at its neutral position only when there is zero load on the actuator. It has the disadvantage of reducing overall efficiency since flow is ever present, but is, however, insensitive to temperature, and hence viscosity changes since a turbulent flow condition is assured at all times.

Due to the rate of change of fluid momentum through the valve, forces are developed which oppose the displacement of spool type valves. These forces are of importance in electrohydraulic servos when a valve is operated by a torque motor or solenoid which have distinct force limitations. This causes a limitation to the maximum size of the servovalve, or requires design of two stage configurations or some technique to reduce or compensate the steady state flow force. Investigations into these forces were led by Lee and Blackburn [22], followed by Noton and Turnbull [23]. Clark [24] suggested three methods of force compensation in addition to those suggested by Lee [25]. Since the force available for stroking the spool is provided by the carriage drive on the copying machine and the template is assumed to be rigidly mounted to the bed, these forces can be ignored in this study.

The linear actuator is a double acting, balanced piston configuration that divides the cylinder into two equal compartments. The fluid passages and the spool sleeve are an integral part of the actuator housing. By interconnecting the return lines at the sleeve, a "four way" valve results which allows actuator

directional reversal whether the piston is balanced or unbalanced. By contrast, a three way valve could be employed [33] which could require only two spool lands, but in order to obtain cylinder direction reversal the piston must be unbalanced; supply pressure is ported to one land and directly to the smaller area of the unequal area piston.

In valve controlled systems, the power is supplied by a constant pressure delivery pump. Two configurations are common: one consists of a constant delivery pump with a pressure relief valve, another consists of a variable delivery pump with a stroke control to regulate the pressure. The latter is more efficient, as no flow is delivered unless demanded by the servovalve. In practice, the pressure does drop slightly upon sudden, large flow demands. This variation is ignored in the analysis of the copying system. The effect on the system of different constant supply pressures is, however, included.

1.3 System Operation

Operation of the copying system as applied to a center lathe can be explained with the aid of sectional diagram Fig. 1-2 and of Fig. 1-3 in which direct mechanical feedback is employed. The cutting tool is fixed to the hydraulic actuator which forms the copying slide. Transverse movement of the copying slide is relative to the piston, which is rigidly connected to the carriage. During a turning operation, the carriage travels at a uniform longitudinal speed fn along the lathe bed. The template is fixed to the bed and thus provides the input signal to the spool. For a constant workpiece diameter the template profile is parallel to the workpiece axis and the spool is at neutral. For a spool displacement x from neutral as shown, supply pressure P_s causes fluid to flow through control orifice 1 to the load chamber 1. Return flow is from chamber 2 through orifice 4 to the reservoir, and the actuator moves a distance y with respect to the workpiece. The difference e between the required (template) input and the actual (copying slide) output position provides the control error which activates the spool. If the spool displacement is halted, the actuator

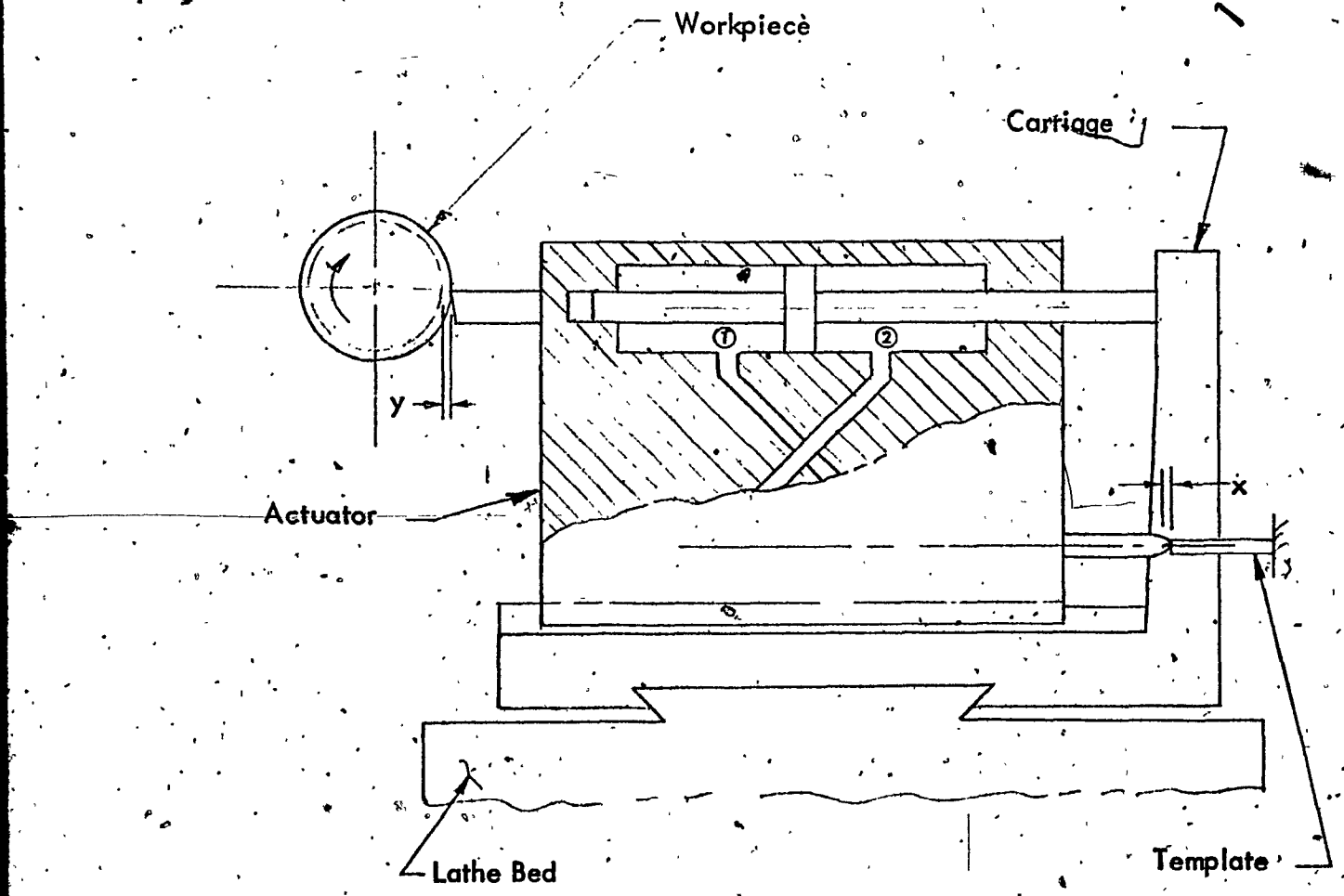

FIGURE 1-3 Copying System With Direct Feedback

will continue to travel until the spool-actuator combination returns to neutral. It is readily seen that the behavior of the system is dependent upon many factors; the nature of the cutting loads at the tool, the velocity of the input, leakages, friction, inertia, supply pressure, flow rates, and elastic deformation of the components.

Fig. 1-4 is a schematic presentation showing the copying slide axis re-arranged from the right angle position of Fig. 1-3, to some angle γ with the workpiece axis. This is commonly employed to more easily control the machining of shoulders and surfaces which lie at 90° to the turning axis. Two angles, 45° and 60°, are used in the study. A feedback lever, or error bar, connected to the spool and pivoting at the actuator is included since it is a common feature resulting from design considerations of accessibility, simplicity and general mechanical arrangement of the copying system. Various lever ratios are simulated in the study for the sake of completeness, but it is assumed that this arrangement is free of backlash, has negligible inertia, and undergoes zero structural deflection.

1.4 Cutting Operations and Limitations

During system operation, the carriage is driven by the leadscrew in a direction parallel to the workpiece axis, at a uniform rate fn. For a given template slope the input velocity of the mechanical linkage in a direction parallel to the copying actuator (cylinder) axis is a function of the carriage velocity. The result of a graphical solution of the vector addition $fn + \dot{X}_c$ is given in Fig. 1-5 for two values of γ.

The system is physically restricted to an operating range of template slopes which is dependent upon the γ employed, due to the requirement that the carriage velocity be positive during a copying cycle; the range being greater than $\gamma°$ and less than $180° + \gamma$. This can be illustrated using the template slope definition of Fig. 1-4 by considering a hypothetical case in which the leadscrew is disengaged, ($fn = 0$) and linkage inputs are supplied directly by the machine tool operator. An actuator extension command would produce the

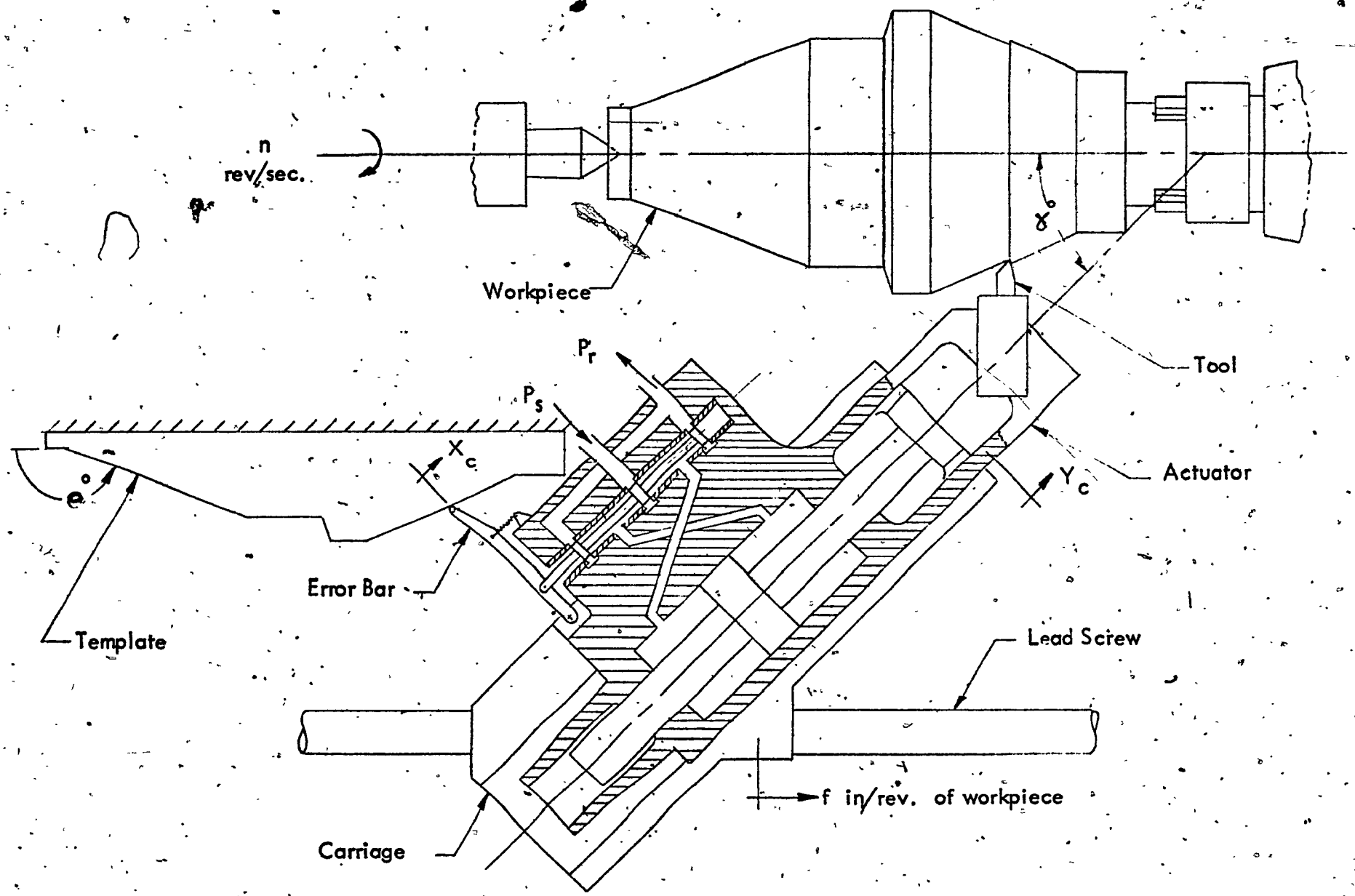

FIGURE 1-4. Sectional Diagram of the Copying System

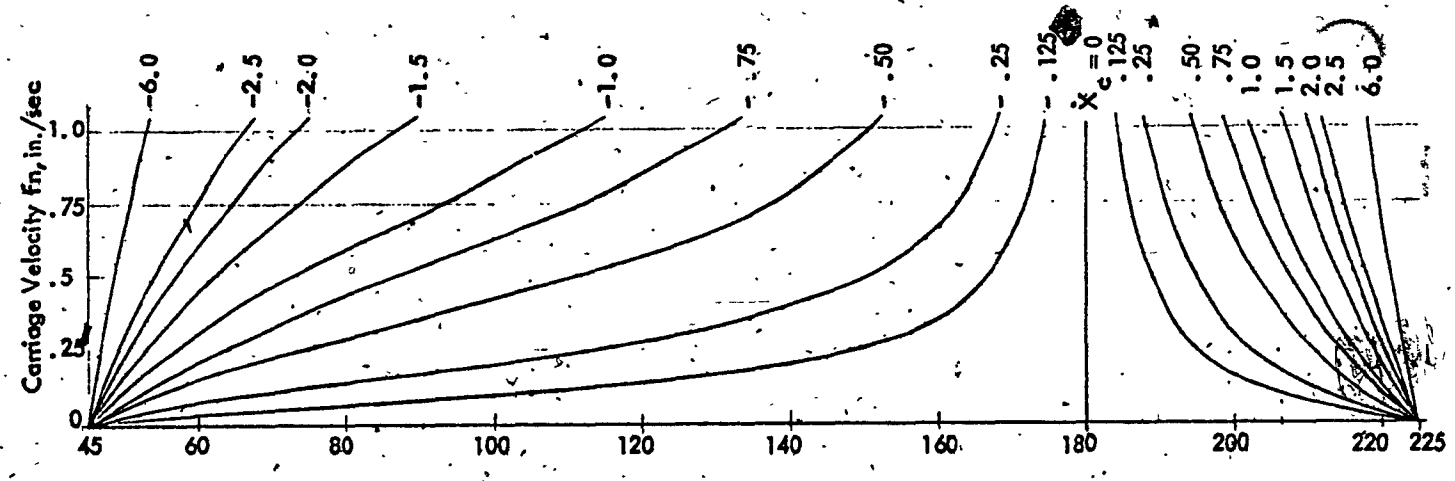

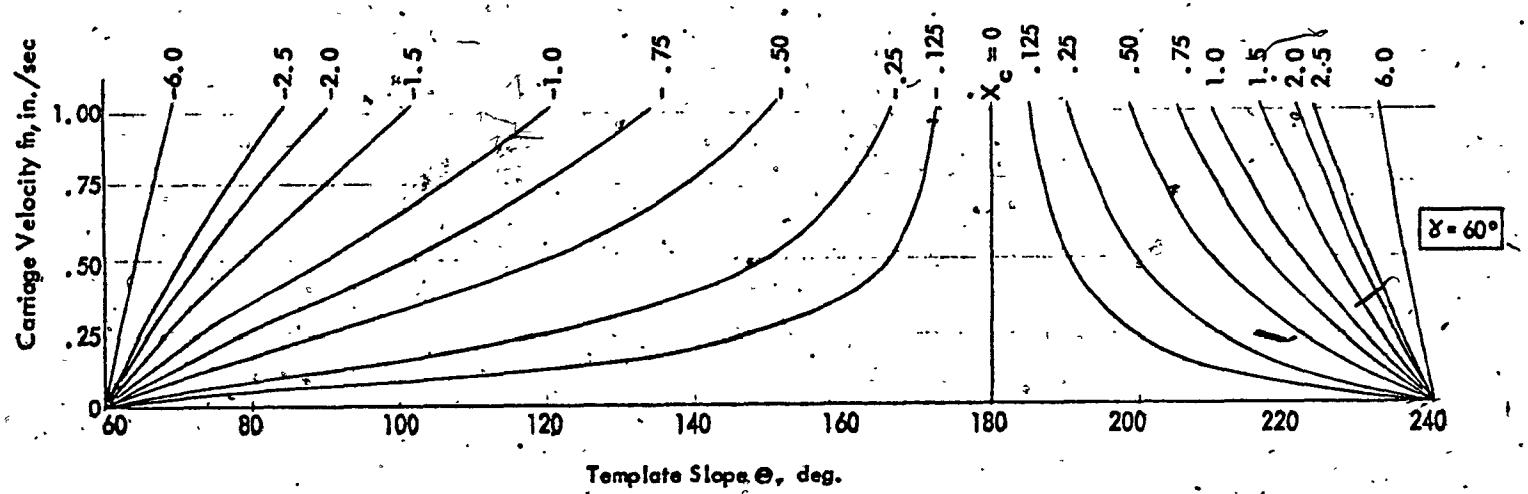

FIGURE 1-5. Template Slope - Carriage Velocity With Parameter $\dot{X}_c$

maximum machined slope of $180° + \gamma$. To increase the resultant slope, the leadscrew would have to drive the carriage in a reverse (negative) direction. The minimun slope limit can be established in a similar way by considering an actuator retraction stroke.

The actual machined slope is further restricted by the existing tool geometry which is discussed in the next chapter. A workpiece requiring machined surfaces which are beyond the template slope limitations can be obtained on a machine tool while maintaining a constant γ, by employing a second copying lathe and template, operating from the opposite side of the workpiece. A restriction which exists in both cases, however, is that the tool tip radius and the template follower radius must be smaller than a given template corner or fillet radius.

The carriage feed rate and depth of cut are selected in combination with the workpiece rotational speed, dependent upon workpiece and tool materials, and the degree of surface finish required. The ratio of depth of cut to feed is given in machinery handbooks as having a value of ten for roughing operations, and three for finish operations. Surface cutting speeds for finish cuts are in general five times that of rough cuts, the limitations being the sacrifice to tool life, and the capabilities of the lathe. It is possible that a combination of speeds, feeds, and depth of cut can be selected that require a greater horsepower than is available at the drive spindle. Values of b, f, n, γ and the geometry of the tool determine the magnitude of a force component and a force constant which are a part of the dynamic cutting force derived in Chapter 3. Investigations of rough and finish cuts for some tool geometries and template slopes are included in the simulation.

1.5 System Analysis

Accuracy of the actuator displacement to follow the template is the prime consideration in the copying system. The difference between the input to the spool linkage (X_c) which is applied by the template and the actual

actuator displacement (Y_c) results in a workpiece diametral error having a magnitude of $2(X_c - Y_c) \sin \gamma$. Ideally, small parameter changes should result in small changes in dynamic performance of the fluid power system. An analog simulation provides a very effective engineering tool for the study of parameter sensitivity. Due to its rapid, real time solution rate, it is possible to examine a large number of operating conditions and quickly reject or verify postulated causes or solutions for undesired performance. It also allows artifically holding constant certain variables of the system so as to gain insight into its effect on the system.

Important dynamic characteristics such as stability can be studied, stability implying that pressure and motion transients decay, leaving the desired steady state behavior.

In order to explore the effect of the system loading in as simple a way as possible, a basic system performance criterion was adopted by integrating the absolute value of the workpiece radial error and noting the resulting effect of changes due to different cutting operations, for a given input displacement.

CHAPTER 2

OBLIQUE CUTTING AND THE COPYING SYSTEM

2.1 Geometry of Oblique Cutting

The major geometrical difference between two dimensional (orthogonal) and oblique cutting is the angle of inclination, or obliquity 'i' which exists between the cutting edge and a normal to the cutting velocity vector, as illustrated in Fig. Fig 2-1. The geometry involved in oblique cutting based on a single thin shear plane model for a single cutting edge as suggested by Merchant [27] can be represented as shown in Fig. 2-2 [26]. The primary, or normal rake angle is measured from the true side view of the rake face to a line perpendicular to the cutting velocity vector V_w, and is designated α_n. The angle measured in a plane that is normal to the cutting edge, to the plane containing the formed work surface is the normal shear angle, Φ_n. The ratio of the uncut chip thickness t_1, to the final chip thickness t_2, is called the chip ratio r_t. From the geometry, an expression can be derived from which the normal shear angle can be calculated, knowing the chip ratio (a value less than unity) and the normal rake angle:

$$\tan \Phi_n = \frac{r_t \cos \alpha_n}{1 - r_t \sin \alpha_n} \qquad (2.1)$$

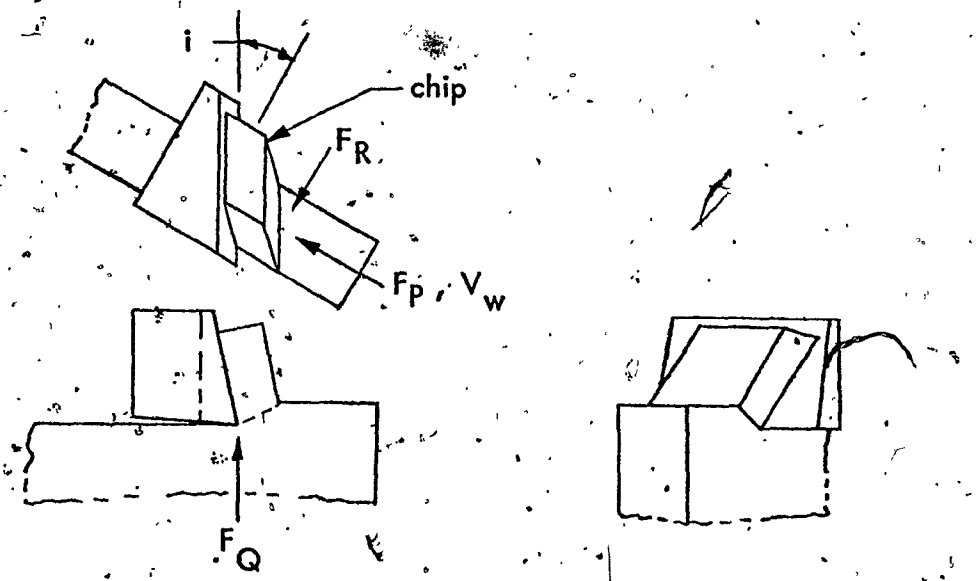

FIGURE 2-1 Oblique Cutting

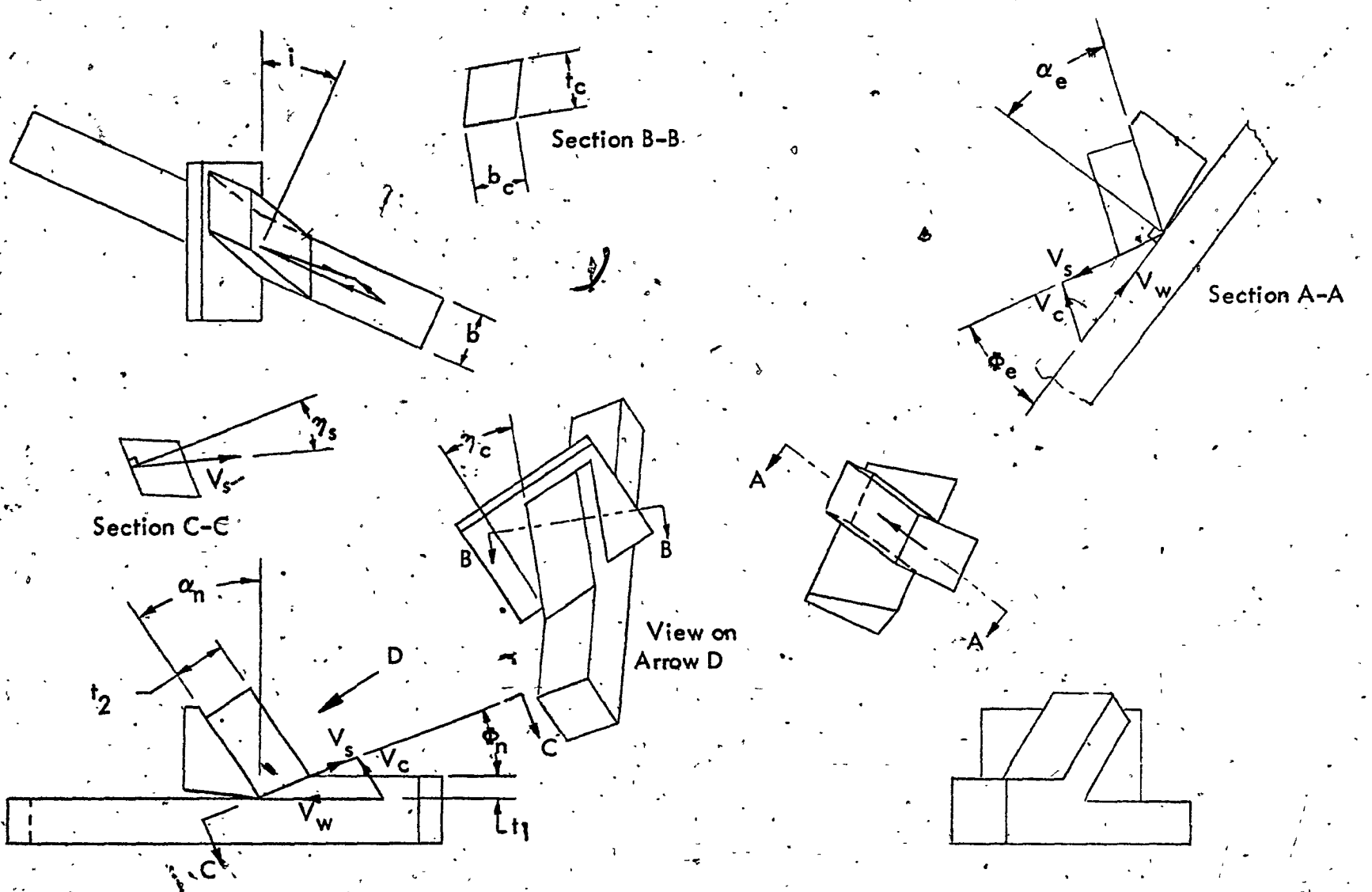

FIGURE 2-2 Chip Formation in Oblique Cutting

The three velocity components lie in one plane and are identified as the approach velocity V_w, the shear velocity V_s in the shear plane, the chip velocity V_c in the plane of the tool face.

As can be seen in the figure, the chip cross section is a parallelogram. The angle between the shear velocity in the shear plane and the normal to the cutting edge is the shear flow angle η_s. In the rake face plane, the angle between the chip flow velocity and the normal to the cutting edge is called the chip flow angle η_c. Stabler [28] [29] reported that experimentally the chip flow angle is equal to the angle of obliquity for all test conditions he investigated including tool and work materials, rake angles and speeds, and he proposed the Chip Flow Law;

$$\eta_c = i \qquad (2.2)$$

As noted by Choi [30] further researches [31] revealed that not all experimental results are in agreement with Merchant's model or Stabler's Chip Flow Law. This approximation, however, is utilized in this investigation.

2.2 Force and Stress Relationships

Armarego and Brown [26] have derived steady state, or average force relationships for single edge oblique cutting using a thin shear plane model. The results of these derivations are presented below, modified slightly to adapt to the turning operation. Three basic assumptions were made:

1. The tool tip is sharp and no rubbing or ploughing forces act on the tool tip.
2. The stress distributions in the shear plane are uniform.
3. The resultant force acting on the chip at the shear plane is equal, opposite and collinear to the force acting on the chip at the rake face.

Three force components were chosen: the power contributing force component (F_P) which is parallel with the velocity approach vector V_w, one perpendicular to the finished work surface (F_Q), and a third (F_R) which is perpendicular to the other two. Component F_P is at 90° to the hydraulic cylinder longitudinal axis during the

copying operation, and results in frictional forces on the moving cylinder. This type of loading is not simulated, so that an expression for F_p is not included here.

Two components of the resultant force were considered to act on the shear plane and two on the rake face. A normal friction angle β_n was defined in terms of the two components on the rake face and the angle between the friction force and the normal to the cutting edge, η'_c. Assuming that the chip velocity and friction force are collinear and that the shear velocity (hence shear strain) and shear force (hence shear stress) in the shear plane are also coincident, a geometrical relationship between α_n, Φ_n, β_n, η_c and i was derived, and expressed as:

$$\tan(\Phi_n + \beta_n) = \frac{\tan i \cos \alpha_n}{\tan \eta_c - \sin \alpha_n \tan i}$$

By substituting the previous assumption that $\eta_c = i \neq o$, this expression is simplified to:

$$\tan(\Phi_n + \beta_n) = \frac{\cos \alpha_n}{1 - \sin \alpha_n} \qquad (2.3)$$

The force components F_Q and F_R (pounds force for each revolution of the workpiece) assuming $\eta_c = i = \eta'_c$ are given by:

$$F_Q = \frac{\tau_s \, b \, f_q \, \sin(\beta_n - \alpha_n)}{\sin \Phi_n \cos i \sqrt{\cos^2(\Phi_n + \beta_n - \alpha_n) + \tan^2 i \, \sin^2 \beta_n}}$$

$$F_R = \frac{\tau_s \, b \, f_q \, (\cos(\beta_n - \alpha_n) \tan i - \tan i \sin \beta_n)}{\sin \Phi_n \sqrt{\cos^2(\Phi_n + \beta_n - \alpha_n) + \tan^2 i \, \sin^2 \beta_n}} \qquad (2.4)$$

Figure 2-3 shows the geometrical relationship of these force components when applied to the copying system. The angle C_s is the side cutting edge angle of the tool and is defined with respect to the cylinder. The carriage feed rate is designated as f (inches per revolution of the workpiece) and the rotational speed of the work piece is n (rev/sec). As described in Chapter 1, for a given cutting

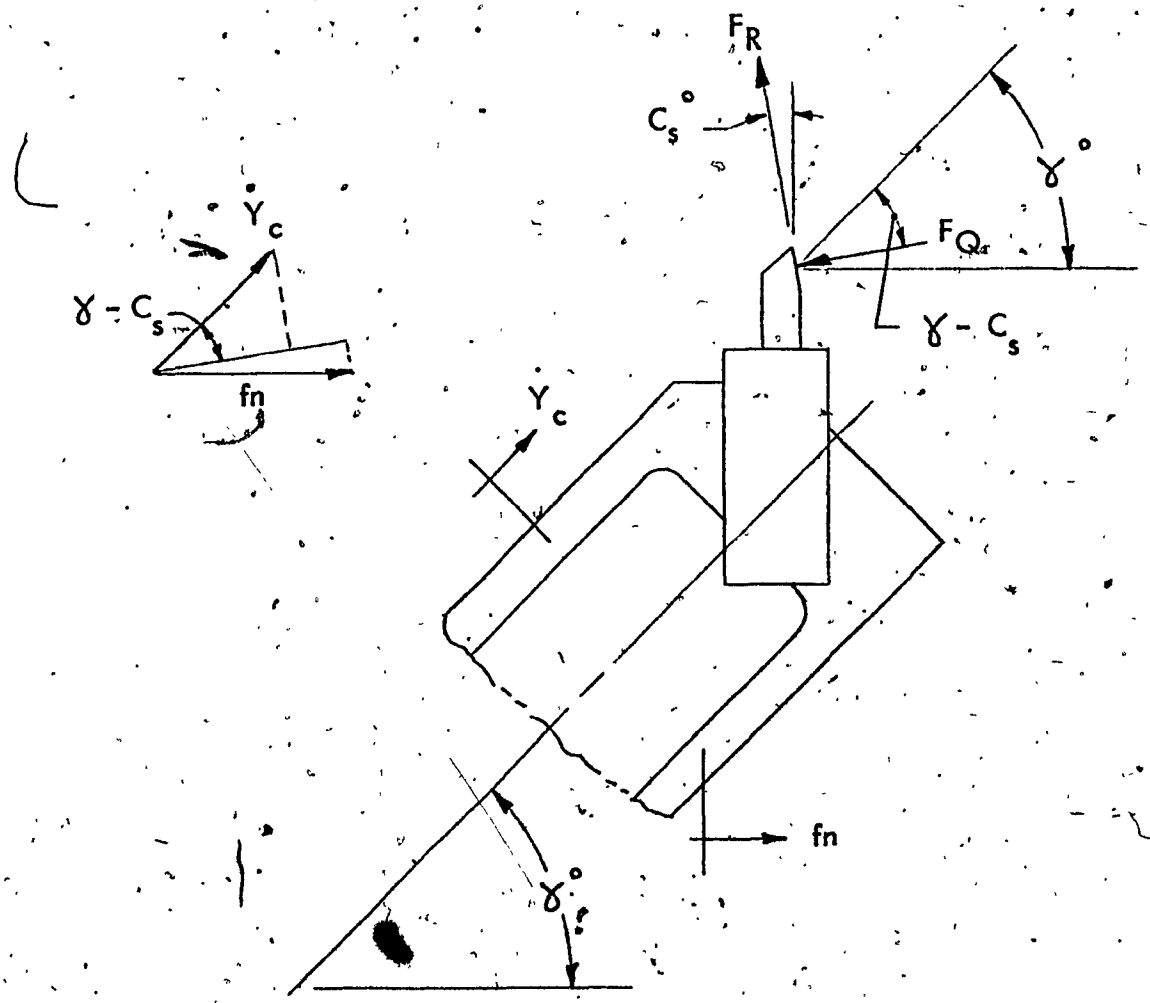

FIGURE 2-3. Cylinder Effective Feed Rate

operation the carriage travels at a uniform velocity fn (inch/sec) along the lathe bed and remains positive as shown. The velocity of the cylinder with respect to the carriage, $\dot{Y}_c$, is positive (as shown), or negative, depending upon the template shape. For directions shown in the figure, the resulting component of cylinder velocity in the direction of F_Q is therefore:

$$V_{cq} = \dot{Y}_c \cos(\gamma - C_s) + fn \cos C_s$$

The feed rate in this direction is V_{cq}/n, so that:

$$f_q = \dot{Y}_c \frac{\cos(\gamma - C_s)}{n} + f \cos C_s \qquad (2.5)$$

Thus the cutting force components are dependent upon the response of the piston - cylinder control system. This will be discussed in Chapter 3. The force component acting along the cylinder axis, opposing cylinder extension can also be obtained from the figure, and is expressed:

$$F = F_Q \cos(\gamma - C_s) - F_R \sin(\gamma - C_s) \qquad (2.6)$$

Force components F_Q and F_R can be expressed (equations 2.4) as:

$$F_Q = K_Q b f_q \text{ and, } \quad F_R = K_R b f_q$$

where

$$K_Q = \frac{\tau_s \sin(\beta_n - \alpha_n)}{\sin \Phi_n \cos i \sqrt{\cos^2(\Phi_n + \beta_n - \alpha_n) + \tan^2 i \sin^2 \beta_n}}$$

and

$$K_R = \frac{\tau_s (\cos(\beta_n - \alpha_n) \tan i - \tan i \sin \beta_n)}{\sin \Phi_n \sqrt{\cos^2(\Phi_n + \beta_n - \alpha_n) + \tan^2 i \sin^2 \beta_n}} \qquad (2.7)$$

A relationship for the shear strength on the shear plane (τ_s) has been given by Merchant [27] as:

$$\tau_s = \frac{\tau_o}{1 - K \tan (\Phi_n + \beta_n - \alpha_n)} \qquad (2.8)$$

Values to τ_o and K were stated to be 69000 psi and .175 respectively for steel SAE 4340.

Numerical values of K_Q and K_R can therefore be obtained from a given set of values of i, r_t, α_n, τ_o and K, by assuming $\eta = i$, calculating Φ_n from equation 2.1, β_n from equation 2.3, and substituting into expressions 2.7.

CHAPTER 3

MATHEMATICAL MODEL OF THE SYSTEM

3.1 Spool Flow Equation

For steady state flow, the volume flow rate through each orifice of the valve sleeve can be obtained by applying Bernoulli's equation for incompressible flow, resulting in the turbulent flow equation:

$$Q = C_d A_o \left[\frac{2}{\rho} (P_{Up} - P_{Down})\right]^{1/2} \qquad (3.1)$$

Because the spool valve chambers are small, compressibility flows are ignored and the relationship is thereby assumed to be valid for the dynamic state. Compressibility flows are included when considering the combination of valve, actuator and lines (ref. Appendix A).

The discharge coefficient, mass density and supply pressure are considered constant. With the notation of Fig. 1-2 for non cavitating condition with zero leakage and lpp at the spool, application of (3.1) gives:

$$Q = C_d A_1 \left[\frac{2}{\rho} (P_s - P_1)\right]^{1/2} = C_d A_4 \left[\frac{2}{\rho} (P_2 - P_r)\right]^{1/2} \qquad (3.2)$$

Similarly, for $e < o$;

$$Q = -C_d A_2 \left[\frac{2}{\rho} (P_s - P_2)\right]^{1/2} = -C_d A_3 \left[\frac{2}{\rho} (P_1 - P_r)\right]^{1/2} \qquad (3.3)$$

For orifices that are matched and symmetrical we see from equations (3.2) and (3.3) that:

$$P_s = P_1 + P_2 \qquad (3.4)$$

if the return pressure P_r is zero.

By defining the load pressure, or pressure drop across the load as $P_L = P_1 - P_2$ and using equation 3.4,

$$P_1 = 1/2\,(P_s + P_L)\ ; \quad P_2 = 1/2\,(P_s - P_L) \tag{3.5}$$

Using rectangular ports, the flow area is

$$A = G_a\, e \tag{3.6}$$

The valve area gradient G_a is the total width of all the rectangular slots at a particular orifice (see Fig. 1-1). Using (3.5) and (3.6) equations (3.2) and (3.3) become:

$$Q = C_d\, G_a\, e\, \frac{1}{\sqrt{\rho}}\, (P_s - P_L)^{1/2} \quad \text{for } e > o \tag{3.7}$$

$$Q = -C_d\, G_a\, e\, \frac{1}{\sqrt{\rho}}\, (P_s + P_L)^{1/2} \quad \text{for } e < o \tag{3.8}$$

The load flow equations can therefore be given as a single relation:

$$Q_L = C_d\, G_a\, e\, \frac{1}{\sqrt{\rho}}\, \left(P_s - \frac{e}{|e|}\, P_L\right)^{1/2} \tag{3.9}$$

where $\frac{e}{|e|}$ is the sgn function.

It must be noted that when cavitation does exist, the inflow and outflow are not equal and the flow through each orifice must be treated separately. The non-linear pressure flow characteristics defined by (3.9) are presented in a normalized form in Appendix A, from which linear flow-spool displacement characteristics due to the rectangular ports can be obtained.

For a symmetrical and balance spool-sleeve combination having a spool overlap of e_o inches, equation (3.9) becomes:

$$Q_L = \frac{C_d G_a (e - e_o)}{\sqrt{\rho}} \left(P_s - \frac{e}{|e|} P_L\right)^{1/2} \quad \text{for } e > e_o$$

$$Q_L = \frac{C_d G_a (e - e_o)}{\sqrt{\rho}} \left(P_s - \frac{e}{|e|} P_L\right)^{1/2} \quad \text{for } e < -e_o$$

$$Q_L = 0 \qquad -e_o < e < e_o \quad (3.10)$$

The orifice discharge coefficient and fluid density are assumed constant, with values of .61 [11] and $.78 \times 10^{-4}$ lb-sec^2/in.^{4}

Rounding of edges strengthens the tendency of the flow to form a boundary layer, so that the transition from laminar to turbulent flow occurs at a higher Reynold's number.

Investigations [32] for annular ports showed that the laminar flow coefficient, which is a function of the edge geometry, decreased from a value of .1 to less than .03, which shifted the transition R_e from 40 to 400. This had the effect of tripling the velocity time constant, which had an initial value of four milliseconds. The effect on rectangular ports was not described.

3.2 Actuator Flow Equation

The load flow is consumed by flow to displace the actuator, flow stored due to compressibility, and leakage flow. The equation can be written (ref. Appendix A) as:

$$Q_L = A \dot{Y}_c + \frac{V_o}{2\beta_e} \dot{P}_L + L_t P_L \quad (3.11)$$

The assumptions made are: constant fluid mass density, supply pressure and effective bulk modulus of elasticity, laminar (annular) leakage flows at the piston and piston rod ends, and that the piston is centered along the cylinder.

To study the effect of a small hole drilled longitudinally through the piston, the equation can be expanded to:

$$Q_L = A\,\dot{Y}_c + \frac{V_o}{2\beta_e}\,\dot{P}_L + L_t P_L + Q_h \qquad (3.12)$$

Assuming turbulent flow, an expression for this flow can be written:

$$Q_h = C_d A_h \sqrt{\frac{2}{\rho}\,|P_1 - P_2|}\quad \text{sgn}\,(P_1 - P_2)$$

$$= \sqrt{\frac{2}{\rho}}\; C_d A_h \sqrt{|P_L|}\quad \text{sgn}\,P_L \qquad (3.13)$$

3.3: Mechanical Feedback Equation

The displacement of a critical closed centre spool from its neutral position can be expressed by the kinematic equation of the error bar for small angular movements. From Figure 3-1, defining the mechanical gain G_m as the ratio of level lengths $\frac{\ell_1 + \ell_2}{\ell_2}$, a small lever input displacement of X_c produces a spool travel of X_c/G_m, for zero motion of the cylinder. By considering the input end fixed at this displacement, the cylinder would have to travel distance Y_c before the spool would again be at neutral. For this cylinder travel, the spool displacement equals $\left[\frac{\ell_1}{\ell_1 + \ell_2}\right] Y_c$, or, $\left[1 - \frac{1}{G_m}\right] Y_c$.

The spool displacement from neutral, e, can therefore be related to the input displacement and the resulting output (cylinder) displacement, since error e = total spool travel - Y_c.

$$= \frac{X_c}{G_m} + \left(1 - \frac{1}{G_m}\right) Y_c - Y_c$$

so that,

$$e = \frac{1}{G_m}\,(X_c - Y_c) \qquad (3.14)$$

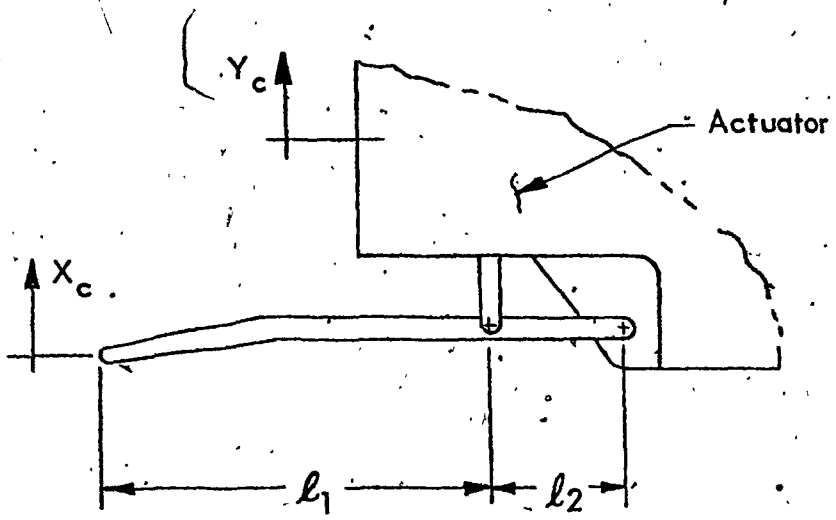

FIGURE 3-1 Mechanical Feedback Linkage

3.4 Equilibrium Equation

For a positive cylinder displacement Y_c, the total axial load is balanced by the pressures P_1 and P_2 prevailing in the two cylinder chambers (ref. Fig. 1-2). By applying Newton's second law to the forces on the cylinder, the force equation can be written:

$$P_L A = F + m \ddot{Y}_a - B \dot{Y}_c \qquad (3.15)$$

3.5 Cutting Force Equation

Substituting force components expressed by equation 2.7 into the expression for the resultant force acting along the cylinder axis, equation 2.6 yields:

$$F = b f_q (K_Q \cos (\gamma - C_s) - K_R \sin (\gamma + C_s))$$

Upon substitution of equation 2.5 this becomes:

$$F = F_1 + F_2 \dot{Y}_c \qquad (3.16)$$

where

$$F_1 = b\, f \cos C_s \left[K_Q \cos (\gamma - C_s) - K_R \sin (\gamma - C_s) \right]$$

and

$$F_2 = \frac{b}{n} \cos (\gamma - C_s) \left[K_Q \cos (\gamma - C_s) + K_R \sin (\gamma - C_s) \right]$$

For a constant cylinder velocity, F is the average static cutting force. By the addition of a fluctuating component having a magnitude ratio ϵ with the static force, and assuming a sinusoidal waveform, the dynamic cutting force F_{dyn} can be written as: [35] [36]

$$F_{dyn} = F + \epsilon F \sin \omega t \qquad (3.17)$$

where ω, the frequency of force variation, is dependent upon cutting conditions.

Upon substitution for F, equation (3.17) becomes: [35] [36]

$$F_{dyn} = (F_1 + F_2 \dot{Y}_c)(1 + \epsilon \sin \omega t) \qquad (3.18)$$

3.6 Linear Analysis Transfer Function

Substituting for P_L, $\dot{P}_L$ from equation (3.15) into (3.11) the expression for the load flow becomes:

$$Q_L = A \dot{Y}_c + \frac{L_t}{A}(m \ddot{Y}_c + B \dot{Y}_c + F) + \frac{V_o}{2 \beta_e A}(m \dddot{Y}_c + B \ddot{Y}_c + \dot{F})$$

Letting $S = d/dt$, the equation of the actuator and load is:

$$Y_c = \frac{\frac{2 \beta_e A}{m V_o} Q_L - \left(\frac{1}{m} S + \frac{2 \beta_e L_t}{m V_o} \right) F}{S \left\{ S^2 + \left(\frac{2 \beta_e L_t}{V_o} + \frac{B}{m} \right) S + \frac{2 \beta_e L_t B}{m V_o} + \frac{2 \beta_e A^2}{m V} \right\}}$$

For constant P_L, C_d, G_a, P_s and e, equation (3.9) can be written as:

$$Q_L = K_q e$$

With this substitution, the equation of the actuator, load and valve is:

$$Y_c = \frac{g_1 e - g_2 (1 - TS) F}{S \left\{ \frac{S^2}{\omega_h^2} + \frac{2 \delta_h}{\omega_h} S + 1 \right\}}$$

where;

$$\omega_h = \left[\frac{2 \beta_e A^2}{m V_o} \left(1 + \frac{L_t B}{A^2} \right) \right]^{1/2}$$

$$T = \frac{V_o}{2 \beta_e L_t}, \quad g_1 = \left(\frac{2 \beta_e A}{m V_o \omega_h^2} \right) K_q, \quad g_2 = \frac{1}{m T \omega_h^2}$$

and

$$\delta_h = \frac{1}{2 T \omega_h} + \frac{B}{2 m \omega_h}$$

If $\frac{L_t}{A^2}$, the inverse of the damping coefficient due to the actuator leakage is $<< B$,

then

$$\omega_h = \left[\frac{2 \beta_e A^2}{m V_o} \right]^{1/2}, \quad T \text{ is unchanged,}$$

$$g_1 = \frac{K_q}{A}, \quad g_2 = \frac{L_t}{A^2}, \quad \delta_h = \frac{L_t}{A} \left[\frac{m \beta_e}{2 V_o} \right]^{1/2} + \frac{B}{2 A} \left[\frac{V_o}{2 m \beta_e} \right]^{1/2}$$

The resulting transfer function is:

$$Y_c = \frac{\frac{K_q}{A} e - \frac{L_t}{A^2} (1 - TS) F}{S\left\{\frac{S^2}{\omega_h^2} + \frac{2\delta_h}{\omega_h} S + 1\right\}} \qquad (3.19)$$

From this dynamic response equation, we can identify the first term of the numerator at the no load velocity, and the second term as the drop in velocity due to the applied loading. Servovalves have fast responses so that the actuator-load natural frequency ω_h is usually the lowest break-frequency in the loop and therefore dominates dynamic performance, i.e. it establishes the overall speed of response of the valve-actuator combination. By analogy to a mechanical system of a mass suspended between two springs (each having a spring rate k), whose natural frequency is $\sqrt{\frac{2k}{m}}$, we can define the total hydraulic spring rate, $K_h = \frac{2\beta_e A^2}{V_o}$. The hydraulic natural frequency can thus be described as due to the interaction of the two trapped "springs" within the cylinder and lines, with the mass of the system.

CHAPTER 4

SYSTEM SIMULATION

4.1 Introduction

The magnitude and time scaled equations of the mathematical model, and the analog circuit are given in Appendix C. The general template profiles simulated are shown in Figure 4-1, and consist of straight line elements, or slopes. As defined, slopes Θ are measured from a datum line parallel to the workpiece rotational axis, in a counter-clockwise direction. A template slope greater than 180° therefore generates a positive actuator linkage input, with a resulting actuator extension in which the tool travels toward the workpiece axis. The simulation assumes that for any given cutting operation, the workpiece has previously been machined to the general desired shape, so that a constant width of cut, b, exists.

Values for the cutting force component F_1 and the force constant F_2 are pre-selected to define a particular cutting operation, since they are a function of the chip ratio r_t, tool geometry i, C_s, α_n, the width of cut b, the cylinder-to-workpiece, angle γ, the carriage feed rate f in the case of F_1, and the workpiece rotational speed n, in the case of F_2. Selection of F_1, F_2 values for a given set of conditions is illustrated by the following example of a typical rough machining operation. Assuming a four inch diameter workpiece, and a desired cutting velocity of 480 ft/min establishes the required workpiece rotational speed (n) of 7.64 rev./sec. Selecting a width of cut (b) of .09 inch, a carriage feed rate (f) of .009 inch/rev., $\gamma = 45°$, $i = 10°$, $\alpha_n = 17.5°$, $C_s = 0$, $r_t = .5$, a value of 5.6 for F_1, 47. for F_2 is obtained from Figures A2-3(b) and A2-4(b) respectively of Appendix B. Selecting a template slope of $\Theta = 223°$, Figure 1-5 can be used (since fn is now defined), to obtain the required linkage input velocity $\dot{X}_c$ of 1.5 in/sec. A negative input velocity of the same magnitude is seen to represent a template slope of 47°.

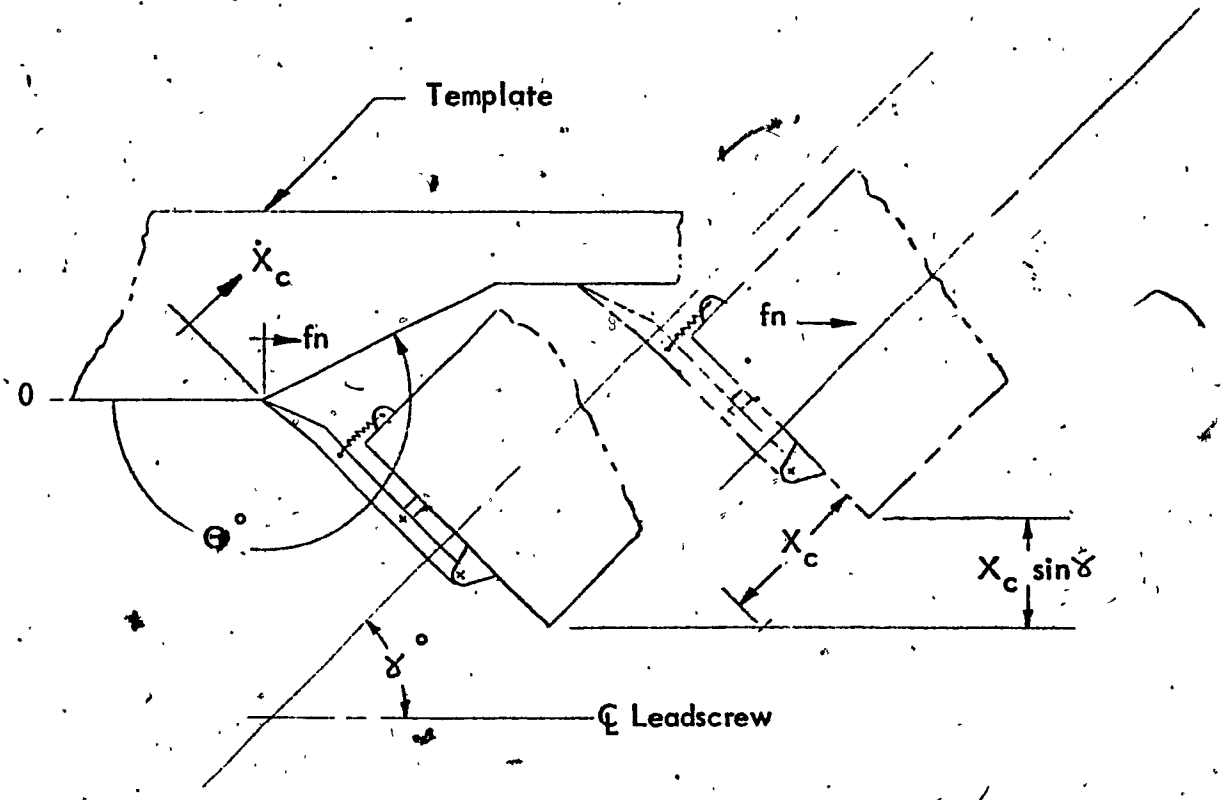

Actuator Extension

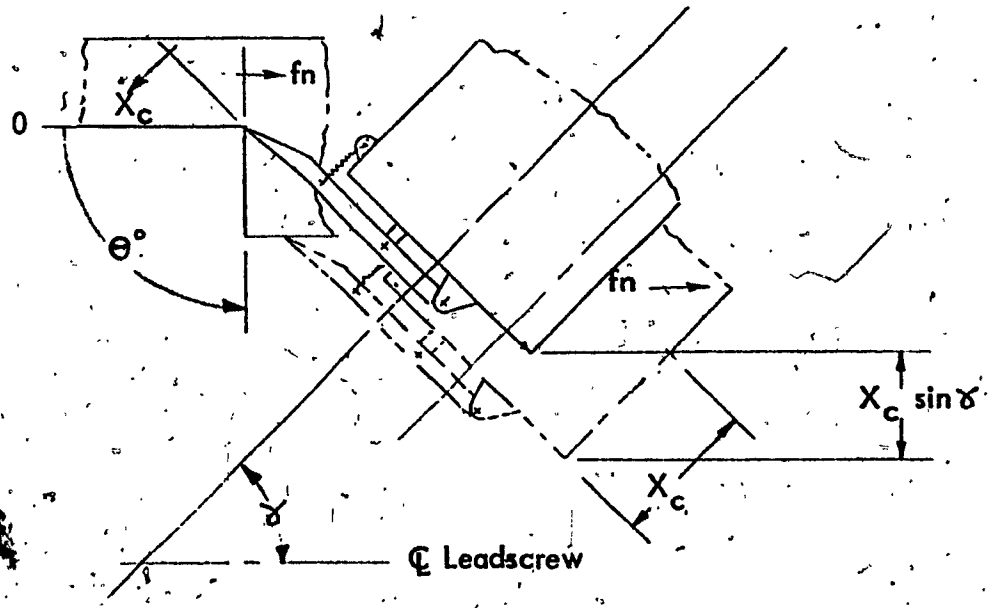

Actuator Retraction

FIGURE 4-1 Simulated Template Profiles

Five loading conditions were investigated ranging from a heavy roughing (b = .15) to a finish operation (b = .009), based on the parameters listed in Table 4.1.

Constants of the system are:

$V_o = 7$ in.^{3} $\quad C_d = .61$ $\quad B = .20$ lb-sec/in.

$A = 1$ in.^{2} $\quad \rho = .78 \times 10^{-4}$ lb - sec^2/in.^{4}

The following parameters were varied; values that are listed represent the "normal" system. Deviations from these values are noted on the Figures given in Section 4.2.

$\beta_e = 1 \times 10^5$ psi $\quad \epsilon = .05$

$L_t = 5 \times 10^{-3}$ in^3/sec/psi $\quad \omega = 0$ rad/sec.

$A_h = 3.25 \times 10^{-5}$ in.^{2} $\quad P_s = 1500$ psi

$m = .13$ lb.-sec^2/in. $\quad \gamma = 45°$

$G_m = 4$ $\quad \dot{X}_c = 1.5$ in/sec.

$G_a = .14$ in^2/in. $\quad X_c = 0$ to .15 in.

$e_o = 0$ in.

TABLE 4.1

Cutting Conditions For Simulated Template Profiles

Condition	b	f	n	γ	i	r_t	α_n	C_s	F_1	F_2	θ	$\dot{X}_c$
A	.15	.015	79	45°	5°	.5	1°	15°	132	101	205° 98°	1.5 -1.5
B	.09	.009	7.6	45°	10°	.5	17.5°	0°	5.0	47	223° 47°	1.5 -1.5
C	.15	.025	42	45°	5°	.5	5°	15°	169	141	206° 90°	1.5 -1.5
D	.049	.012	46	45	5	.5	10°	15°	17	28	220° 51°	6 -6
E	.009	.003	53	45	5	.5	1°	15°	1.6	9	204° 110°	.17 - .17

4.2 Results

In addition to the simulation of the five load conditions described in Table 4.1 which range from the heavy rough machining operation, condition A, to a finish machining operation, condition E, the results include the response of the system to a .06 inch step input under no load, a .03 inch step input under F_1 and F_2 values of condition A, and a sample of the performance under zero load.

For the zero load condition, the absence of a set of values of F_1 and F_2 does not permit a template slope to be quantatively identified.

In keeping with the template profiles illustrated in Figure 4-1, the simulation of an actuator extension or retraction stroke terminates with a constant template slope of 180°. During this latter part of the travel, the F_1 and F_2 values listed in Table 4.1 continue to be applied to the actuator but the spool linkage input velocity at the template in a direction parallel to the actuator axis, $\dot{X}_c$ is zero (ref. Figure 1-5).

Load conditions A and E are based on identical values of tool geometry, chip ratio, cylinder workpiece angle and nearly identical template slopes. Differences in tool geometry i, α_n, C_s and machine settings f, n, between load conditions B and D result in the large (6 inch/sec) servo linkage input rate of condition D although the template profiles are similar. The carriage velocity of 1.05 inch/sec of condition C along with the values of b, γ, i, r_t, C_s, Θ make this condition similar to condition A, but the larger f and smaller n of condition C have resulted in larger values of F_1 and F_2, suppressing the benefits of a larger α_n.

The workpiece radial error E as defined in the nomenclature can be related to the spool valve displacement error (equation 3.14) by the expression $e\, G_m \sin \gamma$. The spool linkage input displacement X_c and actuator output displacement Y_c such as displayed in Figure 4-11 (b) and 4-11 (d) assist in understanding the physical significance of the associated spool displacement but are not a pictorial presentation of the actual template or workpiece profiles.

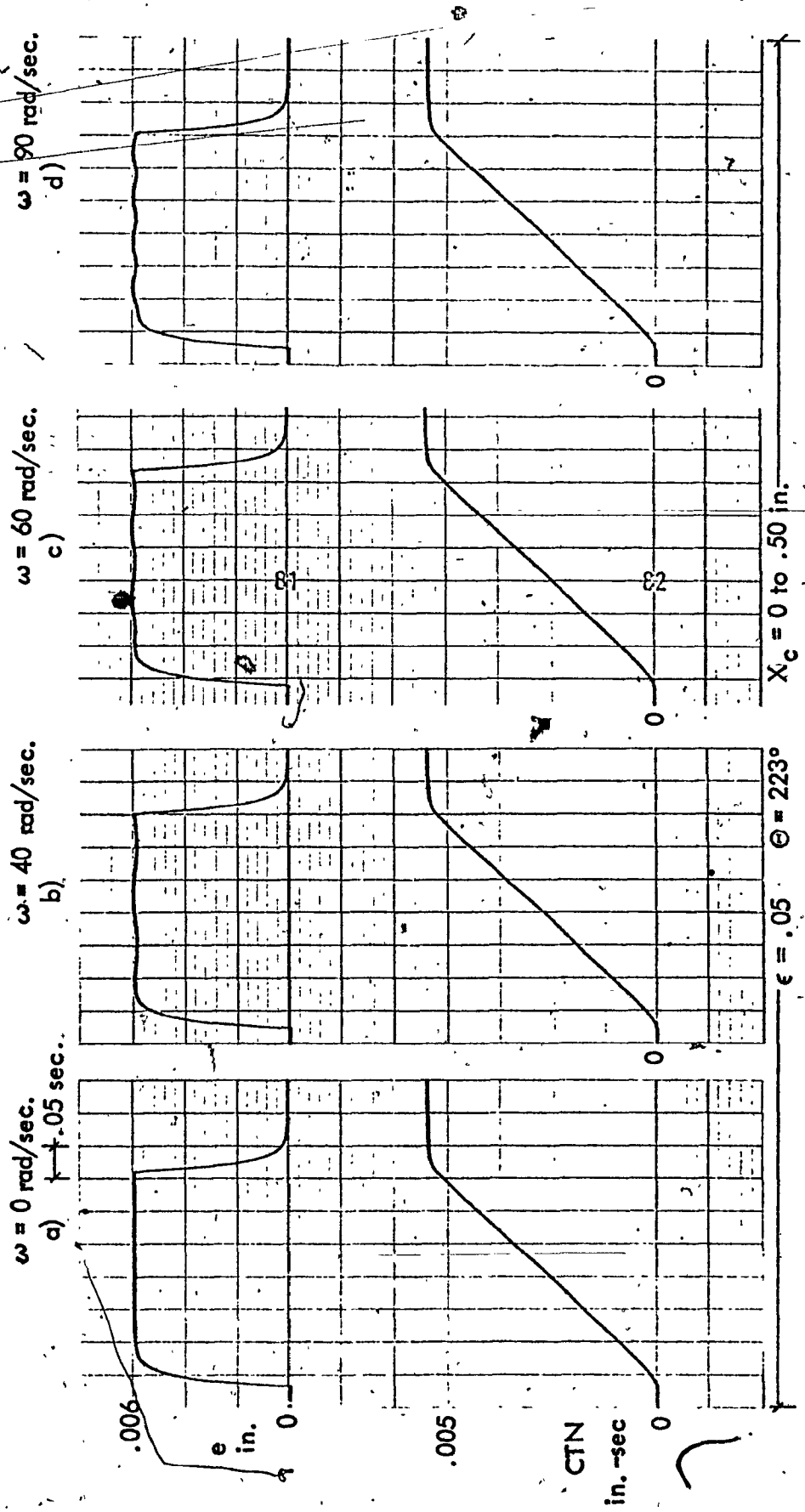

FIGURE 4-2. Effect of Increasing Frequency of the Force Variation on the Spool Displacement and Criterion: Actuator Extension Under Load Condition B

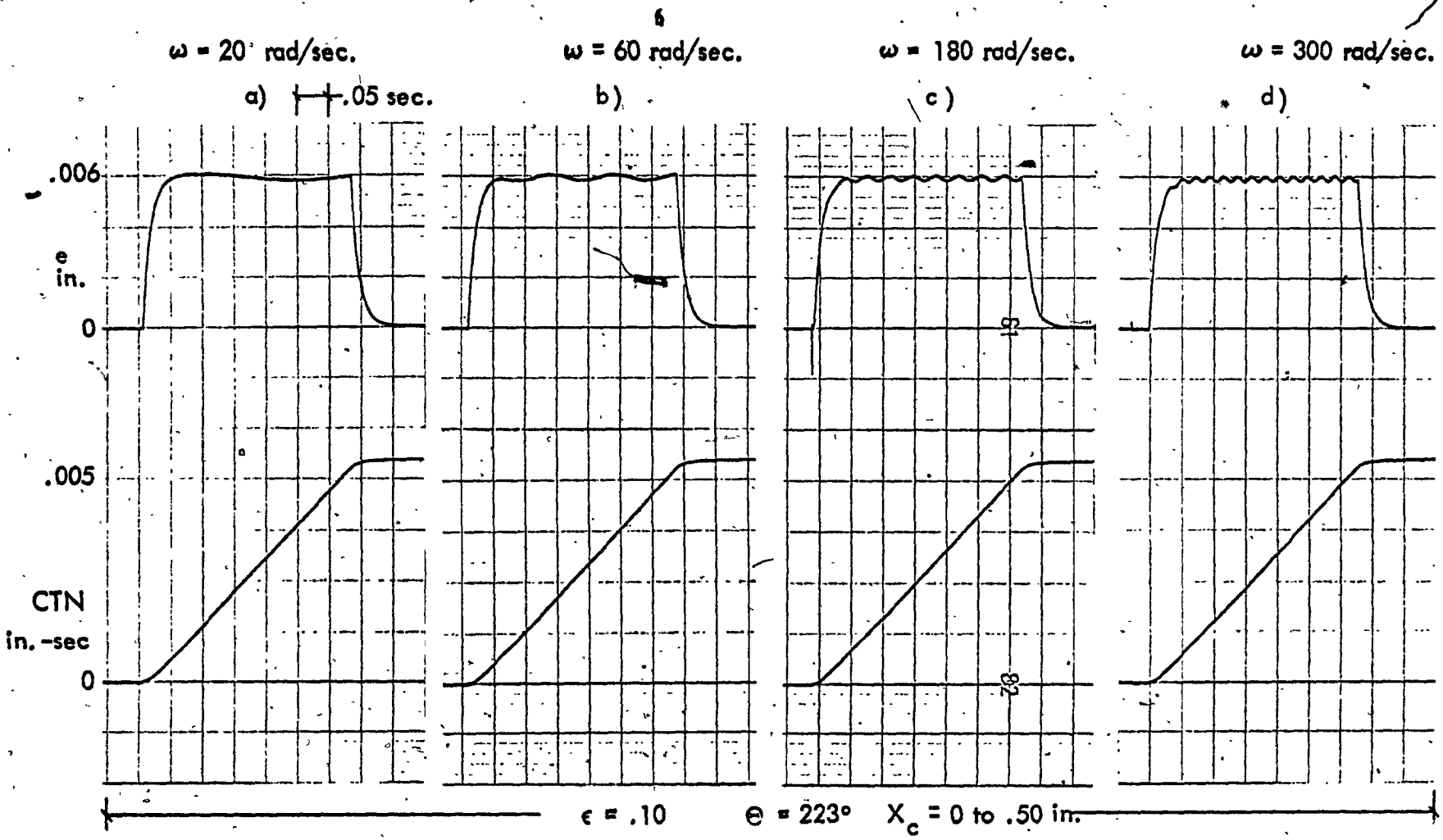

FIGURE 4-3. Effect of Increasing Frequency of the Force Variation on the Spool Displacement and Criterion: Actuator Extension Under Load Condition B With Fluctuating Force Magnitude Ratio of .10

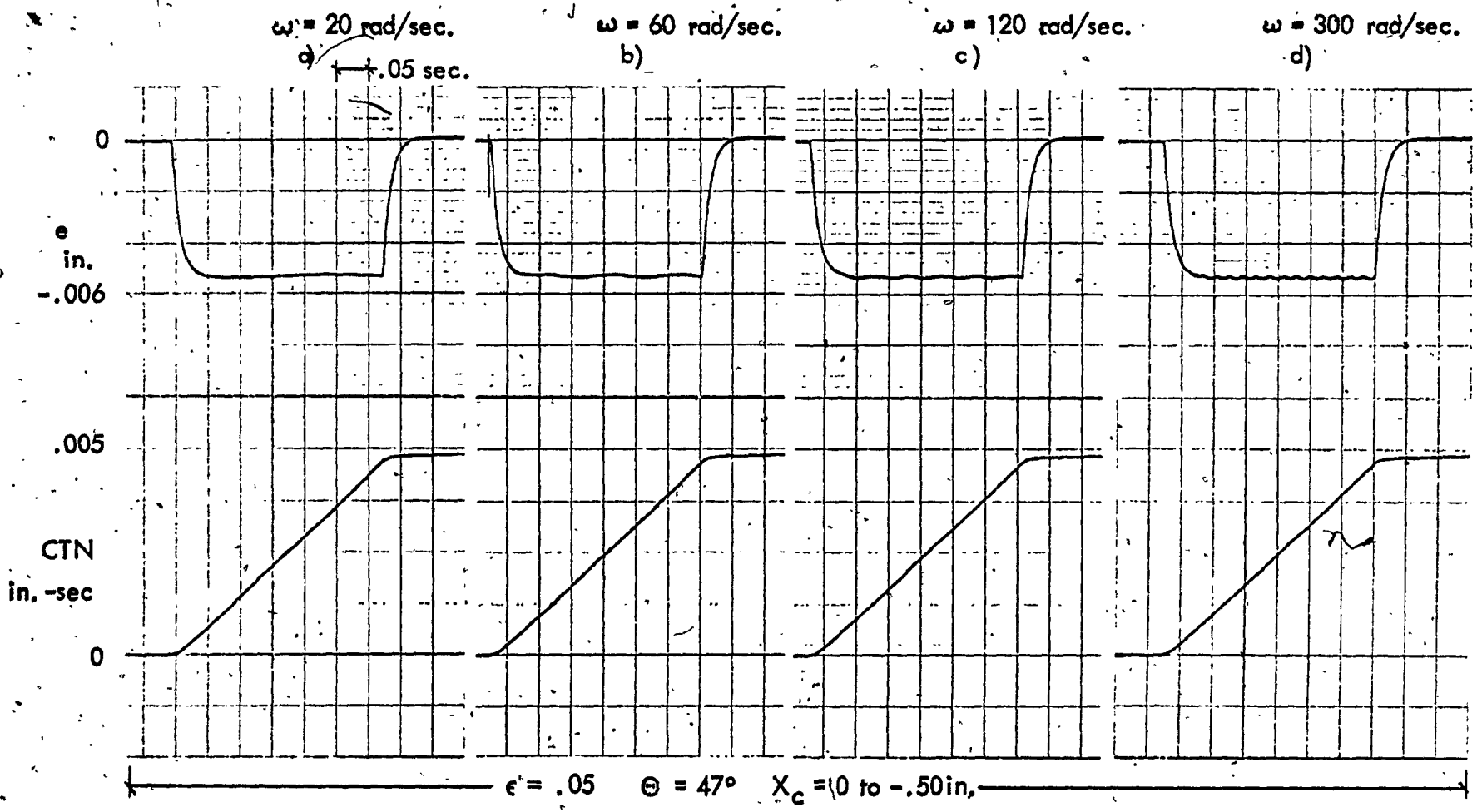

FIGURE 4-4. Effect of Increasing Frequency of the Force Variation on the Spool Displacement and Criterion: Actuator Retraction Under Load Condition B.

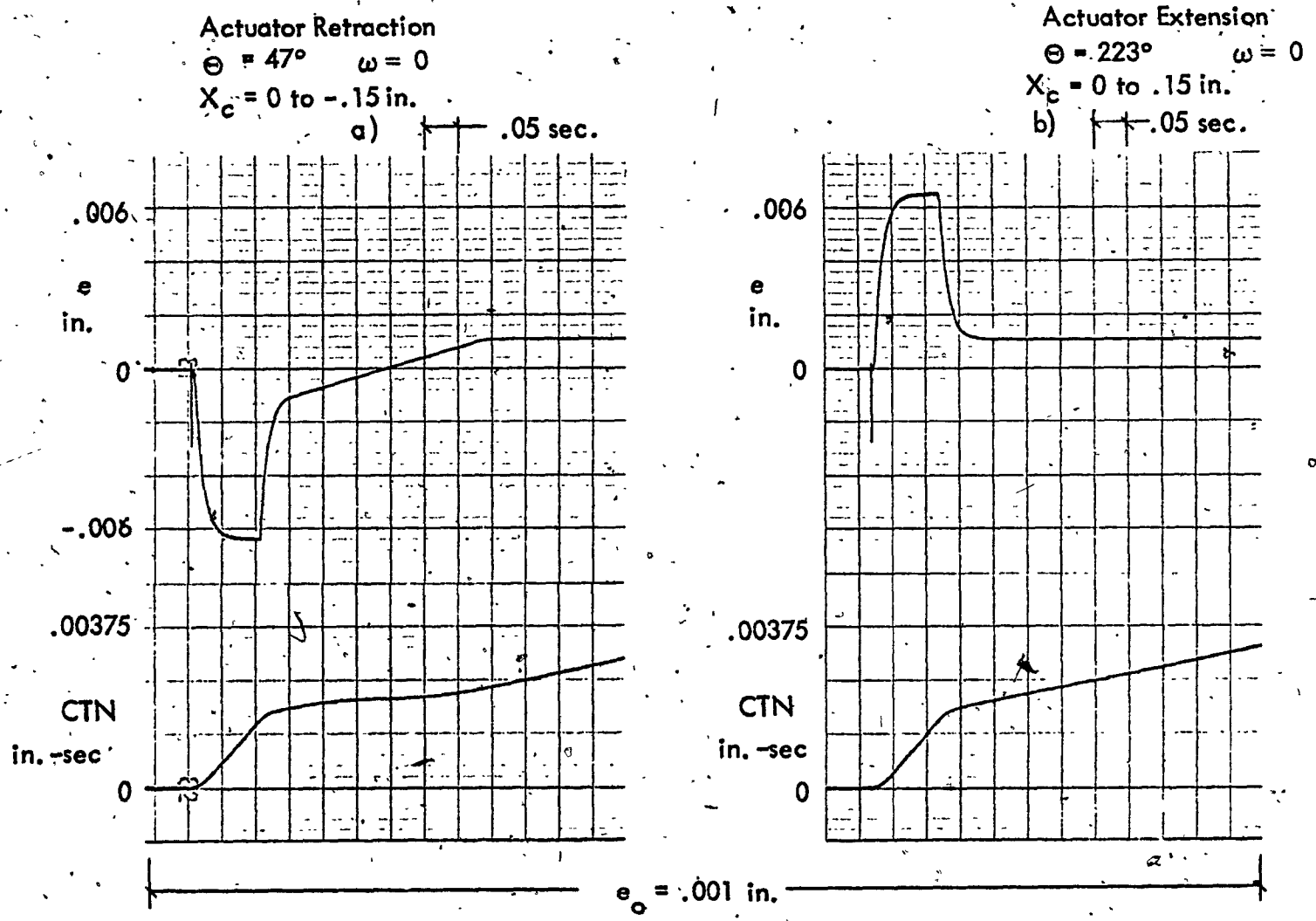

FIGURE 4-5. Effect of Spool Valve Overlap on the Spool Displacement and Criterion; Actuator Retraction vs. Extension Under Load Condition B

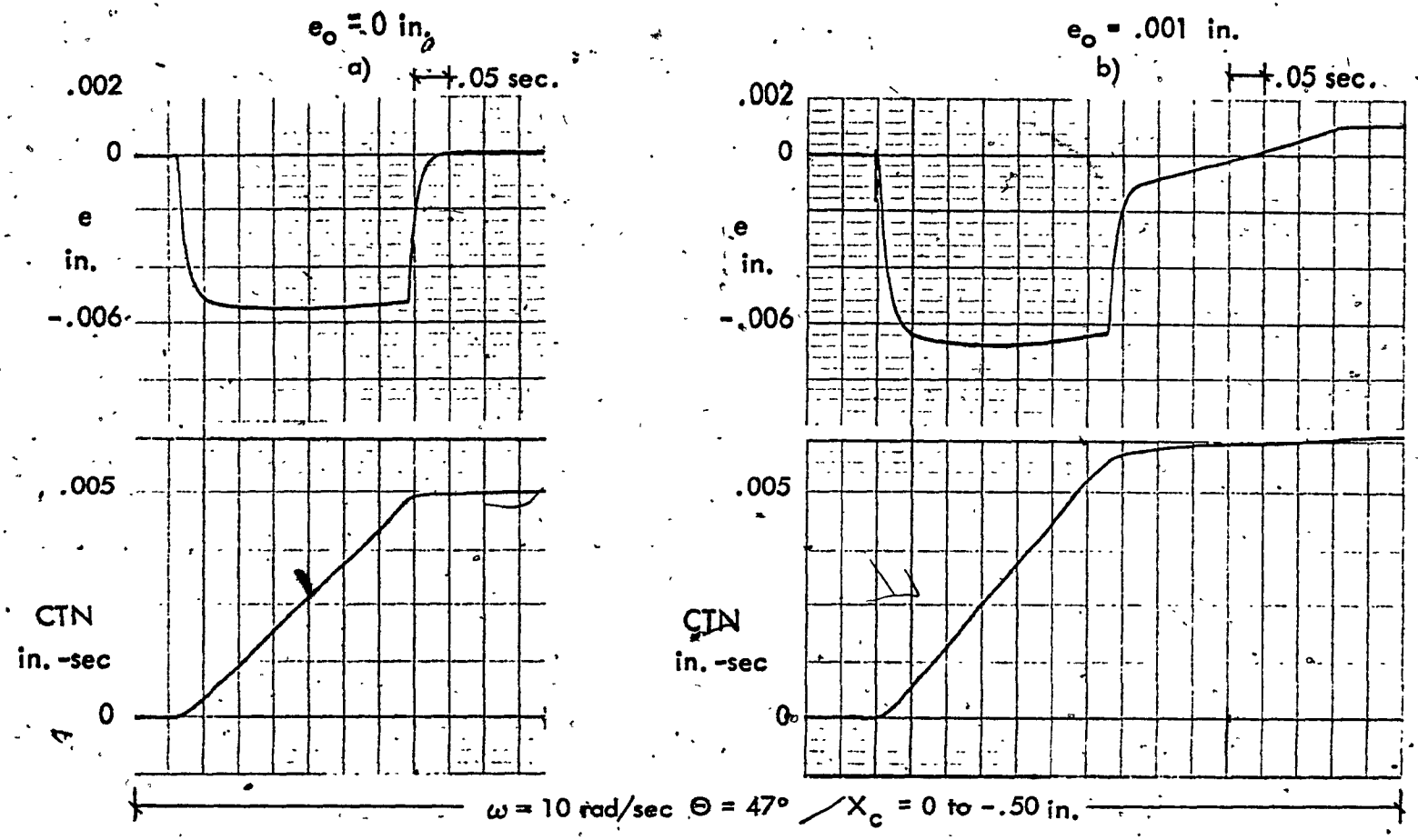

FIGURE 4-6. Effect of Spool Valve Overlap on the Spool Displacement and Criterion: Actuator Retraction Under Load Condition B.

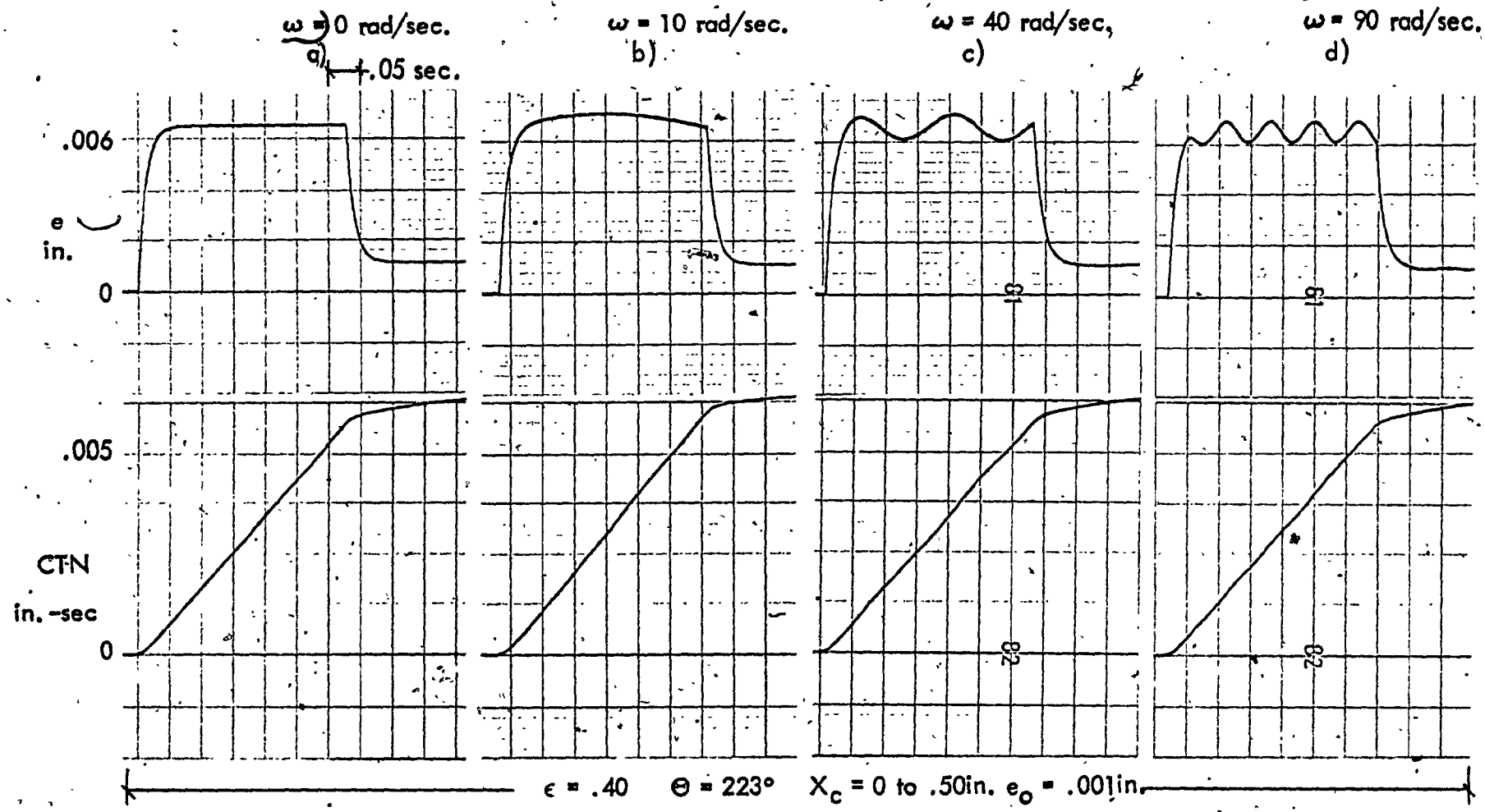

FIGURE 4-7. Effect of Increasing Frequency of the Force Variation on the Spool Displacement and Criterion: Actuator Extension With Spool Valve Overlap Under Load Condition B.

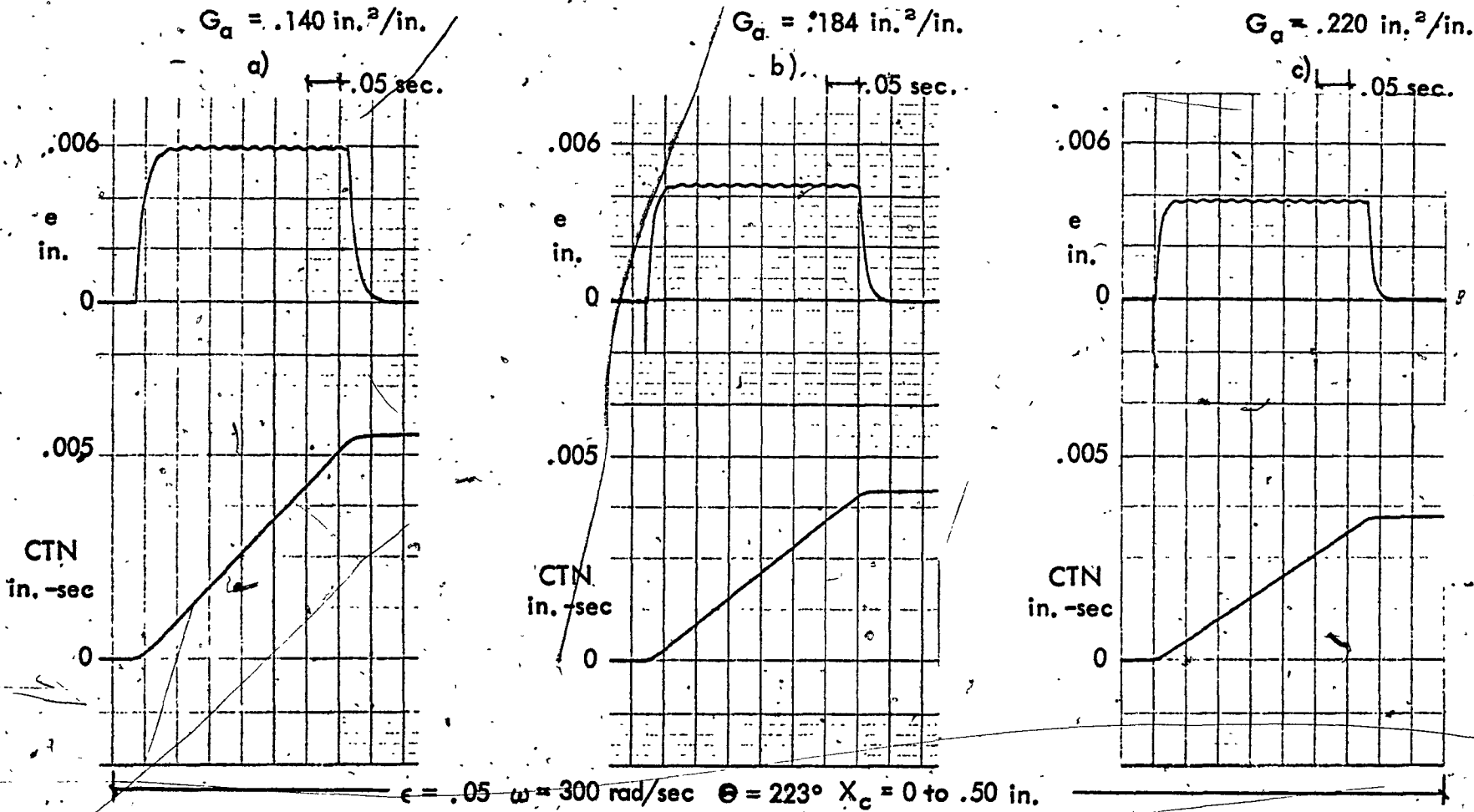

FIGURE 4-8. Effect of Increasing Spool Valve Area Gradient on the Spool Displacement and Criterion; Actuator Extension Under Load Condition B.

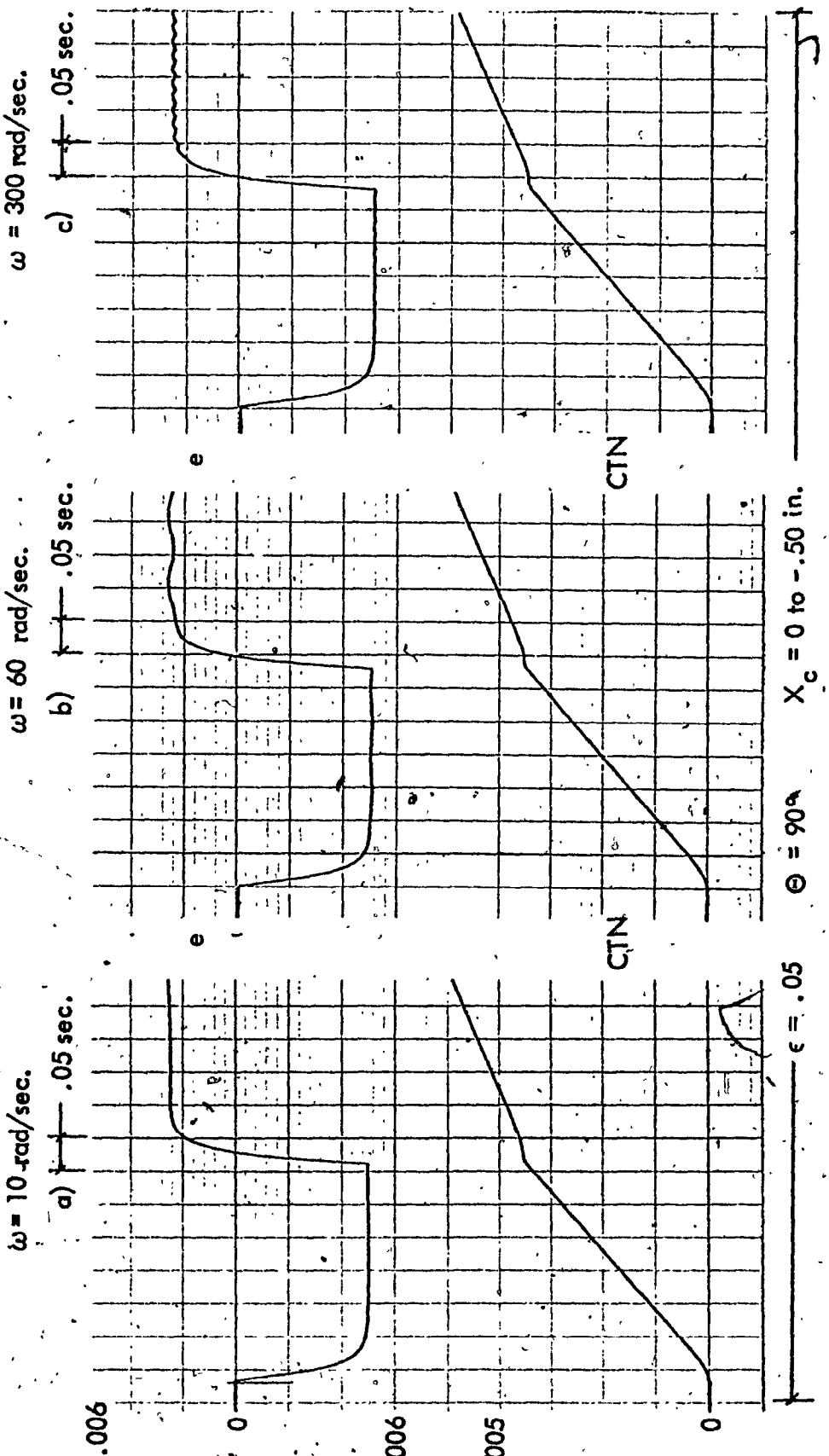

FIGURE 4-9. Effect of Increasing Frequency of the Force Variation on the Spool Displacement and Criterion; Actuator Retraction Under Load Condition C.

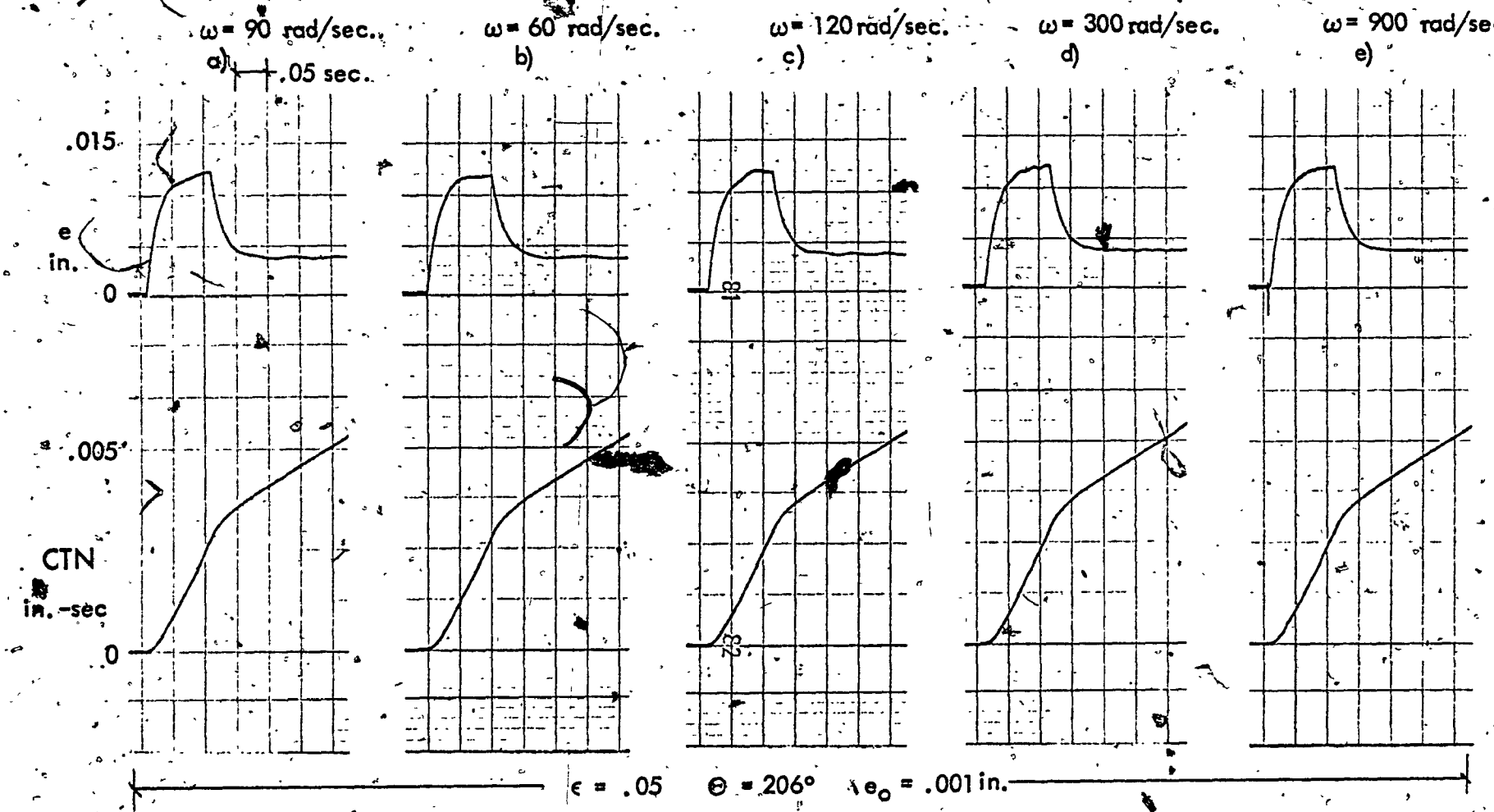

FIGURE 4-10. Effect of Increasing Frequency of the Force Variation on the Spool Displacement and Criterion; Actuator Extension With Spool Valve Overlap Under Load Condition C With Fluctuating Force Magnitude Ratio of .05

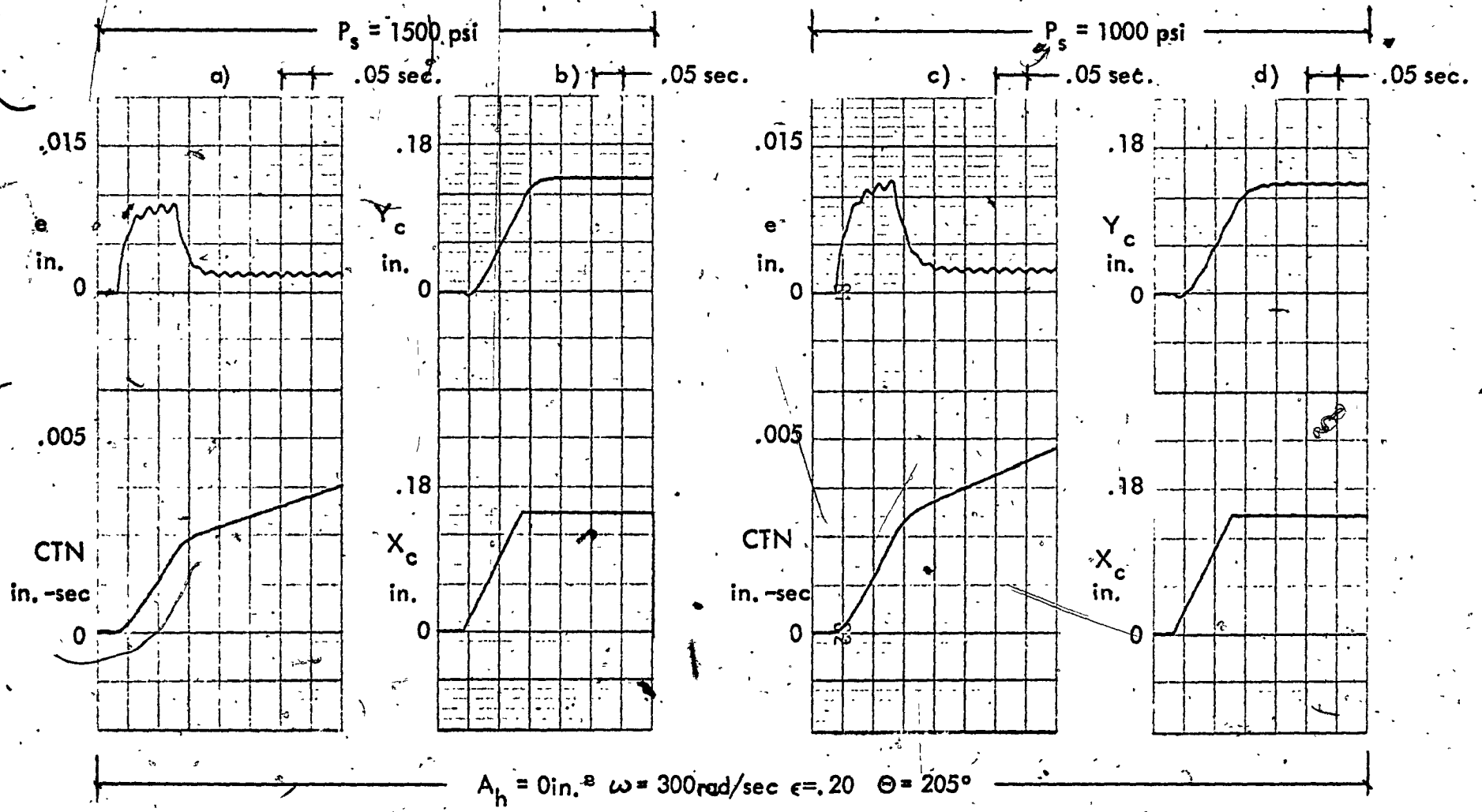

FIGURE 4-11. Effect of Decreasing Supply Pressure on the Spool Displacement, Criterion, and Actuator Displacement; Actuator Extension Under Load Condition A.

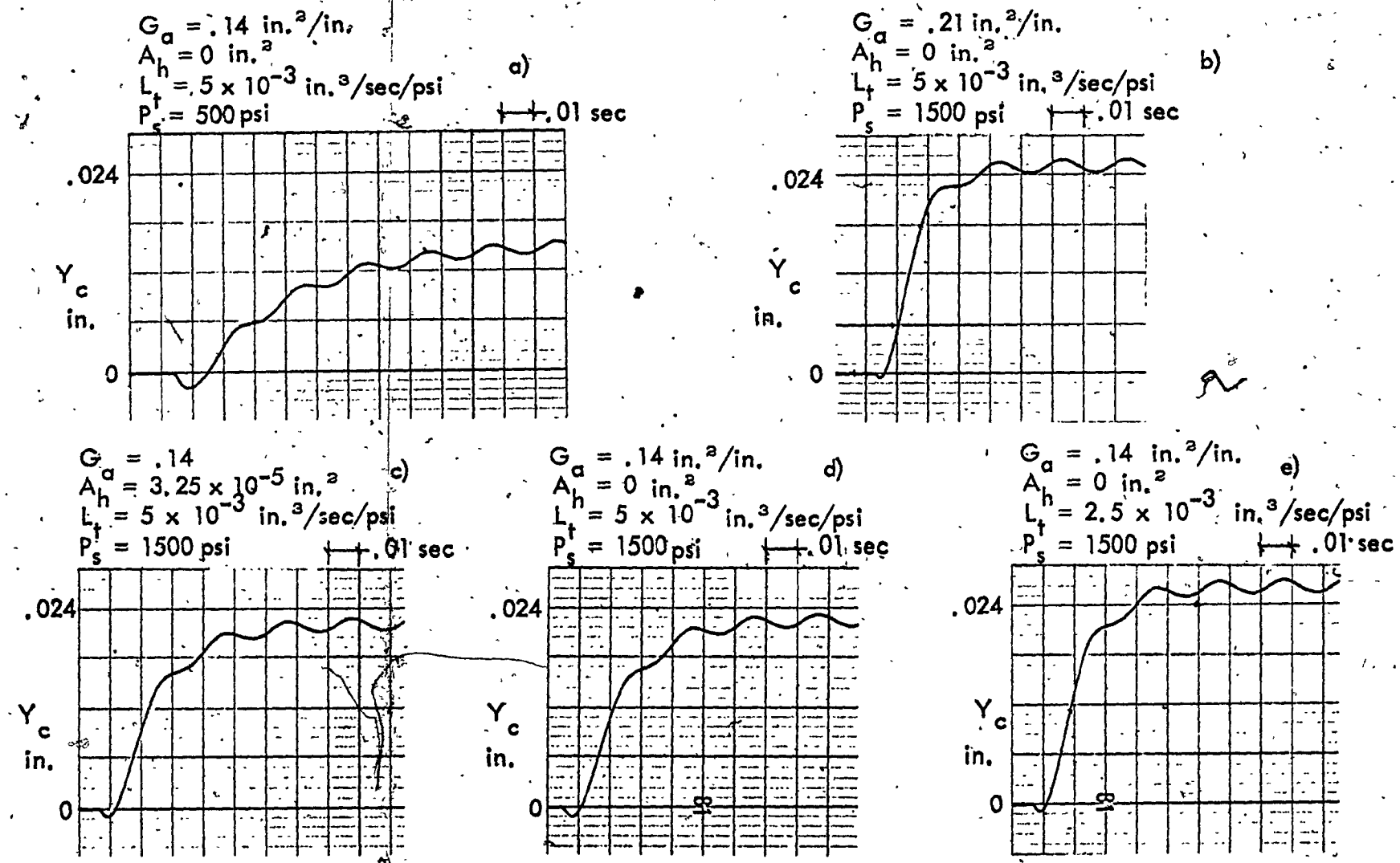

FIGURE 4-12. Effect of Leakage, Supply Pressure, and Axial Piston Hole Dia. on the Actuator Displacement; .03 Step Input Under Cutting Force Component and Force Constant of Load Condition A.

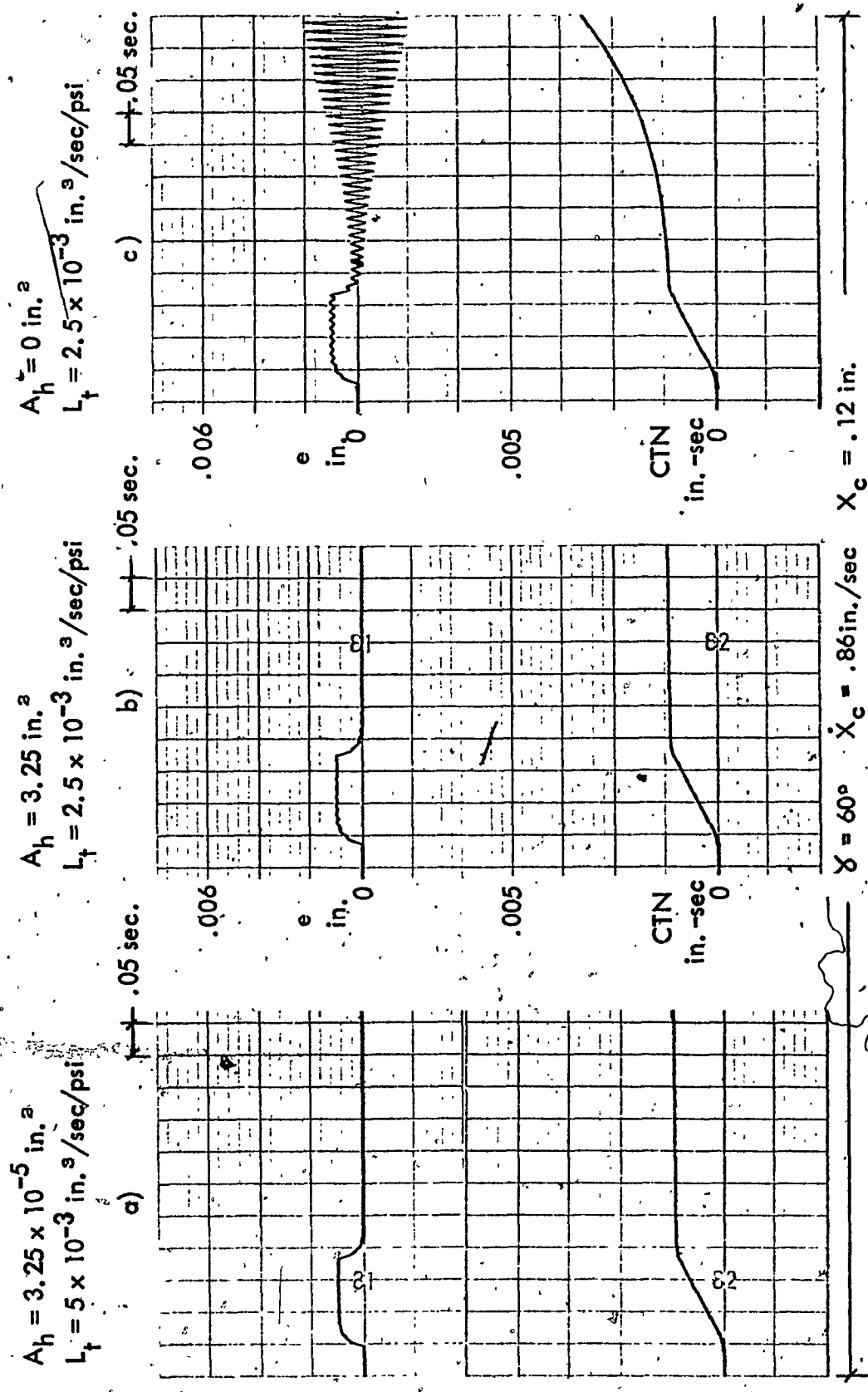

FIGURE 4-13. Effect of Decreasing Actuator Leakage and Axial Piston Hole Dia. on the Spool Displacement and Criterion; Actuator Extension Under No External Load Condition.

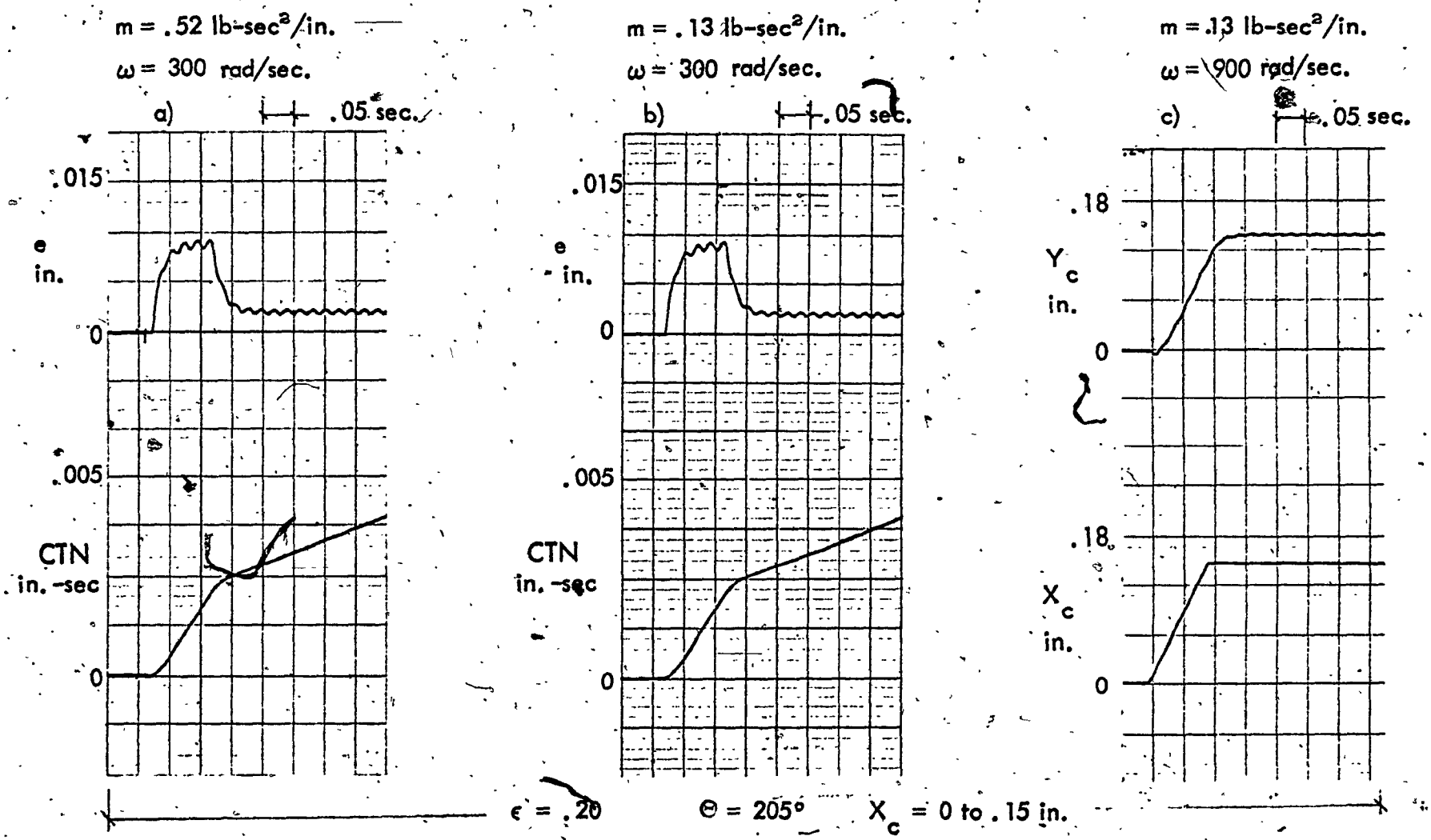

FIGURE 4-14. Effect of Increasing Actuator Mass on the Spool Displacement, Criterion, and Actuator Displacement; Actuator Extension Under Load Condition A

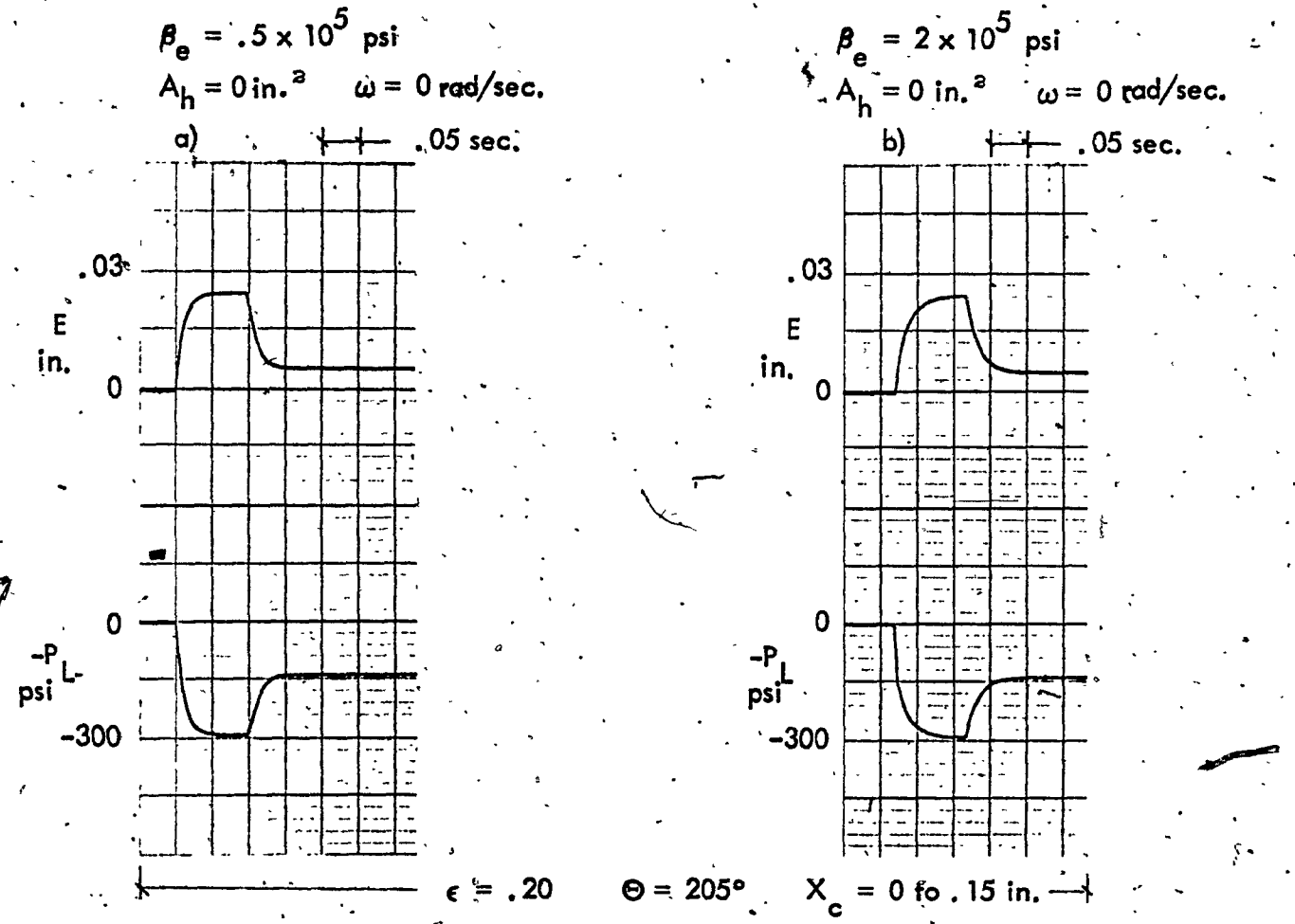

FIGURE 4-15. Effect of Increasing Effective Bulk Modulus on the Workpiece Radial Error and the Load Pressure; Actuator Extension Under Load Condition A

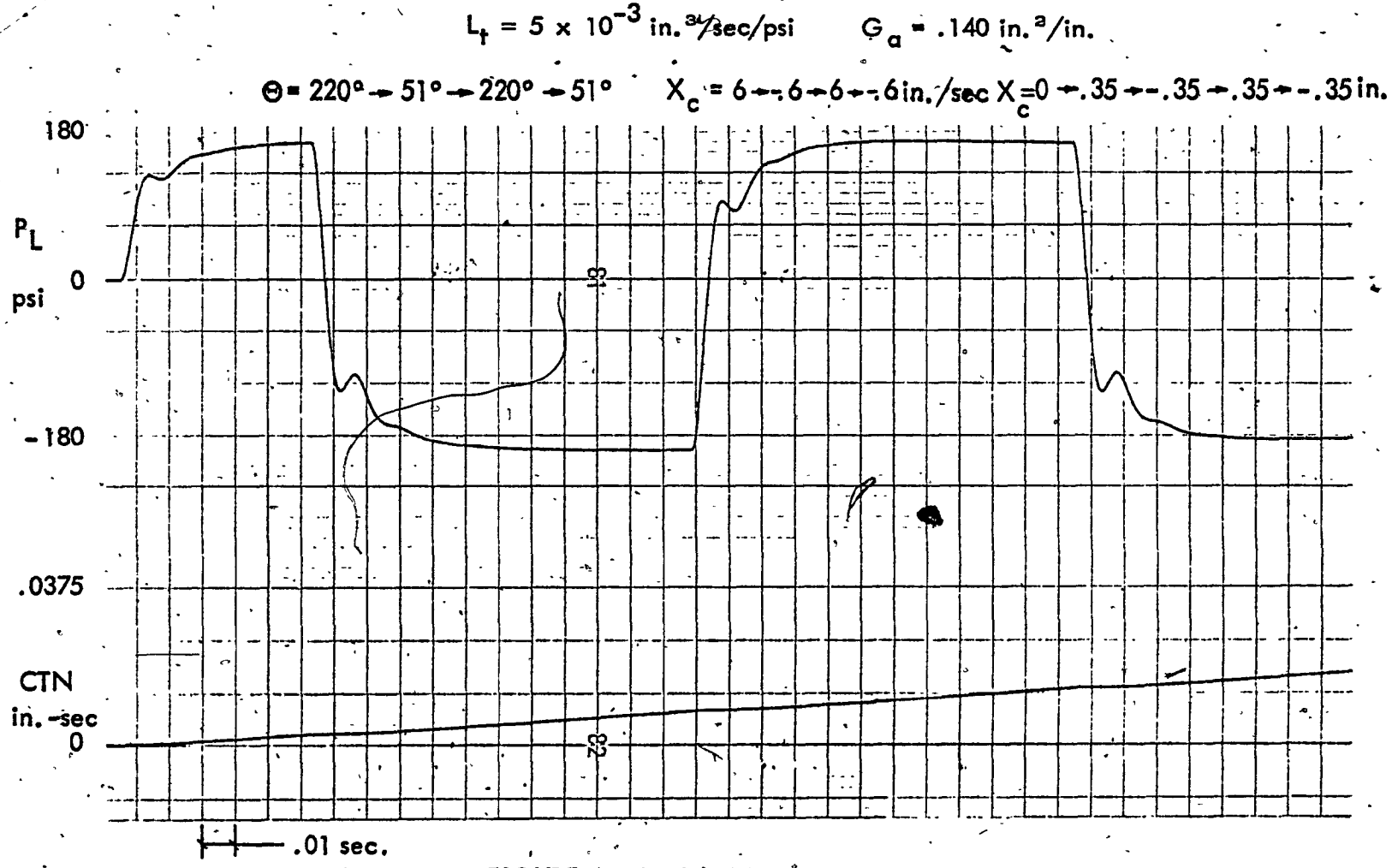

FIGURE 4-16. Load Pressure Response to Sawtooth Input Under Load Condition D

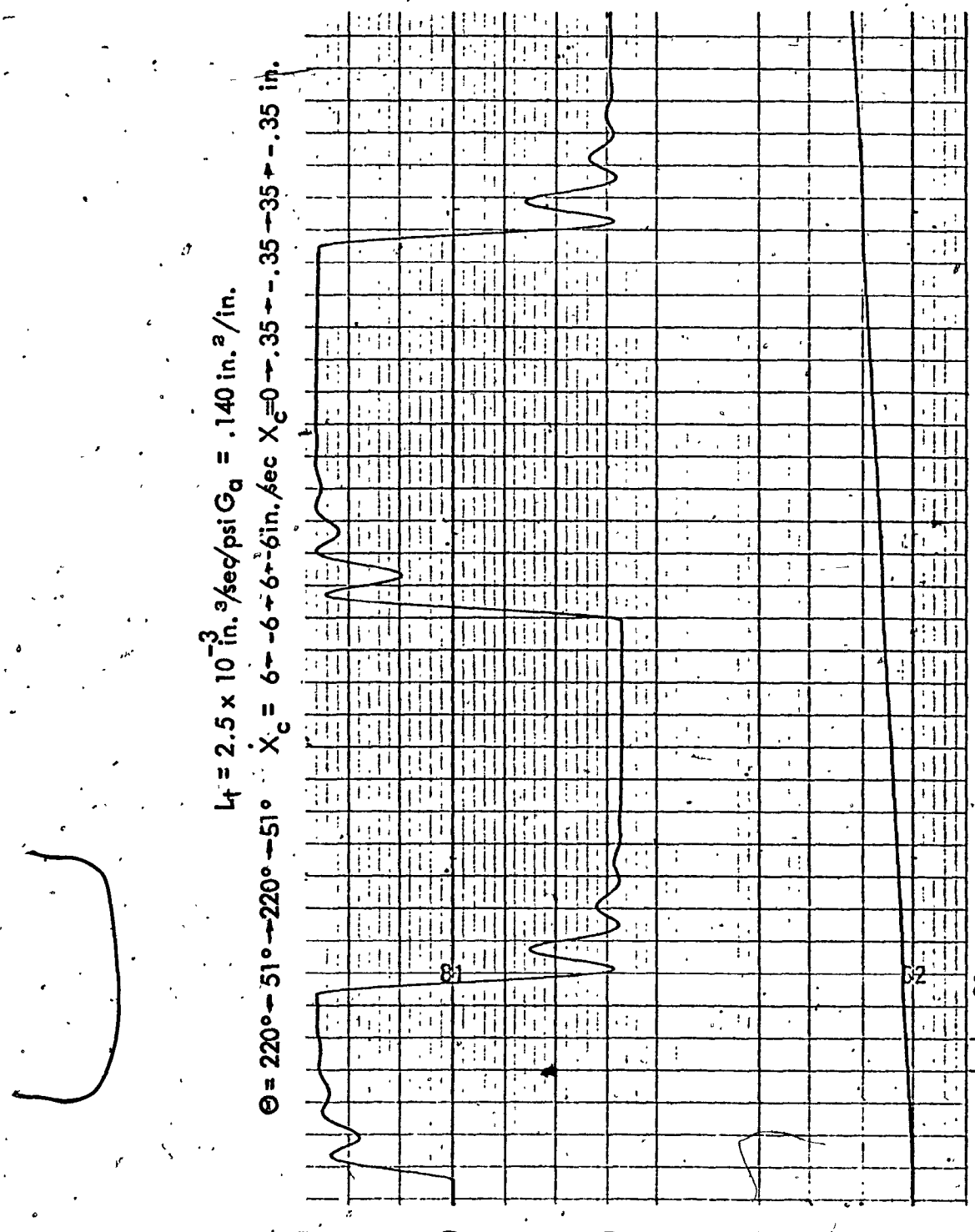

FIGURE 4-17. Load Pressure Response to Sawtooth Input Under Load Condition D; Actuator Total Leakage Coefficient One Half of Normal Value.

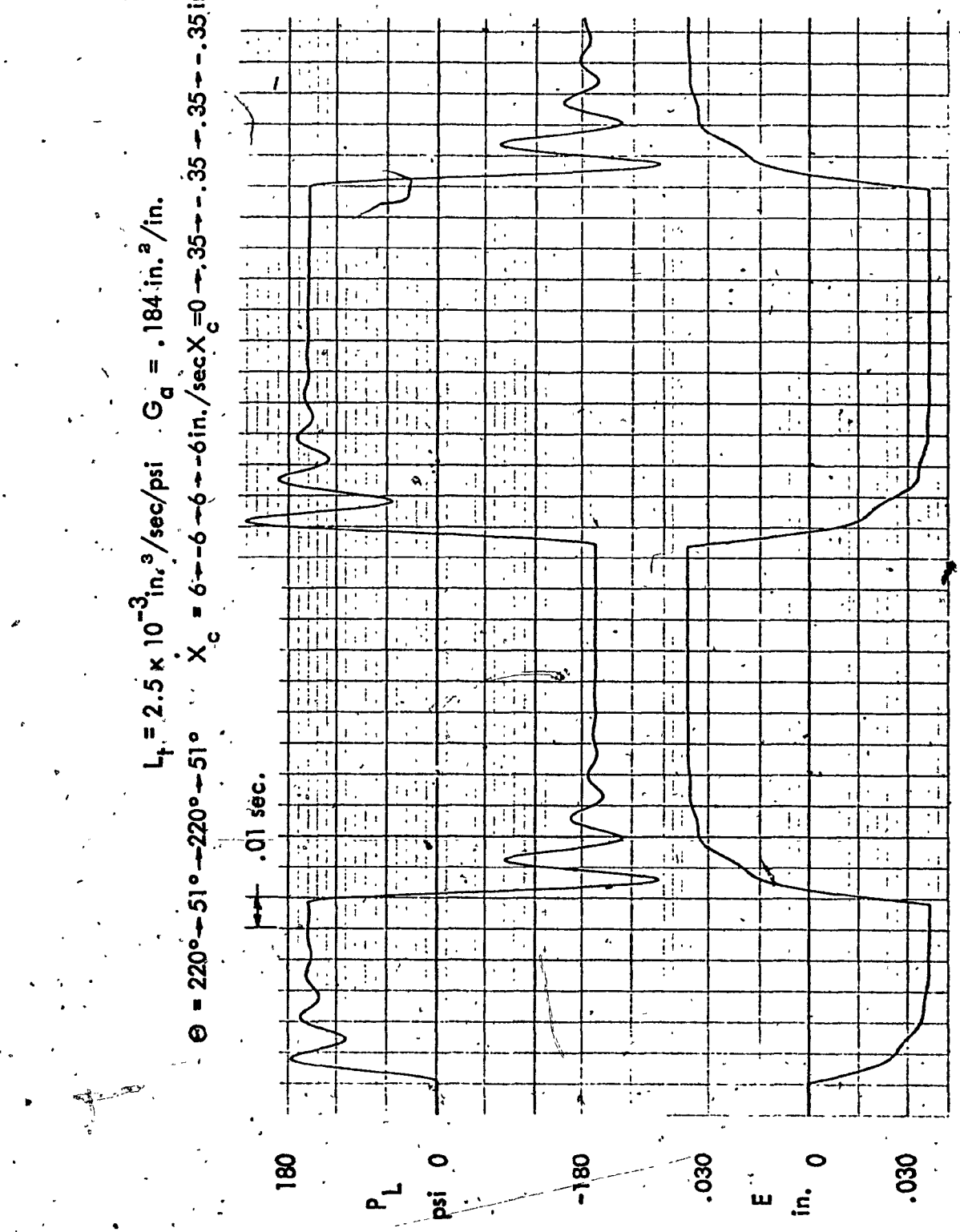

FIGURE 4-18 Load Pressure Response to Sawtooth Input Under Load Condition D; Actuator Total Leakage Coefficient One Half of Nomal Value, Spool Valve Area Gradient Increased

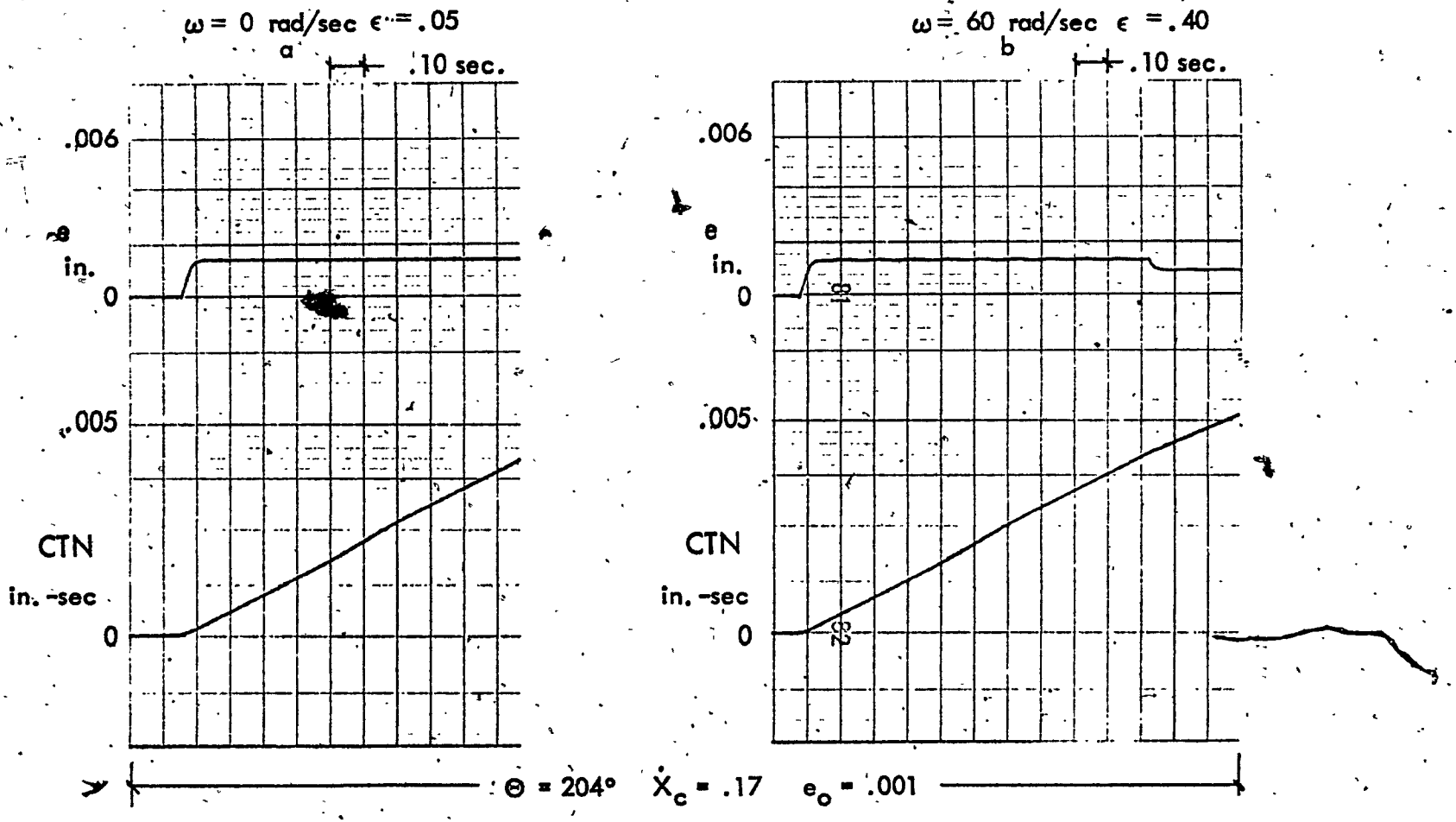

FIGURE 4-19. Effect of Increasing the Fluctuating Force Magnitude Ratio on the Spool Displacement and Criterion; Actuator Extension With Spool Valve Overlap Under Load Condition E.

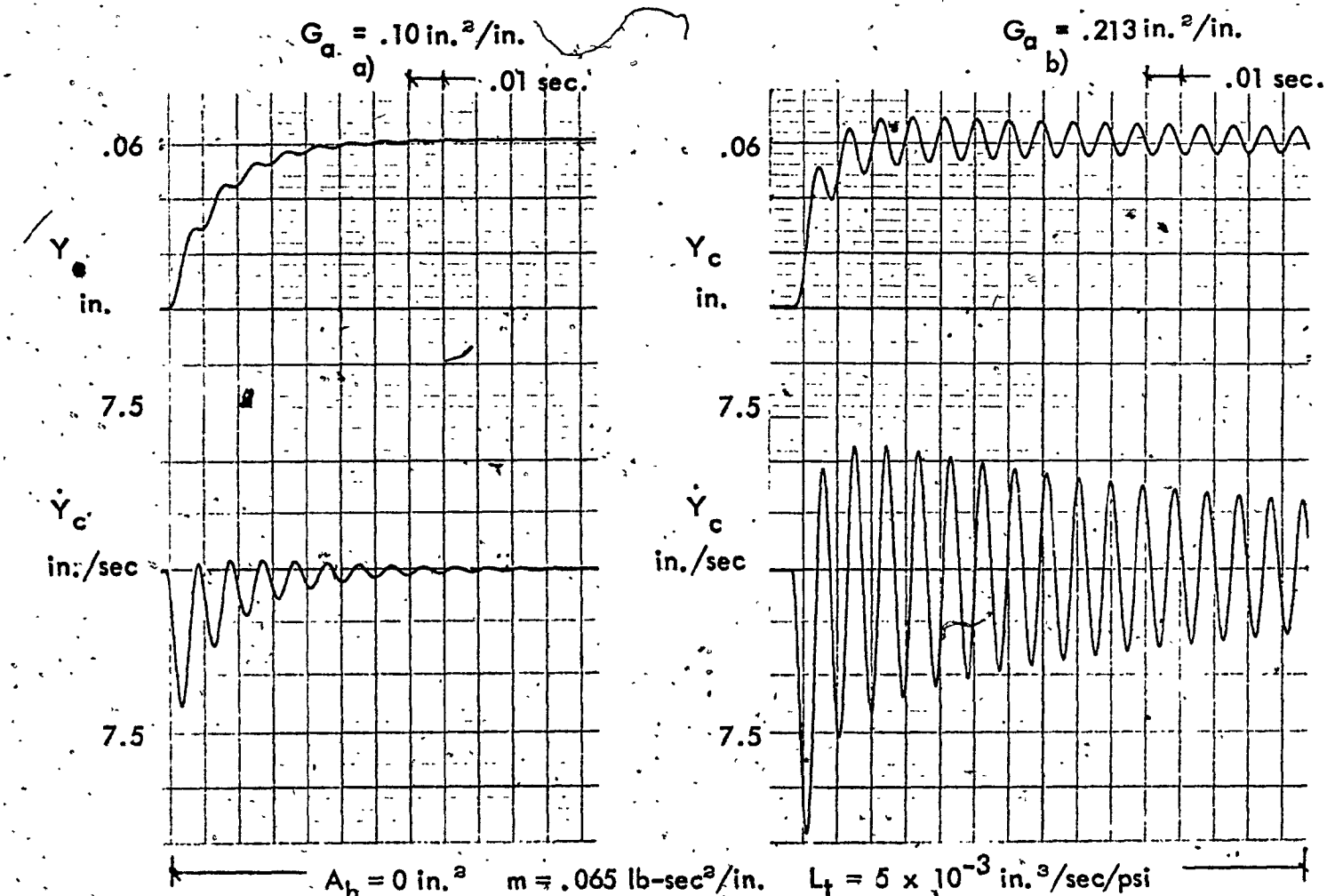

FIGURE 4-20. Effect of Increasing the Spool Valve Area Gradient on the Actuator Output Displacement and Velocity Response to a .06 Step Input Under No Load

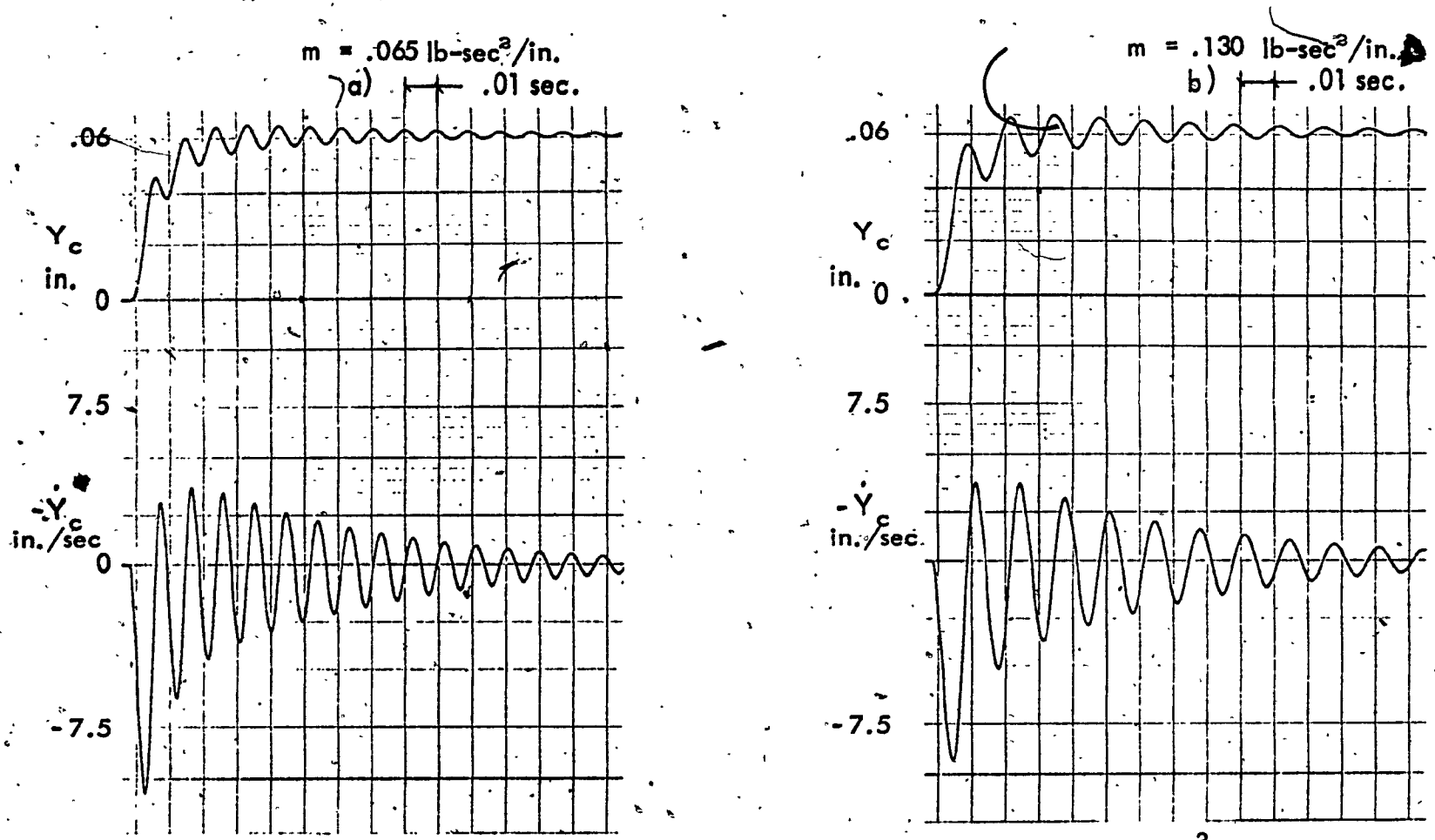

$A_h = 3.25 \times 10^{-5}$ in.² $G_a = .184$ in.²/in. $L_t = 5 \times 10^{-3}$ in.³/sec/psi

FIGURE 4-21. Effect of Increasing the Actuator Mass on the Actuator Output Displacement and Velocity Response to a .06 Step Input Under No Load

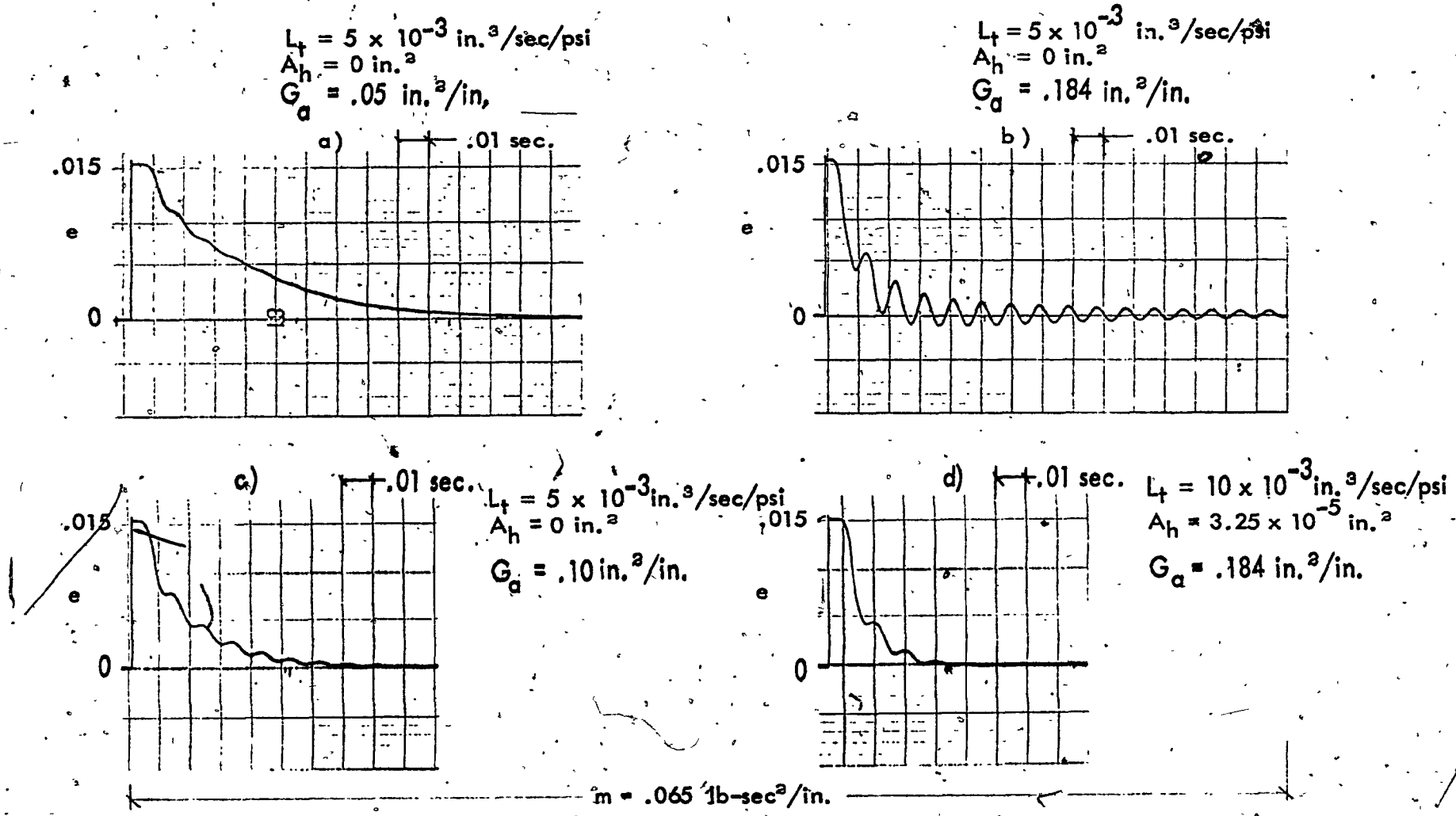

FIGURE 4-22. Effect of Increasing Actuator Leakage, Axial Piston Hole Dia. and Spool Valve Area Gradient on the Spool Displacement Response to a .06 Step Input Under No Load

CHAPTER 5

DISCUSSION AND CONCLUSIONS

A significant indication of the performance of the system is obtained by examining the spool valve displacement error, e. To compliment this output a criterion has been employed, which is the time integral of the absolute value of the workpiece radial error, itself directly related to e through the angle γ.

During extension or retraction strokes with the actuator under load but with zero frequency of force variation, the spool displacement reaches a maximum steady state value which is maintained until the template slope of 180° is reached, at which time the spool displacement begins to decrease. With the addition of a fluctuating force component having a sinusoidal waveform, the spool oscillates about the steady state value with the same frequency as that of the force variation. As the magnitude ratio of the fluctuating force is increased, so also is the magnitude of the fluctuation of the spool displacement. This is shown in Figures 4-2 and 4-3 for the system under study having the parameters listed in Section 4.1 (except that X_c has a value of .50 in.) for cutting condition B as defined in Table 4-1. With this combination, the maximum spool displacement of .006 inch is reached after .05 seconds. The same length of time is seen to exist during the decreasing spool displacement which reduces to a value of zero. It is seen that the criterion remains the same in slope(s) and magnitude as the frequency and the magnitude ratio of force variation increases. Figure 4-4 shows that the maximum spool displacement during a retraction stroke is less than during an extension stroke and this is reflected in the lower maximum value and the lower initial slope, .0139 in. of Figure 4-4 compared with .0166 in. of Figure 4-2 or 4-3.

The existence of a .001 inch spool overlap results in an increase in the maximum spool displacement error during both extension and retraction strokes, being greater in the retraction case, and produces a spool error having a magnitude equal to the overlap upon termination of the stroke, as seen in Figure 4-5(a), (b) and Figure 4-6. The additional spool displacement error existing during the

actuator retraction stroke as seen in Figure 4-6(a) and (b) is an increase of 20% in the spool error. The 20% increase in error is reflected in the slope of the first segment of the criterion, having a value of .017 in. shown in Figure 4-6(b), and value of .014 shown in Figure 4-6(a); and in comparing the magnitude of the criterion at the instant the spool returns to or passes through the zero position, these values being .006 in.-sec. in Figure 4-6(b) and .005 in.-sec. in Figure 4-6(a).

In comparing Figure 4-2(a) with Figure 4-7(a) it is found that the .001 inch spool overlap causes an increase of 7% to the maximum spool displacement error during the extension stroke. The effect of the eightfold increase in the magnitude ratio of the fluctuating force on the spool displacement fluctuations is also readily apparent when comparing Figure 4-7(d) with Figure 4-2(d), having a peak to peak amplitude of .0014 inch.

The beneficial effect of increasing the spool valve area gradient is shown in Figure 4-8. Comparing Figure 4-8(b) with 4-8(a), it is seen that a 31.4% increase in G_a reduces the average spool displacement during the extension stroke by 29%. Similarly, comparison of Figures 4-8(c) with (a) shows that a 57% increase in G_a reduces the spool displacement error by 40%. In both cases, the stability of the system which is continually under load, remains unchanged.

With the system operating under much larger values of the cutting force constant the spool does not return to zero and the frequency of force variation is seen to exist at the spool both during and at the end of the stroke. This is seen in Figure 4-9 for load condition C in which the F_1 value (ref. Table 4.1) is thirty-four times larger than for condition B. Failure to re-zero is due to the combination of loading, actuator leakage and of the small hole through the piston.

With the addition of spool overlap, the spool error remaining at the end of the stroke is further increased, as shown in Figure 4-10. Comparing Figure 4-10 with Figure 4-9, it is seen that the maximum spool displacement required during an extension stroke under load condition C has twice the magnitude reached during a retraction stroke when the cutting forces act in a direction aiding the actuator displacement. The effect on the criterion cannot be directly compared between

Figures 4-9 and 4-10 except for the slope of the first segment since the value of X_c for conditions of Figure 4-10 and 4-9 are .15 inch and .50 inch respectively.

The effect of a 33% reduction in the supply pressure on the spool displacement is shown in Figure 4-11 for the rough machining condition A. The maximum spool displacement has been increased from .009 inch for the system operating under a supply pressure of 1500 psi, to .0115 inch when operating under a supply pressure of 1000 psi. The mean spool displacement remaining after completion of the stroke is also greater for the case of the lower pressure operation; .0025 inch compared to .002 inch.

Insight into the inter-relationship of supply pressure, leakage, spool area gradient and the effect of an axial hole through the actuator piston can be obtained from examining Figure 4-12. Figure 4-12(c) shows the actuator displacement with parameters G_a, A_h, L_t and P_s at the normal values defined in Section 4.1. In comparing Figure (c) with (d) it is seen that eliminating the small axial hole has produced no noticeable change to the actuator displacement response. A reduction in supply pressure from 1500 psi to 500 psi causes an increase in rise time of approximately .05 seconds and an increase in the final average displacement error from a value of .008 inch to .015 inch as can be seen when comparing (a) with (d). Increasing G_a decreases the rise time and the resulting maximum actuator displacement error, as can be seen by comparing (b) with (d), as does the reduction of the total leakage coefficient as can be seen by comparing (d) with (e).

Operation of the system under no external load and with an X_c of .86 in/sec compared to 1.5 in/sec of load conditions A, B and C, results in a maximum spool displacement error of .0025 inch as can be seen in Figure 4-13. With the value of the leakage coefficient reduced to 2.5×10^{-3} in.^{3}/sec/psi (the same value as shown in Figure 4-12(e) for the step input under load) and the absence of the piston hole, the system becomes unstable during operation along the template slope of 180°, as can be seen in Figure 4-13(c).

Increasing the mass of the actuator system has produced no noticeable changes to the spool displacement response when operating under load condition A_n as demonstrated in the results of Figure 4-14. Increasing the effective bulk modulus of elasticity from a value of $.5 \times 10^5$ psi to 2×10^5 psi decreases the workpiece radial error during the early part of the extension stroke but does not reduce the maximum error reached at the end of the stroke, as can be seen in Figure 4-15. This increase in the speed of response is in agreement with the expression developed in Section 3.6 for the linear transfer function in which it was shown that the hydraulic natural frequency can be increased by employing a larger piston area, smaller oil volume and system mass, and increasing the effective bulk modulus. The simulation did not include changes in piston area or oil volumes but it is apparent that one disadvantage in selecting too large a piston area is that the resulting higher flow rates would increase the size of the supply pump, lines, etc. The relationship between oil pressure and the fluid bulk modulus which is lowered by entrained air were not included but Koenigsberger [33] has shown that the use of high oil pressure reduces the influence of entrained air significantly.

Figures 4-16 through 4-18 show the load pressure response to a sawtooth input under load condition D in which the template slope(s) and carriage feed rate combine to produce spool linkage input displacement rates during each actuator extension and retraction of 6 in./sec. Comparison of Figure 4-16 with 4-17 shows the increase in pressure fluctuations caused by the sudden reversal in actuator direction as the total leakage coefficient is halved. Figure 4-18 shows the effect of the smaller leakage coefficient combined with a 31% increase in G_a. In both cases the rise time has been decreased at the expense of the effective damping.

For the finish machining operation (condition E) the spool displacement error caused by the presence of a .001 inch spool overlap is shown in Figure 4-19 to represent 80% of the total error during the extension stroke and 100% of the error at the end of the stroke. The larger magnitude ratio of the fluctuating force

component assumed to exist during finishing operations does not contribute to a significant additional error since the initial values of the cutting force component F_1 and the force constant F_2 are small (ref. Table 4.1).

The step response of the servo actuator under zero external load, Figures 4-20 through 4-22 illustrate the low damping nature characteristic of hydraulic systems and the destabilizing effect of inertia loading as the spool area gradient is increased. Comparing Figure 4-20(a) with (b), it is seen that an increase in the area gradient from a value of .10 to .213 decreases the actuator output displacement rise time from a value of .03 sec to .01 sec but the settling time for the latter case has been greatly increased. A decrease in the mass of the system is seen to produce a similar faster response as can be seen by comparing Figure 4-21(a) with (b). In this case, the increase in mass from a value of .065 lb-sec^2/in. to one of .130 lb-sec^2/in. has increased the rise time from .012 sec to .015 sec. Figures 4-22(a), (b) and (c) show the increased rise time of the spool error displacement as the area gradient is increased.

Backlash and friction were not included in the simulation, and the limited investigation into the effect of the linkage mechanical gain on the spool displacement response indicated that the value of the gain had negligible effect on the criterion.

Conclusions

The simulation of a single stage hydraulic servo actuator operating under a dynamic load has been carried out, with particular emphasis on the effect of various cutting conditions on the accuracy of the system. Values of the cutting force component and the cutting force constant for the dynamic loads developed are applicable to SAE 4340 steel, and take into consideration the tool geometry, the cylinder to workpiece angle, and the machine tool settings of feed, speed and width of cut.

The model does not permit evaluation of the degree of surface roughness developed during the cutting operations but the comparatively low dynamic

loading resulting from finish machining operations permits high servo input rates to be applied without serious degradation of system performance, unless a spool valve overlap condition exists; also, the model does not include coulomb friction or structural dynamics which could conceivably alter the overall response during all cutting conditions.

The mathematical model of the spool flow equation was based upon the steady state turbulent orifice equation and a constant value of the discharge coefficient was employed. The simulation could be extended to include a range of values of the discharge coefficient which it is anticipated would be reflected in a decrease of system accuracy, most notably at very small values of spool displacements, where the assumption of turbulent flow is critical to the analysis.

One of the factors affecting the spool displacement error is the rate of input to the spool. A small reduction in the servo linkage displacement rate resulting from a given template slope and carriage velocity can be realized by employing the largest practical cylinder to workpiece angle in the case of an actuator retraction stroke, and the smallest practical angle in the case of an actuator extension stroke. The limits on the cylinder to workpiece angle are defined by the template slope (ref. Figure 1-5) and the compatibility of the tool geometry itself with respect to the uncut workpiece profile.

The pressure drop across the load, can be reduced by operating the system under conditions which decrease the cutting forces themselves. As illustrated in Appendix B (for a fixed chip ratio of .5) the cutting force component F_1 and force constant F_2 are decreased for a given tool geometry as the cylinder to workpiece angle is increased. Thus the cylinder positioning requirements for decreasing F_1, F_2 and the linkage input rate are in accord for an actuator retraction stroke, and conflict for an actuator extension stroke. Both F_1 and F_2 can be decreased by decreasing the width of cut and side cutting edge angle, and increasing the angle of obliquity and the normal rake angle. As shown in Figures A2-3(a) and A2-4(a) attention must be given to the combined selections of the normal rake and side cutting edge angles as the angle of obliquity is increased. Further decreases in F_1 and F_2 are obtained by decreasing the carriage feed parallel to the workpiece axis (for F_1) and increasing the workpiece rotational speed (for F_2).

REFERENCES

1. Ernst, W. - Oil Hydraulic Power and Its Industrial Applications. 2nd ed. New York: McGraw-Hill Book Co. Inc., 1960.

2. Lewis, E.E., and Stern, H. - Design of Hydraulic Control Systems. New York: McGraw-Hill Book Co. Inc., 1962.

3. Guillon, M. - Hydraulic Servo Systems: Analysis and Design. Translated by Griffiths, R.T., New York: Plenum Press, 1969.

4. "Dynamic Pressure Feedback", Aircraft Engineering, June 1960, p. 171. (Dowty Rotol Ltd.).

5. D'Azzo, J.J., and Houpis, C.H. - Feedback Control System Analysis and Synthesis. New York: McGraw-Hill Book Co. Inc., 1960.

6. Kuo, B.C. - Automatic Control Systems. New Jersey: Prentice-Hall, Inc., 1962.

7. Levine, L. - Methods For Solving Engineering Problems Using Analog Computers. New York: McGraw-Hill Book Co. Inc., 1964.

8. Jackson, A.S. - Analogue Computation. New York: McGraw-Hill Book Co. Inc., 1960.

9. James, M.L. Smith G.M. and Wolford, J.C. - Analog and Digital Computer Methods in Engineering Analysis. Scranton, International Textbook Co., 1964.

10. Morse, A.C. - Electrohydraulic Servomechanisms. New York: McGraw-Hill Book Co. Inc., 1963.

11. Merritt, H.E. - Hydraulic Control Systems. New York: John Wiley and Sons, Inc., 1967.

12. Harpur, N.F., "Some Design Considerations of Hydraulic Servos of Jack Type," Proc. Conf. Hydraulic Servomechanisms, (Instn. Mech. Engrs., Lond.), 1953, p. 41.

13. Shearer, J.L., "Dynamic Characteristics of Valve-Controlled Hydraulic Servomotors," Trans. A.S.M.E., Vol. 76, 1954, p. 895.

14. Reeves, E.I., Contributions to Hydraulic Control - 7. "Analysis of the Effects of Nonlinearity in a Valve-Controlled Hydraulic Drive," Trans. A.S.M.E. Feb. 1957, p. 427.

15. Reethof, G., "Application of the Analog Computer to Predict Dynamic Performance in Typical Hydraulic Circuits," Trans. A.S.M.E., Aug. 1958, p. 1299.

16. Rausch, R.G., "The Analysis of Valve - Controlled Hydraulic Servomechanisms," Bell System Tech. J., Vol. 38, No. 4-6, 1959, p. 1513.

17. Davies, R.M., and Lambert, T.H., "Transient Response of an Hydraulic Servomechanism Flexibly Connected to an Inertial Load," J. Mech. Engrg. Sci., Vol. 6, No. 1, 1964, p. 32.

18. Glaze, S.G., "Analogue Technique and the Non-Linear Jack Servomechanism," Proc. Symp. Recent Mech. Eng. Dev. Automatic Control (Instn. Mech. Engrs, Lond.), 1960, paper 10, p. 178.

19. Royle, J.K., "Inherent Non-Linear Effects on Hydraulic Control Systems with Inertia Loading," Proc. Instn. Mech. Engrs, Lond., Vol. 173, No. 9, 1959, p. 257.

20. Turnbull, D.E., "The Response of a Loaded Hydraulic Servo-mechanism," ibid., p. 270.

21. Butler, R., "A Theoretical Analysis of the Response of a Loaded Hydraulic Relay," ibid., No. 16, p. 429.

22. Lee, S.-Y., and Blackburn, J.B., Contributions To Hydraulic Control, Trans. A.S.M.E. Vol. 74, 1952. '1. "Steady - State Axial Forces on Control - Valve Pistons," p. 1005; '2. "Transient Flow Forces and Valve Instability," p. 1013.

23. Noton, G.J., and Turnbull, D.E., "Some Factors Influencing the Stability of Piston - Type Control Valves," Proc. Instn. Mech. Engrs. Lond., Vol. 172, No. 40, 1958, p. 1065.

24. Clark, R.N., "Compensation of Steady - State Flow Forces in Spool - Type Hydraulic Valves," Trans. A.S.M.E., Nov. 1957, p. 1784.

25. Lee, S.-Y., Contributions to Hydraulic Control - 6. "New Valve Configurations for High - Performance Hydraulic and Pneumatic Systems," Trans. A.S.M.E. Vol. 76, 1954, p. 905.

26. Armarego, E.J.A. and Brown, R.H. - The Machining of Metals. Englewood Cliffs, N.J., Prentice-Hall, Inc., 1969.

27. Merchant, M.E., "Basic Mechanics of the Metal Cutting Process," J. Appl. Mech., Trans. A.S.M.E., Vol. 66, 1944, p. A-168.

28. Stabler, G.V., "The Fundamental Geometry of Cutting Tools," Proc. Inst. Mech. Engrs. Lond., Vol. 165, 1951, p. 14.

29. Stabler, G.V., "The Chip Flow Law and Its Consequences," Proc. of the 7th International M.T.D.R. Conference, 1964, p. 243.

30. Choi, C.Y., "An Experimental Study of Plastic Deformation Due to Oblique Cutting," Proc. of the 9th International M.T.D.R. Conference, 1968, p. 1081.

31. Shaw, M.C., Cook, N.H., and Smith, P.A., "The Mechanics of Three Dimensional Cutting Operation," Trans. A.S.M.E., Vol. 74, 1952, p. 1055.

32. Viersma, T.J., "Designing Load-Compensated Fast Response Hydraulic Servos," Control Engng., May 1962, p. 111.

33. Koenigsberger, F., Design Principles of Metal Cutting Machine Tools. New York: Macmillan Co., 1964.

34. Khaimovich, E.M., Hydraulic Control of Machine Tools. Oxford: Permagon Press Inc., 1965.

35. S. Sankar and M.O.M. Osman: On the dynamic accuracy of machine tool hydraulic copying system, ASME-paper No. 73-DET-95, Sept. 1973, to be published in ASME-transactions, J. of Engineering for Industry.

36. W.M. Mansour, M.O.M. Osman and G.M.L. Gladwell: Stability and kinematic accuracy of hydraulic copying mechanisms in metal cutting, ASME-paper, No. 73-WA/DE-11, Nov. 1972, to be published in ASME-transactions, J. of Engineering for Industry.

APPENDIX A

Actuator Flow Equations

The Law of Conservation of Mass is expressed by flow equations. Since the cubical expansion coefficients $\Delta V/\Delta T$ are small for liquids, the direct effect of temperature on the fluid mass density ρ, and consequently on fluid flow, is neglected. Pressure can be regarded as being uniform throughout the volume, so that ρ is also uniform, i.e. a function of time only, not a function of position in the volume. For a control volume - ref. Fig. A1-1, the net rate of mass flow rate into the system equals the rate of mass accumulation in the control volume.

Therefore, the continuity equation is:

$$\Sigma \dot{m}_i - \Sigma \dot{m}_o = \frac{dM}{dt}$$

$$= \frac{d}{dt}(\rho V)$$

$$= \frac{\rho\, dV}{dt} + \frac{V\, d\rho}{dt}$$

In terms of volume flow rate, this becomes:

$$\Sigma Q_i - \Sigma Q_o = \frac{dV}{dt} + \frac{V}{\rho}\frac{d\rho}{dt} \qquad (A.1.1.)$$

From the equation of state for a fluid under constant temperature, $\frac{d\rho}{dt} = \frac{\rho}{\beta}\frac{dP}{dt}$, the bulk modulus of elasticity, β, (which is the reciprocal of compressibility) can be expressed as:

$$\beta = \frac{dP}{\left(\frac{d\rho}{\rho}\right)}$$

With this substitution, equation A.1.1. becomes:

$$\Sigma Q_i - \Sigma Q_o = \frac{dV}{dt} + \frac{V}{\beta}\frac{dP}{dt} \qquad (A.1.2.)$$

The first term on the right side is the flow consumed by expansion of the control volume; the second is the compressibility flow, i.e. flow resulting from pressure changes.

Applying equation A.1.2. to the forward and return chambers respectively,

$$Q_1 - (Q_{Li} + Q_{Le}) = \dot{V}_1 + \frac{V_1}{\beta} \dot{P}_1$$

$$Q_{Li} - (Q_{Le2} + Q_2) = \dot{V}_2 + \frac{V_2}{\beta} \dot{P}_2$$

The leakage flows are proportional to the first power of pressure since the leakage for a small annular clearance is laminar, so that:

$$Q_{Li} = L_i (P_1 - P_2); \; Q_{Le1} = L_{e1} (P_1) \; ; Q_{Le2} = L_{e2} (P_2)$$

Substituting these expressions for the leakage flows, assuming that the two external leakage coefficients are equal, the flow rate into and out of the actuator can be written:

$$Q_1 = \dot{V}_1 + \frac{V_1}{\beta} \dot{P}_1 + L_i (P_1 - P_2) + L_e P_1$$

$$Q_2 = -\dot{V}_2 - \frac{V_2}{\beta} \dot{P}_2 + L_i (P_1 - P_2) - L_e P_2$$

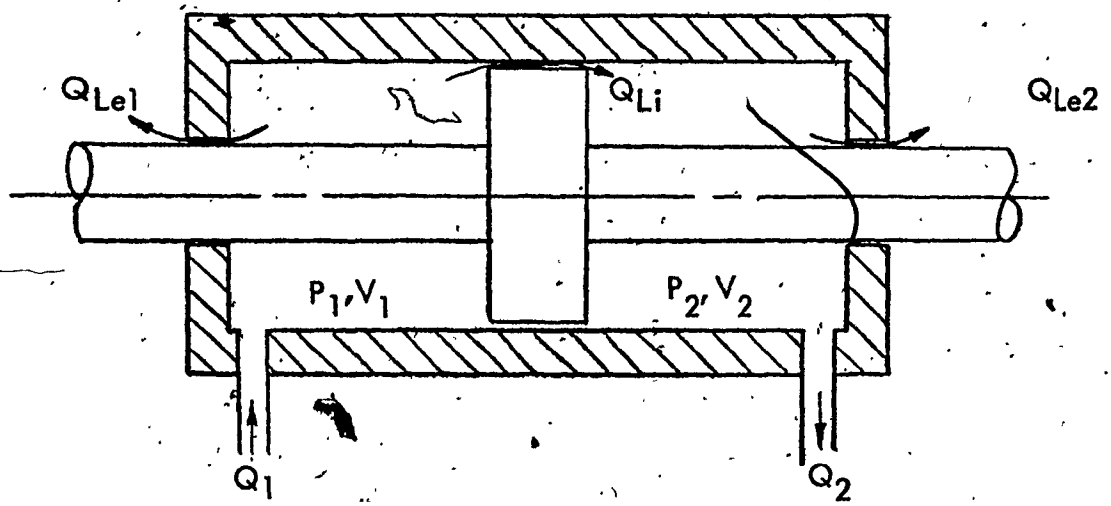

FIGURE A1-1. Actuator Leakage Flow

After a small displacement Y_c of the cylinder,

$$V_1 = V_{o1} + A Y_c \qquad V_2 = V_{o2} - A Y_c$$

where: V_{o1}, V_{o2} are the initial volumes in the forward and return chambers respectively.

The equations are significantly simplified by assuming that the piston is centered along the cylinder. With this assumption,

$$V_{o1} = V_{o2} = V_o$$

where V_o is a constant, equal to half the total trapped volume.

With this substitution, the equations become:

$$Q_1 = A\dot{Y}_c + \left(\frac{V_o + AY_c}{\beta}\right)\dot{P}_1 + L_i(P_1 - P_2) + L_e P_1$$

$$Q_2 = A\dot{Y}_c - \left(\frac{V_o - AY_c}{\beta}\right)\dot{P}_2 + L_i(P_1 - P_2) - L_e P_2$$

By defining load flow, Q_L as the average flow $\frac{Q_1 + Q_2}{2}$, the equations can be reduced to a single equation which relates load flow to actuator pressure difference and velocity:

$$Q_L = A\dot{Y}_c + \frac{V_o}{2\beta}(\dot{P}_1 - \dot{P}_2) + \frac{AY_c}{2\beta}(\dot{P}_1 + \dot{P}_2) + L_i(P_1 - P_2) + \frac{L_e}{2}(P_1 - P_2)$$

With the assumption of constant supply press P_s, the third term on the right is eliminated. Defining load pressure $P_L = P_1 - P_2$, total leakage coefficient $L_t = L_i + \frac{L_e}{2}$ and substituting, the final expression is:

$$Q_L = A\dot{Y}_c + \frac{V_o}{2\beta}\dot{P}_L + L_t P_L$$

Thus the load flow is consumed by flow to displace the actuator, flow stored due to compressibility, and leakage flow.

The bulk modulus is lowered by entrained air, mechanical compliance and increased temperature, so that an effective bulk modulus β_e is used in place of β. The bulk modulus of a petroleum base fluid such as MIL-H-5606 is approximately 4×10^5 psi at 100°F. and 1×10^5 psi at 350°F. No attempt is made in this investigation to establish fluid temperature changes during operation, but the effect of β_e values of $.1 \times 10^5$, $.5 \times 10^5$ and 2×10^5 psi are included.

The volumetric flow rate for laminar leakage through an annular clearance is expressed as:

$$Q = \frac{\pi \partial^3 d}{12 \mu l} \Delta P \quad \text{in}^3/\text{sec}$$

where ∂ is the radial clearance, in., ℓ the passage length, in., and d the diameter of the larger circular section, in. Values of the internal and external leakage coefficients can therefore be calculated for a known piston/rod and cylinder geometry, and fluid operating temperature. The leakage can be up to three times larger [11] if the piston is not centered.

Spool Valve Pressure - Flow Characteristics

A non-dimensionalized presentation of the steady state performance (independent of load dynamics) of the non linear flow equation 3.9 for a critical centre 4 way spool valve with zero leakage and having matched and symmetrical orifices is given in Figure A1-2. The maximum load flow, Q_{Lmax} occurs at max spool displacement under no load i. e. $P_L = 0$.

It is seen that the curves are parabolas which pass through the point $P_L = P_s$ in either direction. Above the $Q = 0$ line, the flow is through one set of orifices; below this line, the flow is through the other set. It is possible to be in the second and fourth quadrants of the P - Q curve only during transient operation or when negative, or assisting loads are present. On a force-velocity basis, the first and third quadrants represent useful work done by the piston; the second and fourth quadrants represent the piston being driven by the load. The greatest nonlinearity occurs at higher loads and larger signals. To avoid operating in this region, the system can be sized so that the P_L/P_s ratio is less than unity. Moreover, it can be shown from equation 3.9 (with C_d, ρ, G_a constant) that for maximum power output $P_L = \frac{2}{3} P_s$.

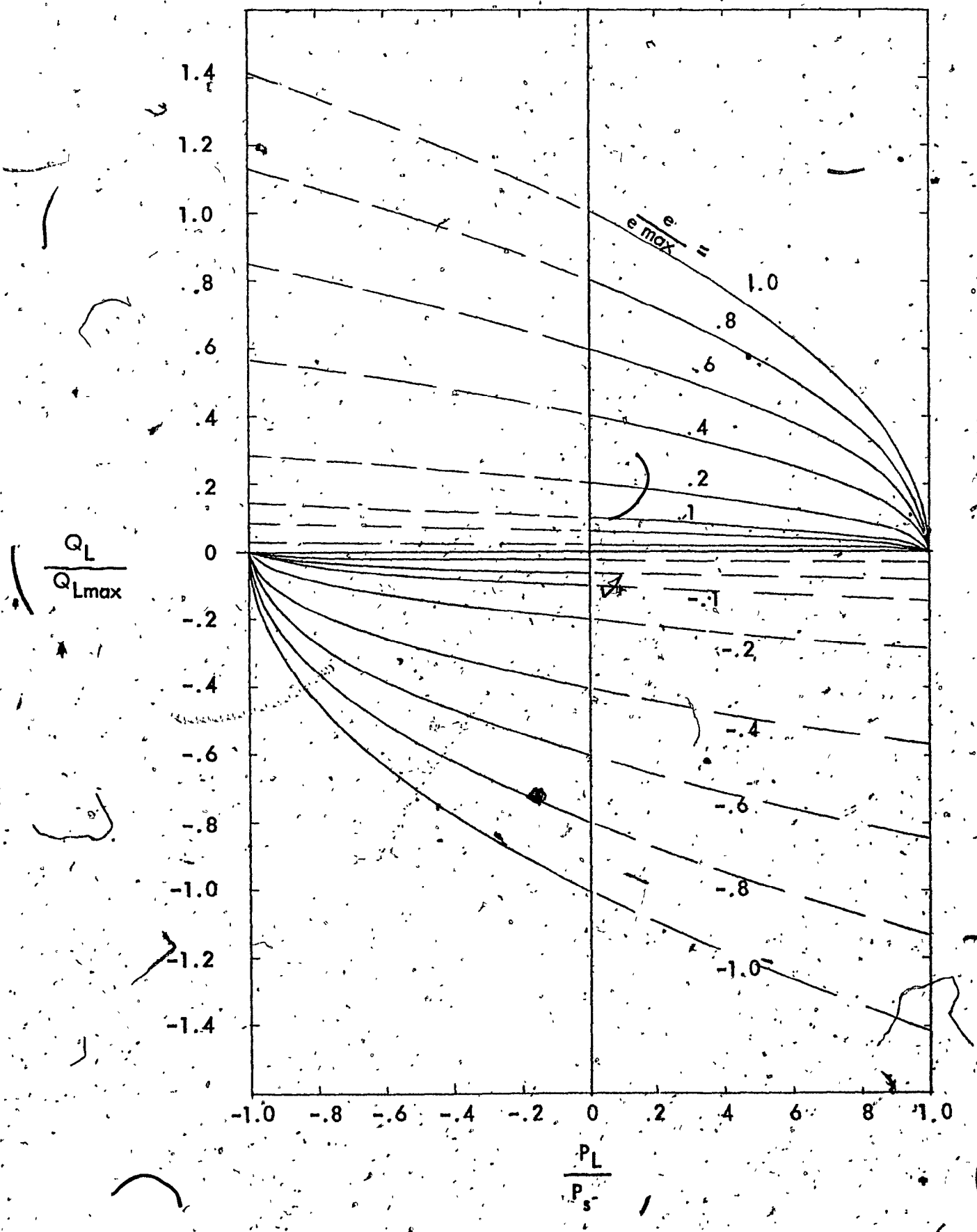

FIGURE A1-2. Spool Valve Pressure-Flow Characteristics

APPENDIX B

Graphical Presentation of the Force Component and Force Constant

As outlined in Chapter 2, with known values of τ_o and K for a given material, K_Q and K_R can be calculated from expression 2.7 for a given tool geometry i, α_n and chip ratio r. Force component F_1 and force constant F_2 of the dynamic force equation 3.18 can then be calculated for a tool side cutting edge angle C_s, copying cylinder axis angle γ and the lathe settings f, n, b. By not assigning values to b, f, and n, $\frac{F_1}{bf}$, $\frac{F_2}{b/n}$ can be calculated from which F_1, F_2 are readily obtainable for a particular desired machine cutting setting.

A digital computer solution is necessary if a range of values of each variable is to be obtained. Figures A2-1 through A2-4 present a solution for two values of γ and i through a range of positive α_n and C_s, with the chip ratio maintained at .5. The solution is applicable only to SAE 4340 steel due to the values of τ_o and K selected. Values of $\frac{F_1}{bf}$ and $\frac{F_2}{b/n}$ are seen to increase for a selected α_n and C_s as γ decreases; increasing the angle of obliquity i lowers the values of both. Increasing C_s increases $\frac{F_1}{bf}$ and $\frac{F_2}{b/n}$; increasing α_n decreases both.

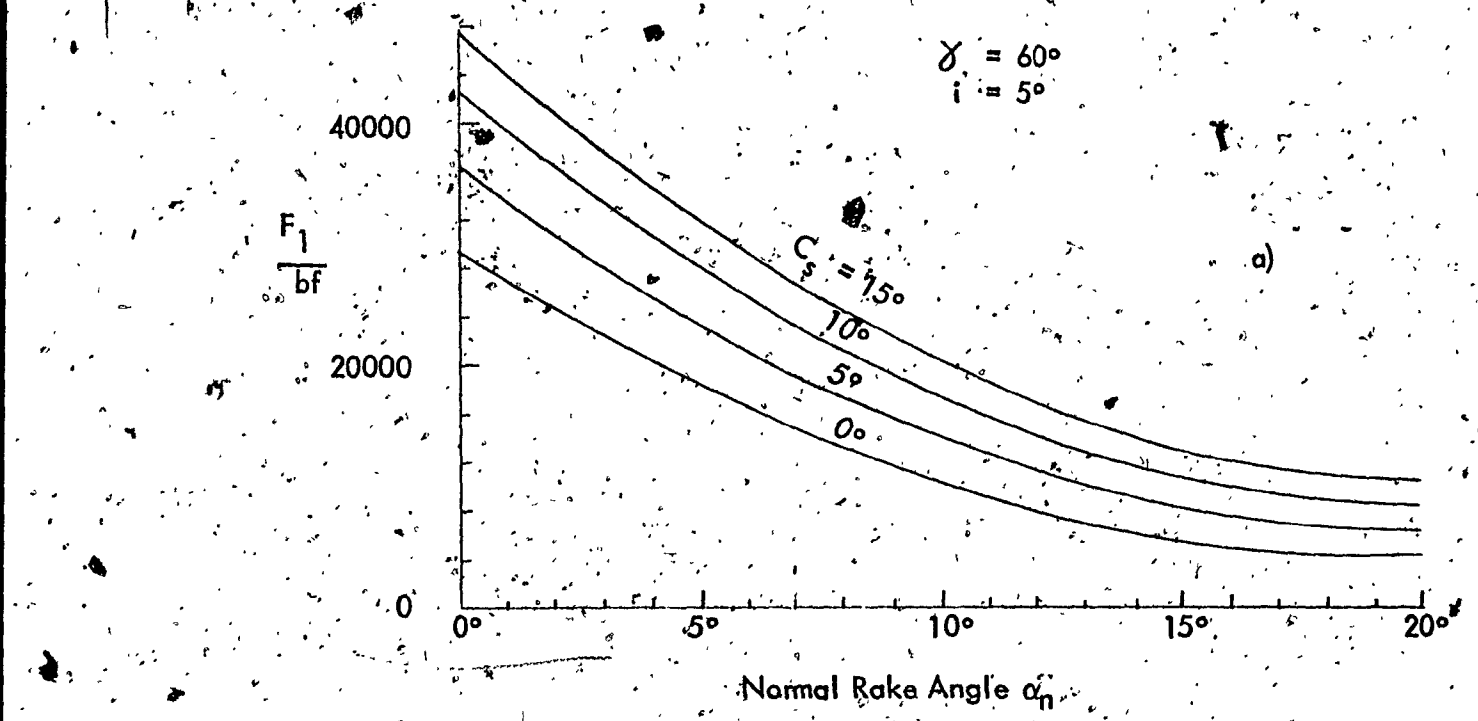
γ = 60°
i = 5°
40000
$\frac{F_1}{bf}$
20000
0
C_s = 15°
10°
5°
0°
a)
0°
5°
10°
15°
20°
Normal Rake Angle α_n

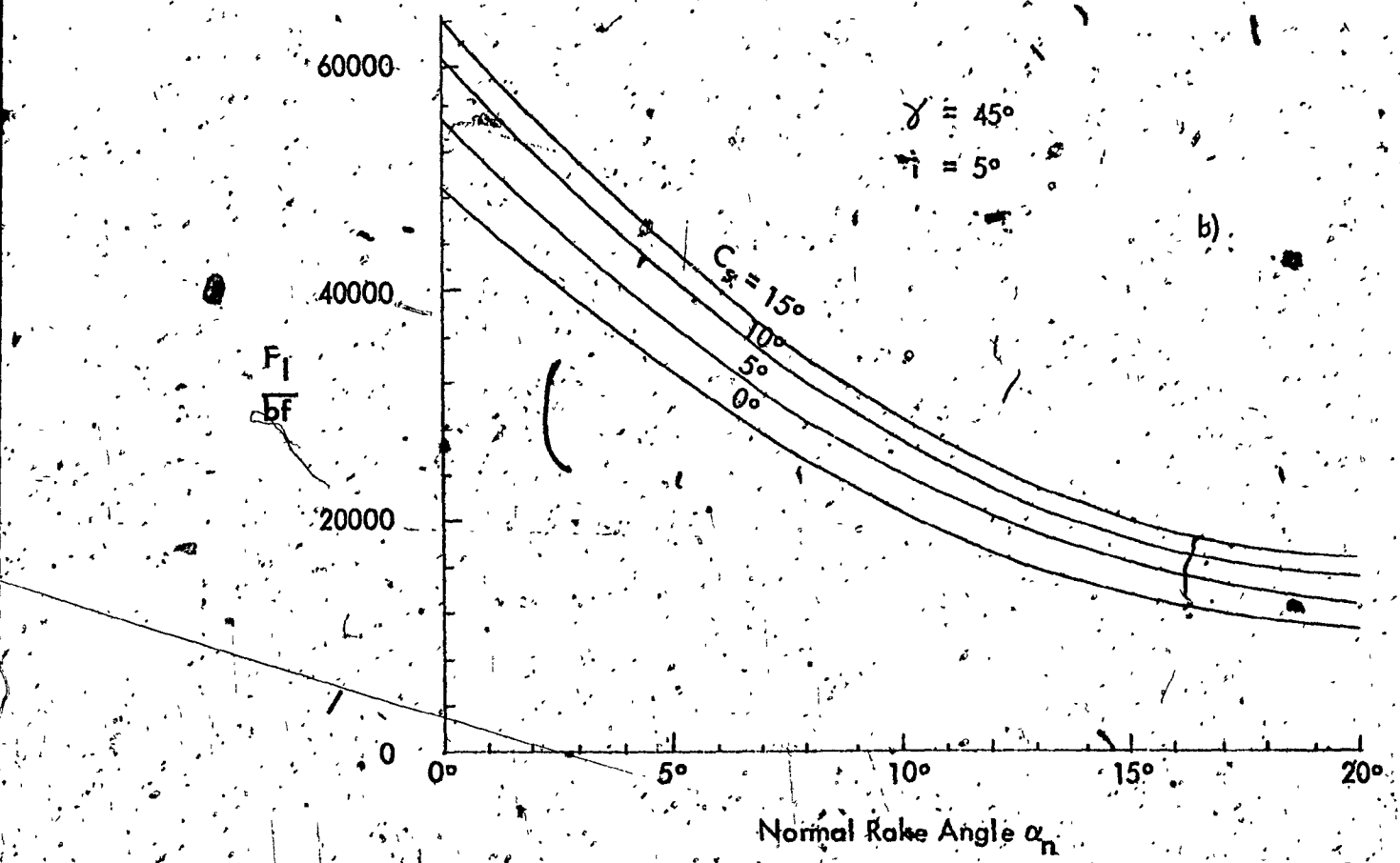
γ = 45°
i = 5°
60000
40000
$\frac{F_1}{bf}$
20000
0
C_s = 15°
10°
5°
0°
b)
0°
5°
10°
15°
20°
Normal Rake Angle α_n

FIGURE A 2-1.

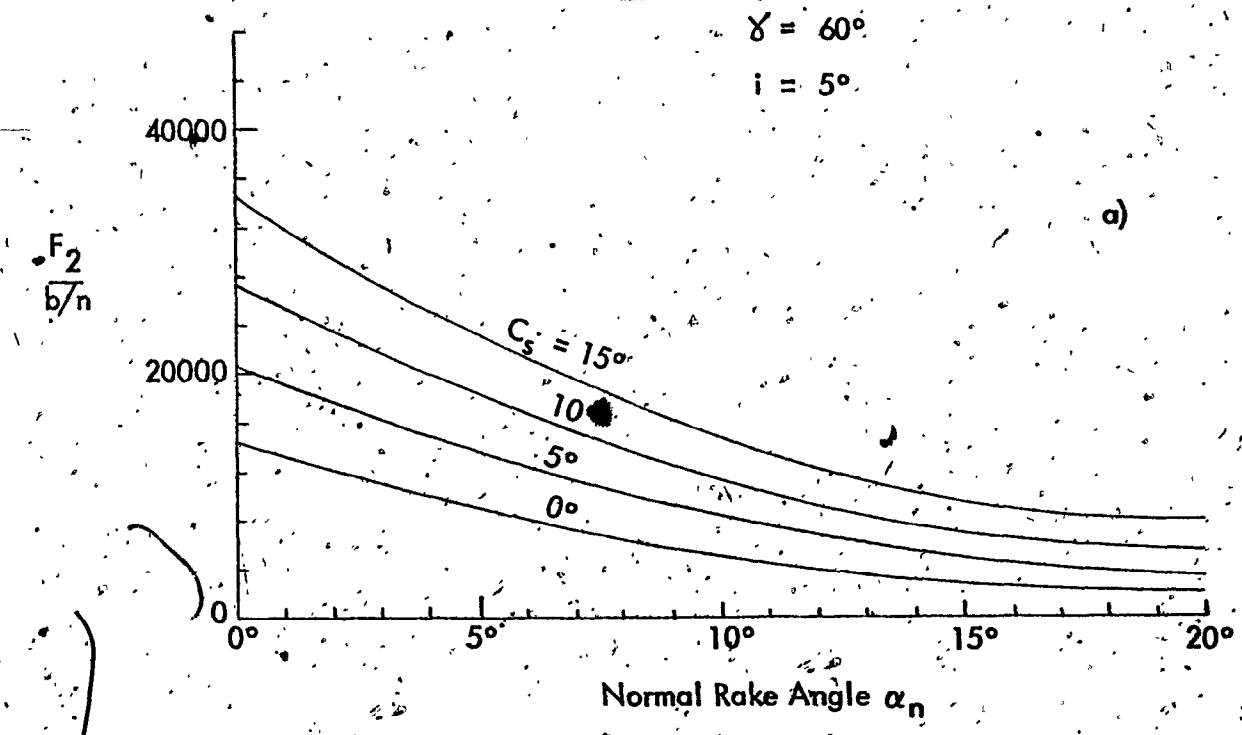
γ = 60°
i = 5°
a)
$\frac{F_2}{b/n}$
40000
20000
0
C_s = 15°
10°
5°
0°
0°
5°
10°
15°
20°
Normal Rake Angle α_n

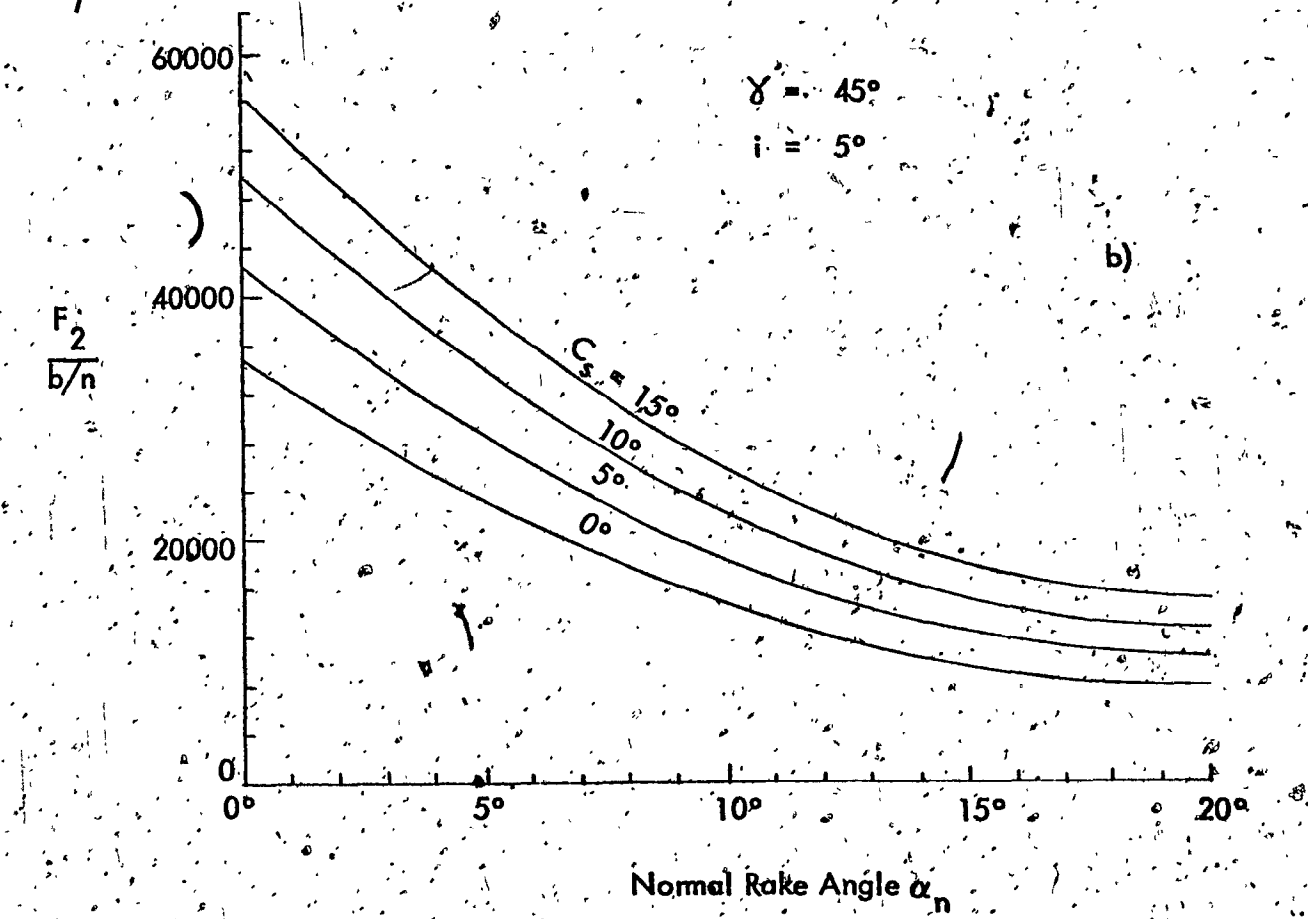
γ = 45°
i = 5°
b)
$\frac{F_2}{b/n}$
60000
40000
20000
0
C_s = 15°
10°
5°
0°
0°
5°
10°
15°
20°
Normal Rake Angle α_n

FIGURE A2-2

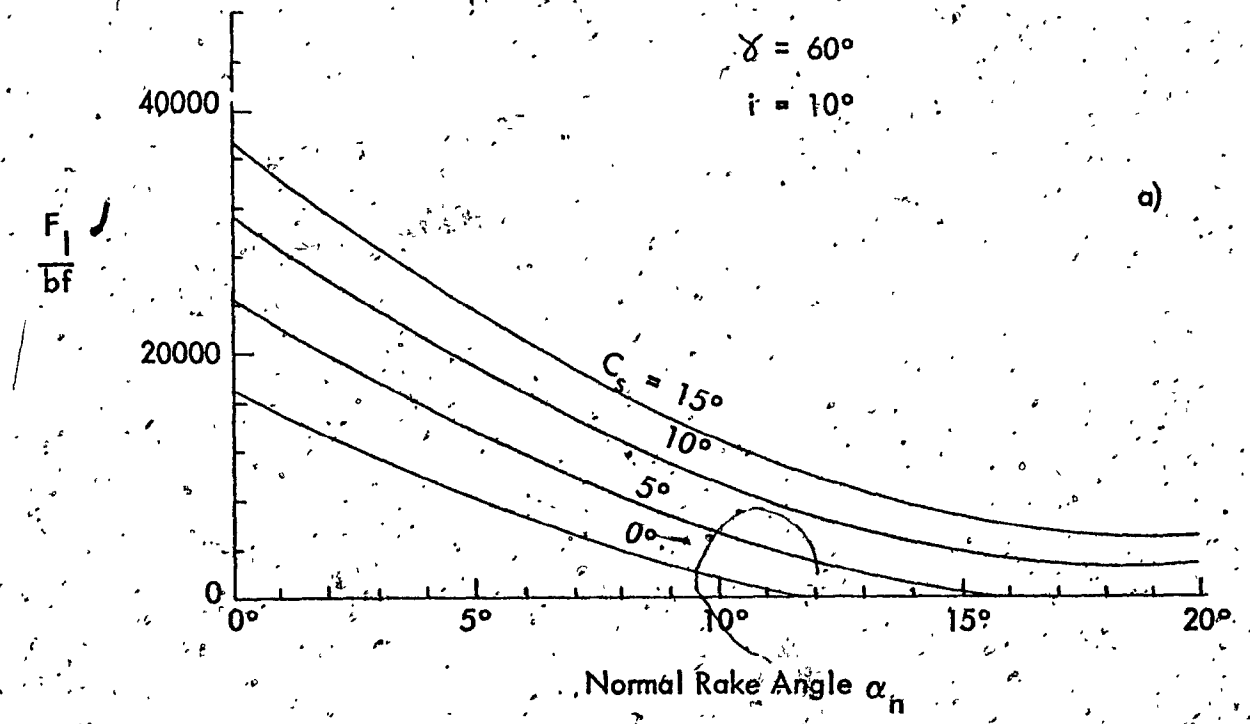
γ = 60°
i = 10°
a)
40000
20000
0
$\frac{F_1}{bf}$
C_s = 15°
10°
5°
0°
0°
5°
10°
15°
20°
Normal Rake Angle α_n

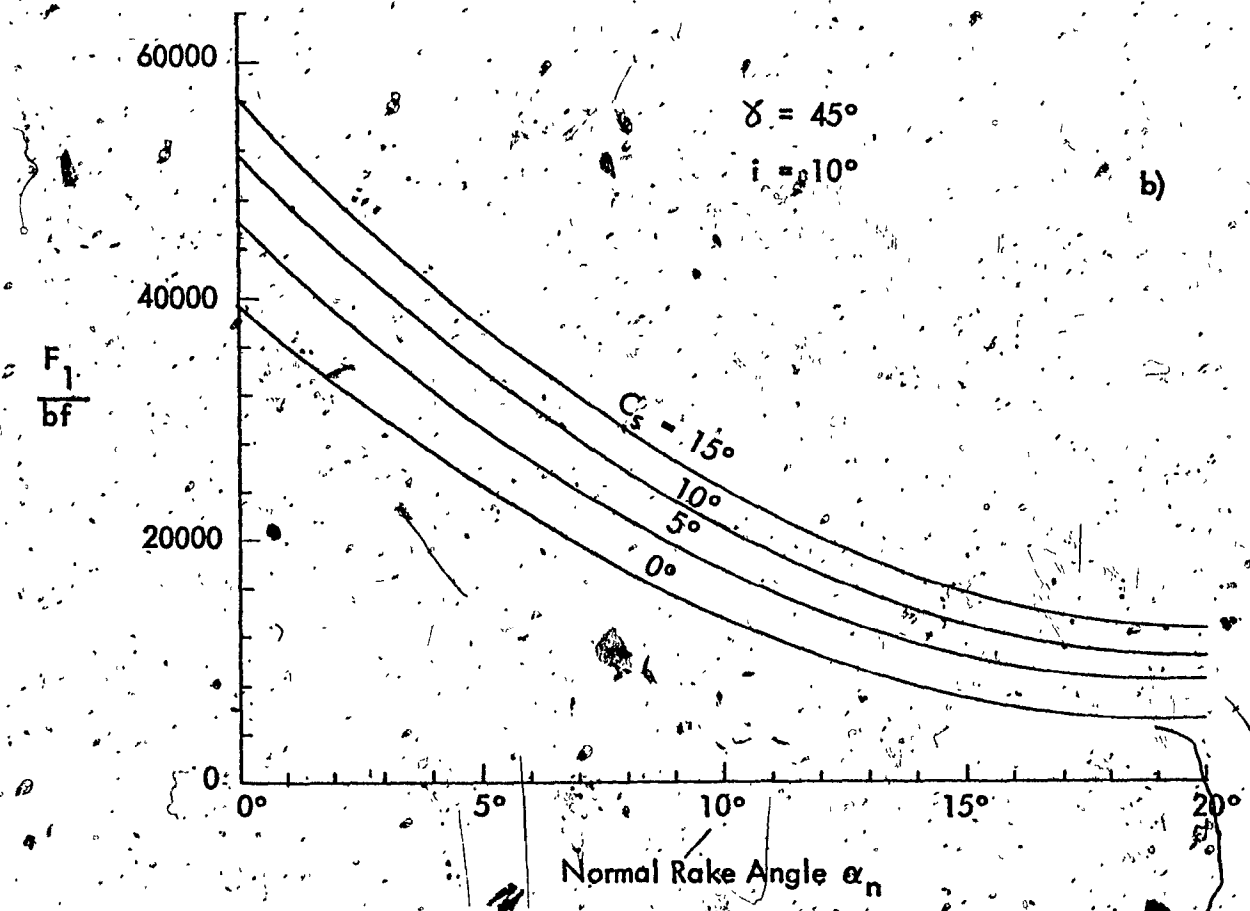
γ = 45°
i = 10°
b)
60000
40000
20000
0
$\frac{F_1}{bf}$
C_s = 15°
10°
5°
0°
0°
5°
10°
15°
20°
Normal Rake Angle α_n

FIGURE A2-3

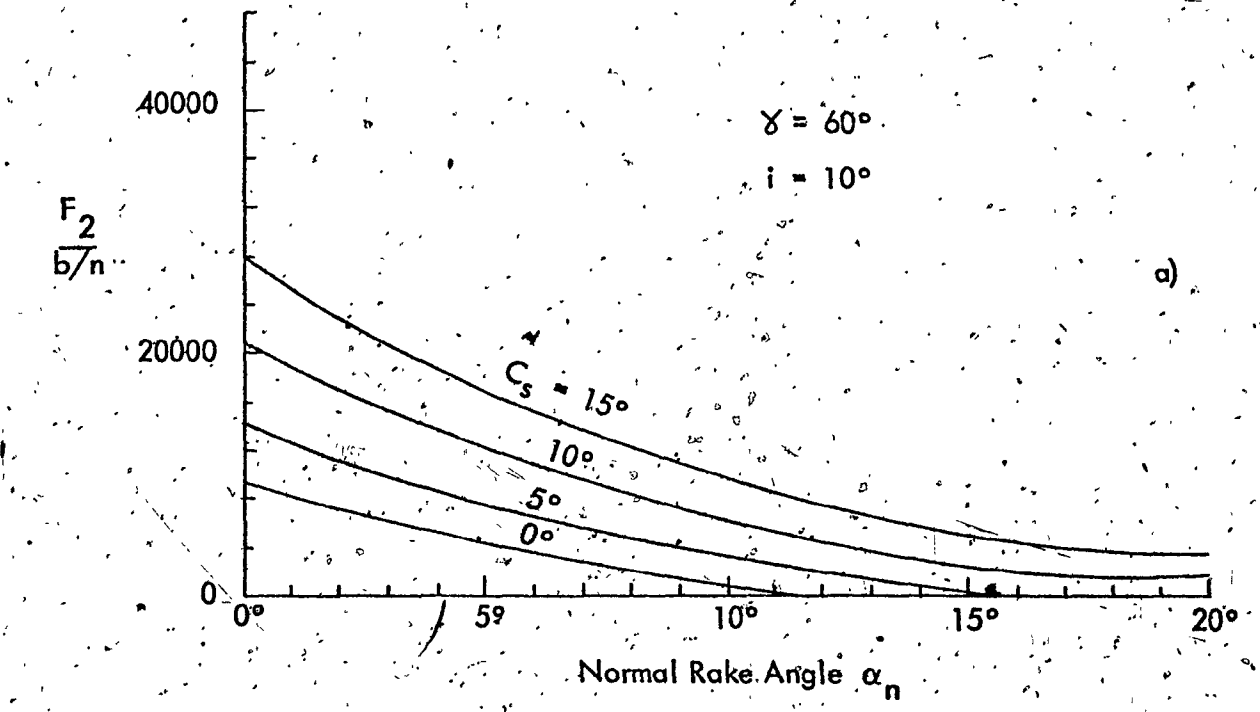
40000
20000
0
$\frac{F_2}{b/n}$
γ = 60°
i = 10°
a)
C_s = 15°
10°
5°
0°
0°
5°
10°
15°
20°
Normal Rake Angle α_n

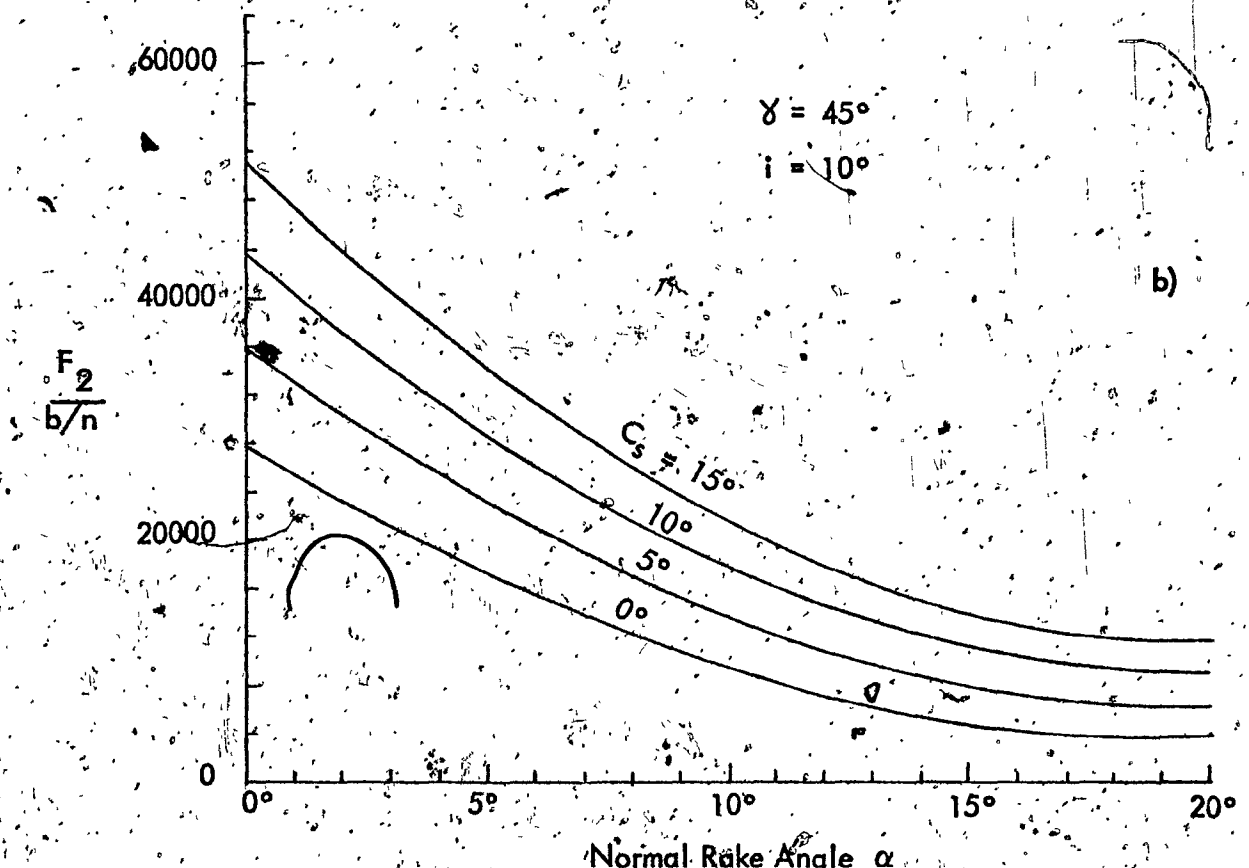
60000
40000
20000
0
$\frac{F_2}{b/n}$
γ = 45°
i = 10°
b)
C_s = 15°
10°
5°
0°
0°
5°
10°
15°
20°
Normal Rake Angle α_n

FIGURE A2-4

APPENDIX C

Analog Simulation of the Mathematical Model

Computer time, T (secs), the independent variable in the computer, is made proportional to the copying system independent variable t (secs), by the expression $T = B_s\, t$ where B_s is the time scale factor. A B_s value of 100 was used throughout the simulation, with the result that the computer solution was a hundred times slower than the problem, or copying system time. The time scale factor appears at all inputs to integrators, since computer integration is with respect to machine time. A problem derivative of dx/dt say, therefore becomes dx/dT at the input after multiplication by $1/B_s$, since $\frac{dx}{dT} = \frac{dt}{dT} \times \frac{dx}{dt} = \frac{1}{B_s} \frac{dx}{dt}$.

The magnitude and time scaled diagram of the copying system mathematical model, Fig. A3-1, lists the potentiometers, amplifiers, and comparators used during the simulation on an EAI 680 computer. The spool mechanical linkage input circuit shown illustrates the simulation of a positive linkage input. The output of integrator 035 simulates the rate of input to the spool linkage (a function of carriage speed and the slope of the template), and is varied by changing the setting of potentiometer 035. The total input displacement, X_c, is represented by potentiometer 036. A given template slope, carriage feed rate, tool geometry, depth of cut, chip ratio, workpiece rotational speed, and workpiece material is simulated by corresponding settings to potentiometers 035, 036, 003 (for F_1) and 005 (for F_2). The cutting component magnitude ratio ϵ, and the frequency of force variation ω, are adjusted via potentiometers 002, 045, and 015. The effect of system parameters for this set of copying input conditions on the overall system response can then be obtained by adjusting the potentiometer(s), containing the parameter under investigation. Conversely, the effect of changes to F_1, F_2, due to changes in tool geometry, or to template slopes, and to ϵ and ω on a given system can be obtained.

Simulation of an actuator retraction stroke is obtained by the addition of an inverter between integrator 035 and amplifier 066. An uninterrupted cylinder

extension, retraction simulation is accomplished by patching a negative unit computer voltage, to the circuit shown, at the negative input to the D/A switch 34B. Simulation of step inputs is achieved by replacing the comparator 34 circuitry with a potentiometer; the input of which is a negative computer unit voltage (for simulating cylinder extensions), the output being patched to amplifier 066.

The computer variables shown in Fig. A3-1 were employed for a number of computer runs, but were re-scaled for other simulations. Simulation of step inputs for example, required re-scaling to prevent overloading of amplifiers. Also, combinations of parameters that would result in potentiometer settings that were too small (causing computation errors), were avoided by re-scaling amplifier variables where possible.

Scaling the System Equations

The following values of parameters are used to illustrate the steps in forming the circuit diagram, and to permit preparation of a potentiometer assignment sheet, useful during static test of programming, scaling, and patching.

Effective area of piston	$A = 1$ in.^{2}
Area of sharp edged hole in piston	$A_h = 3.25 \times 10^{-5}$ in.^{2}
Viscous damping coefficient	$B = .20$ lb-sec/in.
Discharge coefficient (turbulent)	$C_d = .61$
Force component	$F_1 = 17$ lb/rev
Force constant	$F_2 = 155.5$ lb-sec/in.-rev
Spool valve area gradient	$G_a = .05$ in.^{2}/in.
Mechanical linkage gain	$G_m = 4$
Total leakage coefficient $(L_i + \frac{L_e}{2})$	$L_t = 5 \times 10^{-3}$ in.^{3}/sec/psi
Mass of cylinder	$m = .065$ lb-sec^2/in.
Supply pressure	$P_s = 1500$ psi
One half total trapped oil volume	$V_o = 7$ in.^{3}
Effective bulk modulus	$\beta_e = 1 \times 10^5$ psi

Magnitude ratio of fluctuating force	ϵ	$= .05$
Angle between cylinder and workpiece axis	γ	$= 45°$
Fluid mass density	ρ	$= .78 \times 10^{-4}$ lb-sec^2/in.^{4}
Frequency of force variation	ω	$= 10$ rad/sec.

Since a potentiometer setting must always be less than unity, groupings of parameters which would result in a greater magnitude are divided by a constant (usually a value of ten), and an identical value of gain is employed at the associated amplifier.

The system equations are re-arranged as necessary to employ the "general method" technique of programming, and in the unscaled form are as follows:

$$e = \frac{1}{G_m} (X_c - Y_c) \tag{3.14}$$

$$F_{dyn} = (F_1 + F_2 \dot{Y}_c)(1 + \epsilon \sin \omega t) \tag{3.18}$$

$$\ddot{Y}_c = \frac{1}{m} (P_L A - B \dot{Y}_c - F_{dyn}) \tag{3.15}$$

$$\dot{P}_L = \frac{2\beta_e}{V_o} (Q_L - A\dot{Y}_c - L_t P_L - Q_h) \tag{3.12}$$

$$Q_L = \frac{C_d G_a e}{\rho} \sqrt{P_s - P_L \operatorname{sgn} e} \tag{3.9}$$

$$Q_h = \sqrt{\frac{2}{\rho}} C_d A_h \sqrt{|P_L|} \operatorname{sgn} P_L \tag{3.13}$$

The voltage and time scaled equations are written in terms of the computer variables. These variables are themselves based upon best estimates of expected maximum values of the problem variables. The scaled equations are as follows:

Using (3.14), applied to a pot feedback amplifier:

$$\left[\frac{e}{.020}\right] = -\left\{\frac{\left[\frac{-X_c}{.6}\right] + \left[\frac{Y_c}{.6}\right]}{\left(\frac{.020}{.6}\,G_m\right)}\right\}$$

Using (3.18) applied to a multiplier:

$$\left[-\frac{F_{dyn}}{405}\right] = -\left\{\left[\frac{\Theta_1}{300}\right] \times \left[\frac{\Theta_2}{1.35}\right]\right\}$$

where

$$\left[\frac{\Theta_1}{300}\right] = -\left\{\left(\frac{F_1}{300}\right)[-1] + 10\left(\frac{10\,F_2}{300 \cdot 10}\right)\left[\frac{-\dot{Y}_c}{10}\right]\right\}$$

and

$$\left[\frac{\Theta_2}{1.35}\right] = -\left\{\left(\frac{1}{1.35}\right)[-1] + \left(\frac{\epsilon}{1.35}\right)\left[\frac{-\sin\omega t}{1}\right]\right\}$$

Computer variable $\left[\frac{-\sin\omega t}{1}\right]$ is generated from the mechanization on the computer of the second order differential equation of the form $\ddot{y} + \omega^2 y = o$ with initial conditions $y(o) = o$, $\dot{y}(o) = 1$.

Using (3.15) applied to a multiple input integrator whose output is $\left[\frac{-\dot{Y}_c}{10}\right]$;

$$\frac{d}{dT}\left[\frac{-\dot{Y}_c}{10}\right] = -\left\{10\left(\frac{600\,A}{10m\,B_s\,10}\right)\left[\frac{P_L}{600}\right] + \left(\frac{B}{m\,B_s}\right)\left[\frac{-\dot{Y}_c}{10}\right] + 10\left(\frac{405}{10m\,B_s\,10}\right)\left[\frac{-F_{dyn}}{405}\right]\right\}$$

Using (3.12);

$$\frac{d}{dT}\left[\frac{-P_L}{600}\right] = -\left\{10\left(\frac{4\;2\beta_e}{600\,B_s\,10\,V_o}\right)\left[\frac{Q_L}{4}\right] + 10\left(\frac{10\;2\beta_e\,A}{600\,B_s\,10\,V_o}\right)\left[\frac{-\dot{Y}_c}{10}\right] + 10\left(\frac{2\beta_e\,L_t}{B_s\,10\,V_o}\right)\left[\frac{-P_L}{600}\right] + \left(\frac{2\beta_e\,.5}{600\,B_s\,V_o}\right)\left[\frac{-Q_h}{.5}\right]\right\}$$

Using (3.9); for a multiplier with pot feedback:

$$\left[\frac{Q_L}{16} \times \frac{4}{1}\right] = \left\{\frac{\left[\frac{\gamma 1}{800}\right] \times \left[\frac{e}{.020}\right]}{(1/4)}\right\}$$

where $$\left[\frac{\gamma 1}{800}\right] = -\left\{\left(\frac{C_d\, G_a\, 50}{800\sqrt{\rho}}\right)\left[-\sqrt{\frac{\gamma 2}{2500}}\right]\right\}$$

and $$\left[\frac{\gamma 2}{2500}\right] = -\left\{\left(\frac{P_s}{2500}\right)[-1] + \left(\frac{600}{2500}\right)\left[\frac{P_L}{600}\right] \text{sgn } e\right\}$$

A multiplier with pot feed back was used to facilitate rapid magnitude scaling whenever rescaling in the computer was found necessary.

Using (3.13);

$$\left[\frac{-Q_h}{.5}\right] = -\left\{\left(\frac{\sqrt{2}\; C_d\, A_h \sqrt{600}}{.5\sqrt{\rho}}\right)\left[\sqrt{\left|\frac{P_L}{600}\right|}\ \text{sgn } P_L\right]\right\}$$

By forming a computer variable which is the absolute value of the system displacement error and integrating, the criterion for accuracy (referenced in Chapter 1) is generated at amplifier 010.

The spool valve deadband circuit consists of two potentiometers (031 and 038); a positive and negative limit summer (016 and 006), and summer amplifier 036. Pot settings given in Figure A3-1 are for a spool overlap (each side of the neutral zero) of .001 inches.

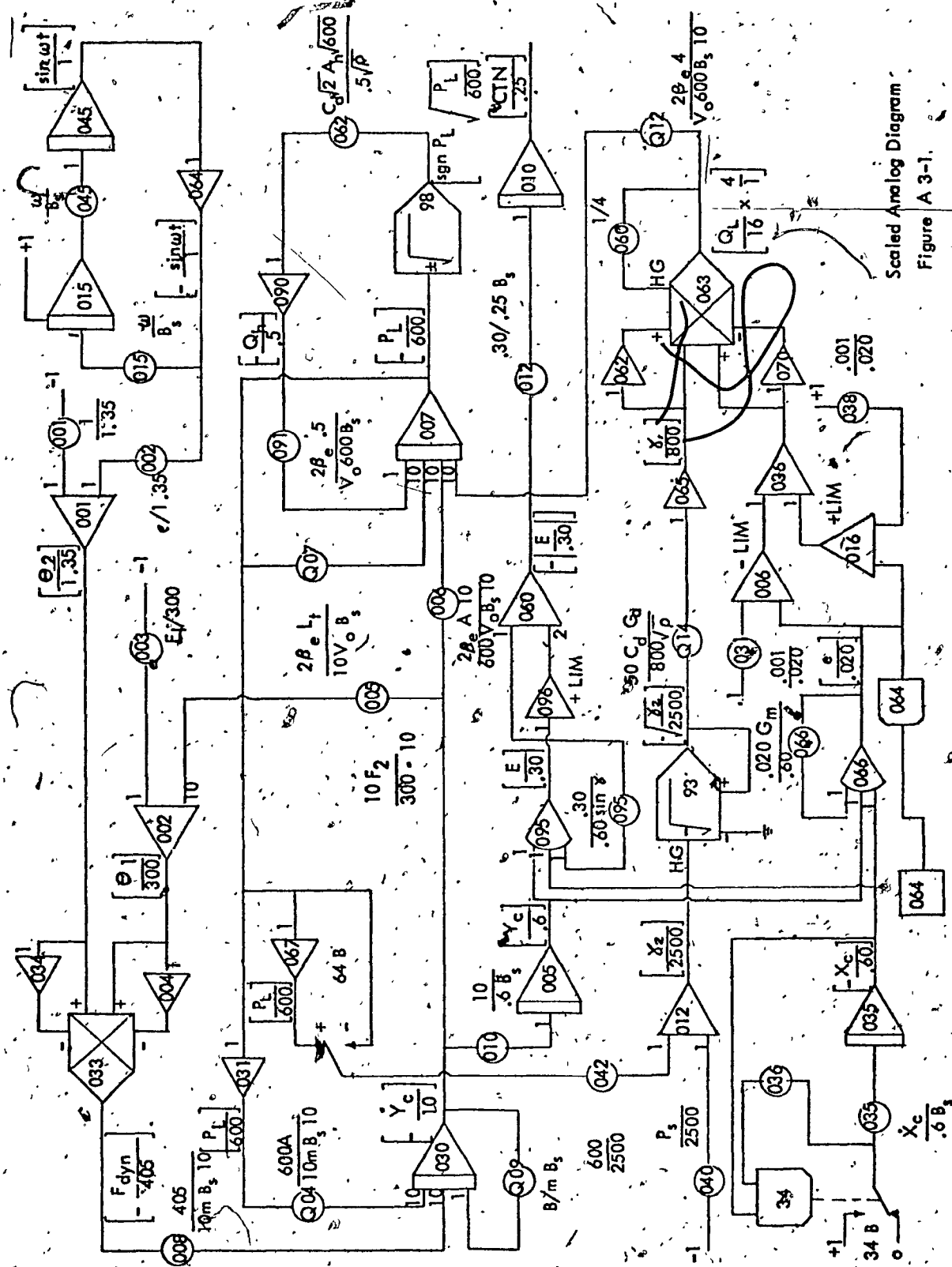

Figure A 3-1. Scaled Analog Diagram